

ปริมาณรังสีเด็กในครรภ์จากการตรวจช่องท้อง กระดูกเชิงกราน และ  
กระดูกสันหลังส่วนเอวด้วยเอกซเรย์ระบบดิจิทัลในหุ่นจำลอง



นางสาวศกามาศ เถายบุตร

## สถาบันวิทยบริการ จุฬาลงกรณ์มหาวิทยาลัย

วิทยานิพนธ์นี้เป็นส่วนหนึ่งของการศึกษาตามหลักสูตรปริญญาวิทยาศาสตรมหาบัณฑิต

สาขาวิชาอาชีวเวชศาสตร์ ภาควิชารังสีวิทยา

คณะแพทยศาสตร์ จุฬาลงกรณ์มหาวิทยาลัย

ปีการศึกษา 2550

ลิขสิทธิ์ของจุฬาลงกรณ์มหาวิทยาลัย

**FETAL DOSE IN RANDO PHANTOM FROM COMPUTED  
RADIOGRAPHY OF ABDOMEN, PELVIS AND LUMBO-  
SACRAL SPINE**



**Miss Phakamart Thaoyabut**

สถาบันวิทยบริการ  
จุฬาลงกรณ์มหาวิทยาลัย

**A Thesis Submitted in Partial Fulfillment of the Requirements  
for the Degree of Master of Science Program in Medical Imaging**

**Department of Radiology**

**Faculty of Medicine**

**Chulalongkorn University**

**Academic Year 2007**


**Copyright of Chulalongkorn University**

Thesis Title FETAL DOSE IN RANDO PHANTOM FROM  
COMPUTED RADIOGRAPHY OF ABDOMEN,  
PELVIS AND LUMBO-SACRAL SPINE

By Miss Phakamart Thaoyabut  
Field of Study Medical Imaging  
Thesis Advisor Associate Professor Sivalee Suriyapee, M.Eng.


---


Accepted by the Faculty of Medicine, Chulalongkorn University in  
Partial Fulfillment of the Requirements for the Master's Degree

  
.....Dean of the Faculty of Medicine  
(Associate Professor Adisorn Patradul, M.D.)

#### THESIS COMMITTEE

  
.....Chairman  
(Associate Professor Anchali Krisanachinda, Ph.D.)

  
.....Thesis Advisor  
(Associate Professor Sivalee Suriyapee, M.Eng.)

  
..... External Member  
(Professor Franco Milano, Ph.D.)

  
..... Member  
(Assistant Professor Kiat Arjhansiri, M.D.)

พจนานุกรม : ปริมาณรังสีเด็กในครรภ์จากการตรวจช่องท้อง กระดูกเชิงกราน และกระดูกสันหลัง ส่วนเอวด้วยเอกซเรย์ระบบดิจิตอลในหุ่นจำลอง. (FETAL DOSE IN RANDO PHANTOM FROM COMPUTED RADIOGRAPHY OF ABDOMEN, PELVIS AND LUMBO-SACRAL SPINE )  
 อ.ที่ปรึกษา: รศ.ศิวลี สุริยาปี, 95 หน้า

ปัจจุบันการถ่ายภาพรังสีด้วยเครื่องเอกซเรย์ระบบดิจิตอลได้เข้ามามีบทบาทเป็นอย่างมากสำหรับการวินิจฉัยโรคในแผนกเอกซเรย์เนื่องจากใช้ง่ายและสะดวกในการใช้งาน แต่พบว่าปริมาณรังสีที่ซึบกลับมากขึ้นเพื่อรองรับการแสดงผลของภาพในระดับต่างๆ อย่างไรก็ตามหากนำมาใช้กับหญิงมีครรภ์โดยไม่ระมัดระวังก็อาจทำให้เกิดผลต่อตัวอ่อนในครรภ์โดยเฉพาะการตั้งครรภ์ในระยะสามเดือนแรก จุดประสงค์ของการศึกษานี้เพื่อหาปริมาณรังสีจากหุ่นจำลองด้วยการวัดค่าปริมาณรังสีที่ได้จากอุปกรณ์วัดรังสีชนิดเทอร์โมลูมิเนสเซนส์โคสมิเตอร์เปรียบเทียบกับปริมาณรังสีที่ได้จากการคำนวณด้วยตัวแปรต่างๆ จากการตั้งค่าในการถ่ายภาพรังสี เพื่อหาความสัมพันธ์ของค่าที่วัดได้จากทั้งสองวิธีนี้

ในการศึกษานี้ หุ่นจำลองถูกถ่ายภาพรังสีด้วยท่า pelvis AP, abdomen AP, lumbo-sacral spine AP และ lumbo-sacral spine LAT จากเครื่องเอกซเรย์ Toshiba รุ่น KX0-80G ซึ่งใช้ระบบรับภาพดิจิตอล Fuji รุ่น FCR XG 5000 ปริมาณรังสีที่ได้จะทำการเปรียบเทียบจากการคำนวณด้วยค่าพารามิเตอร์ต่างๆ จากการตั้งค่าเอ็กโพสเซอร์และจากการวัดด้วยเทอร์โมลูมิเนสเซนส์โคสมิเตอร์ ซึ่งเทอร์โมลูมิเนสเซนส์โคสมิเตอร์แต่ละตัวจะถูกคัดเลือกโดยดูจากค่าความไว ความสัมพันธ์ที่เป็นเส้นตรง และการตอบสนองต่อพลังงาน เปรียบเทียบกับ โคบอลต์-60 จากนั้น เทอร์โมลูมิเนสเซนส์โคสมิเตอร์ ที่ได้จะถูกนำไปใส่ในหุ่นจำลองที่ตำแหน่งต่างๆ โดยที่ pelvis AP, abdomen AP และ lumbo-sacral spine AP วางบริเวณผิวหนังระดับครรภ์ และลึกลงไป 3.0, 6.0 และ 9.0 เซนติเมตร และสำหรับ lumbo-sacral spine LAT วางบริเวณผิวหนังระดับครรภ์ และลึกลงไป 13.0, 16.0 และ 19.0 เซนติเมตร ผลการทดลองพบว่า ปริมาณรังสีที่ตัวอ่อนได้รับ จาก ท่า pelvis AP วัดด้วยเทอร์โมลูมิเนสเซนส์โคสมิเตอร์มีค่าอยู่ในช่วง 0.83 ถึง 1.39 มิลลิเกรย์ และ จากการคำนวณ มีค่าอยู่ในช่วง 0.62 ถึง 1.03 มิลลิเกรย์, abdomen AP การวัดด้วยเทอร์โมลูมิเนสเซนส์โคสมิเตอร์มีค่าอยู่ในช่วง 0.55 ถึง 0.87 มิลลิเกรย์ จากการคำนวณ มีค่าอยู่ในช่วง 0.36 ถึง 0.67 มิลลิเกรย์, lumbo-sacral spine AP วัดด้วยเทอร์โมลูมิเนสเซนส์โคสมิเตอร์มีค่าอยู่ในช่วง 0.46 ถึง 1.10 มิลลิเกรย์ จากการคำนวณ มีค่าอยู่ในช่วง 0.44 ถึง 1.05 มิลลิเกรย์ และ lumbo-sacral spine LAT จากการวัดด้วยเทอร์โมลูมิเนสเซนส์โคสมิเตอร์มีค่าอยู่ในช่วง 0.15 ถึง 0.20 มิลลิเกรย์ และ จากการคำนวณ มีค่าอยู่ในช่วง 0.13 ถึง 0.24 มิลลิเกรย์ ซึ่งจะพบว่าค่าที่ได้จากเทอร์โมลูมิเนสเซนส์โคสมิเตอร์ นั้นสูงกว่าค่าที่ได้จากการคำนวณโดยค่าแตกต่างมากที่สุดคิดเป็น 23.46 เปอร์เซ็นต์ ที่ผิว และลดลงเหลือ 19.19 เปอร์เซ็นต์ ที่ระดับเด็กในครรภ์ ความคลาดเคลื่อนนี้คาดว่าเกิดจากหัววัดรังสีที่ใช้ในการทดลองและความคลาดเคลื่อนจากค่าพารามิเตอร์ต่างๆที่นำมาคำนวณ อย่างไรก็ตามเมื่อนำผลที่ได้จากทั้งสองวิธีมาวาดกราฟพบว่าผลการตอบสนองรังสีเป็นไปในทิศทางเดียวกัน ซึ่งการวัดปริมาณรังสีที่มากกว่า 1.0 มิลลิเกรย์ เป็นค่าที่กำหนดโดย ICRP พบว่าการใช้เทอร์โมลูมิเนสเซนส์โคสมิเตอร์วัดได้ดีกว่าการคำนวณ ดังนั้นในการคำนวณหาค่าปริมาณรังสีในผู้ป่วยที่ตรวจด้วยเอกซเรย์ระบบดิจิตอลให้ค่าต่ำกว่าค่าจากการวัดด้วยเทอร์โมลูมิเนสเซนส์โคสมิเตอร์ประมาณ 23 เปอร์เซ็นต์ จึงควรพิจารณาเมื่อนำค่าเอ็กโพสเซอร์พารามิเตอร์มาใช้ในการคำนวณ

ภาควิชา.....รังสีวิทยา.....ลายมือชื่อนิสิต.....พจนานุกรม 1.เอิบบุตร  
 สาขาวิชา.....ฉายาเวชศาสตร์.....ลายมือชื่ออาจารย์ที่ปรึกษา.....ศิวลี สุริยาปี  
 ปีการศึกษา 2550

# # 4974753030: MAJOR MEDICAL IMAGING

KEYWORDS: FETAL DOSE / COMPUTED RADIOGRAPHY /  
THERMOLUMINESCENT DOSIMETRY/ RANDO PHANTOM

PHAKAMART THAOYABUT: FETAL DOSE IN RANDO PHANTOM  
FROM COMPUTED RADIOGRAPHY OF ABDOMEN, PELVIS AND  
LUMBO-SACRAL SPINE. THESIS ADVISOR: ASSOC. PROF. SIVALEE  
SURIYAPEE, 95 pp.

Computed radiography (CR) has an important role in diagnostic imaging, because of its ease of use and fast processing. However, the patient radiation doses used is highly increased to support multi-resolution results. So it may cause some effects to a fetus in pregnant woman, especially in the first trimester. The purpose of this study is to determine the fetal doses calculating by exposure parameters and measuring with TLD-100 chips in RANDO phantom and to demonstrate the correlation between both methods.

The calculation was performed for surface 3.0, 6.0 and 9.0 cm depths for the pelvis AP, abdomen AP and lumbo-sacral spine AP at surface 13.0, 16.0, 19.0 cm depths for lumbo-sacral spine lateral projection. The machines were Toshiba x-ray model KXO-80G and Fuji CR model XG 5000. Before using, the TLD-100 chips were calibrated with Cobalt-60 gamma rays for sensitivity, linearity and energy response. The average fetal doses at 6.0 cm depth in RANDO phantom measured with TLD-100 chips ranged from 0.83 to 1.39 mGy and the calculation were 0.62 to 1.03 mGy for pelvic AP. For abdomen AP, the measured fetal doses ranged from 0.55 to 0.87 mGy and the calculations were 0.36 to 0.67 mGy. For lumbo-sacral spine AP, the measured fetal dose ranged from 0.46 to 1.10 mGy and the calculations were 0.44 to 1.05 mGy. For lumbo-sacral spine LAT, the measured ranged from 0.15 to 0.20 mGy and the calculations were 0.13 to 0.24 mGy. The TLD doses were mostly higher than the calculated doses. The highest different value was 23.46% which observed at the surface, the difference was reduced to 19.19 % at the fetal depth. The dispersion may be caused mainly by the difference of the chamber type used for dose determination and also the parameters employed for calculation. The graph of fetal doses from measured with TLD-100 chips and parameter calculation showed a good correlation. The fetal doses of greater than 1.0 mGy which was the ICRP dose limit to the pregnant patient and radiation worker were observed in the measured with TLD-100 chips than the calculation. Therefore, the patients undergo the CR examination, estimated dose by exposure parameter will give under doses within 23%. When using parameter calculation, careful consideration should be kept in mind.

Department..... Radiology..... Student's signature *Phakamart Thaoyabut*  
Field of study..... Medical Imaging..... Advisor's signature *Sivalee Suriyapee*  
Academic year 2007

## ACKNOWLEDGEMENTS

I would like to express gratitude and deepest appreciation to Associate Professor Sivalee Suriyapee, Head of Physicist at Division of Radiation Oncology, Department of Radiology, Faculty of Medicine, Chulalongkorn University, my major advisor for her guidance, invaluable advice, supervision, constructive comments and English language proof in this research. I am equally grateful to Mr. Sornjarod Oonsiri and Ms. Petcharleeya Suwanpradit, physicist at Department of Radiology, King Chulalongkorn Memorial Hospital, for their help in the experiment, kind suggestion and constructive comments in the experiments.

I would like to deeply thank Associate Professor Anchali Krisanachinda, at Nuclear Medicine Division, Faculty of Medicine, Chulalongkorn University, my teacher for advice and comments in the research.

I would like to deeply thank Associate Professor Somjai Wangsuphachart, Head of Department of Radiology, Faculty of Medicine, Chulalongkorn University for advice and comments in the research.

I would like to deeply thank to my thesis committee, Assistant Professor Kiat Arjhansiri, Head of Diagnostic Division, Department of Radiology, Faculty of Medicine, Chulalongkorn University and for his kindness in examining the research methodology and provide suggestion for the improvement.

I would like to thank Professor Franco Milano from Florence University Italy, who was the external examiner of the thesis defense for his help in the experiment, kind suggestion, and constructive comments in the experiments and English language proof in this research.

I would like to thank medical staff in Department of Radiology, Faculty of Medicine, Chulalongkorn University, for their help in my research.

I am thankful for all teachers, lecturers and staff at the Master of Science Program in Medical Imaging, Faculty of Medicine, Chulalongkorn University for their unlimited teaching of knowledge in Medical Imaging.

Finally, I am grateful of my family for their financial support, valuable encouragement, entirely care, and understanding during the entire course of study.

สถาบันวิทยบริการ  
จุฬาลงกรณ์มหาวิทยาลัย

# CONTENTS

	<b>Page</b>
ABSTRACT (THAI).....	iv
ABSTRACT (ENGLISH).....	v
ACKNOWLEDGEMENTS.....	vi
LIST OF TABLES.....	xi
LIST OF FIGURES.....	xiii
LIST OF ABBREVIATIONS.....	xv
<b>CHAPTER 1 INTRODUCTION.....</b>	<b>1</b>
1.1 Background and rationale.....	1
1.2 Research objectives.....	1
<b>CHAPTER 2 REVIEW OF RELATED LITERATURES.....</b>	<b>2</b>
2.1 Theory.....	2
2.1.1 Radiation effects in utero.....	2
2.1.2 Ionizing radiations.....	7
2.1.3 Computed radiography.....	10
2.1.4 In utero exposure in diagnostic radiology.....	11
2.1.5 Factors affecting fetal dose in diagnostic radiology.....	11
2.1.6 Fetal dose estimation in diagnostic radiology.....	11
2.1.7 Absorbed dose calibration.....	14
2.1.8 Thermoluminescent dosimetry.....	17
2.1.9 Calibration of thermoluminescent dosimeter.....	23
2.1.10 Determination of unknown radiation dose.....	24
2.1.11 Uncertainty in measurement.....	24

	<b>Page</b>
2.2 Related literatures.....	27
<b>CHAPTER 3 RESEARCH METHODOLOGY.....</b>	<b>30</b>
3.1 Research design.....	30
3.2 Research design model.....	30
3.3 Conceptual framework.....	31
3.4 Key word.....	31
3.5 Research questions.....	31
3.5.1 Primary question.....	31
3.5.2 Secondary question.....	31
3.6 Material.....	32
3.6.1 Thermoluminescent dosimeter, Lithium Fluoride.....	32
3.6.2 Thermoluminescent dosimeter system.....	32
3.6.3 Automatic TLD reader system 5500.....	34
3.6.4 Alderson RANDO phantom.....	35
3.6.5 Ionization chamber.....	35
3.6.6 Electrometer.....	37
3.6.7 Water phantom.....	38
3.6.8 Cobalt-60 teletherapy unit.....	38
3.6.9 Computed radiography system.....	39
3.7 Method.....	40
3.7.1 Calibration and quality control of x-ray equipment.....	40
3.7.2 Calibration of thermoluminescent dosimeters.....	41
3.7.3 Preparation of TLDs in RANDO phantom.....	43
3.7.4 Measurement of fetal doses with TLDs .....	44



	<b>Page</b>
3.7.5 Calculation of fetal doses by using parameters.....	45
3.7.6 Estimation of uncertainties between TLDs measurement and exposure parameter calculation.....	45
3.7.7 Comparison of radiation doses from TLDs measurement and exposure parameter calculation.....	48
3.7.8 Correlation of fetal dose between TLDs measurement and exposure parameter calculation.....	48
3.8 Measurement.....	48
3.9 Data collection.....	48
3.10 Data analysis.....	48
3.11 Benefit of the study.....	48
3.12 Ethic consideration.....	49
<b>CHAPTER 4 RESULTS.....</b>	<b>50</b>
4.1 Calibration and quality control of x-ray machine.....	50
4.2 Calculation of fetal dose with parameters.....	50
4.2.1 Parameters for calculation.....	50
4.2.2 Calculation of fetal doses from each examination...	51
4.3 Thermoluminescent dosimeters calibration.....	53
4.3.1 Sensitivity of TLD-100 chips.....	53
4.3.2 Linearity of TLD-100 chips.....	53
4.3.3 Energy response of TLD-100 chips.....	57
4.3.4 Minimum detectable dose.....	58
4.4 Measurement of fetal doses in RANDO phantom.....	58
4.4.1 Pelvic AP examination.....	58

	<b>Page</b>
4.4.2 Abdomen AP examination.....	59
4.4.3 Lumbo-sacral spine AP examination.....	59
4.4.4 Lumbo-sacral spine LAT examination.....	60
4.5 Estimation of uncertainties for TLDs measurement and exposure parameter calculation.....	60
4.6 Comparison of fetal doses from TLDs measurement and exposure parameter calculation.....	62
4.7 Correlation of fetal doses between TLDs measurement and exposure parameter calculation.....	74
<b>CHAPTER 5 CONCLUSION</b> .....	<b>76</b>
5.1 Discussion.....	76
5.2 Conclusion.....	79
5.3 Recommendation.....	79
<b>REFERENCES</b> .....	<b>80</b>
<b>APPENDICES</b> .....	<b>84</b>
Appendix: Quality control of x-ray equipment.....	85
<b>VITAE</b> .....	<b>95</b>

## LIST OF TABLES

<b>Table</b>	<b>Page</b>
2.1 Conceptus depth in anteverted uteri.....	6
2.2 Estimated doses to the uterus from diagnostic procedures.....	12
2.3 Continuing a pregnancy after radiation exposure as a function of gestation age and dose.....	13
2.4 Effects of radiation exposure on prenatal development.....	14
3.1 The exposure parameters used for each procedure.....	44
3.2 The uncertainty budget to estimate the relative expanded uncertainty of TLDs measurement.....	46
3.3 The uncertainty budget to estimate the relative expanded uncertainty of exposure parameter calculation.....	47
4.1 The output measurement of x-ray machine.....	50
4.2 The parameters for fetal doses calculation.....	50
4.3 The exposure parameters of each procedure for fetal doses calculation.....	51
4.4 The percentage depth dose for fetal doses calculation.....	51
4.5 The fetal doses from exposure parameter calculation of pelvic AP examination.....	51
4.6 The fetal doses from exposure parameter calculation of abdomen AP examination.....	52
4.7 The fetal doses from exposure parameter calculation of lumbo-sacral spine AP examination.....	52
4.8 The fetal doses from exposure parameter calculation of lumbo-sacral spine LAT examination.....	53
4.9 The energy response of TLD -100 chips in kilovoltage relative to Co-60 gamma rays at absorbed dose of 50 mGy.....	57
4.10 The minimum detectable dose.....	58
4.11 The fetal doses in RANDO phantom from TLDs measurement of pelvic AP examination.....	59

<b>Table</b>	<b>Page</b>
4.12 The fetal doses in RANDO phantom from TLDs measurement of abdomen AP examination.....	59
4.13 The fetal doses in RANDO phantom from TLDs measurement of lumbo-sacral spine AP examination.....	60
4.14 The fetal doses in RANDO phantom from TLDs measurement of lumbo-sacral spine LAT examination.....	60
4.15 The uncertainty budget to estimate the relative expanded uncertainty of TLDs measurement.....	61
4.16 The uncertainty budget to estimate the relative expanded uncertainty of exposure parameter calculation.....	61
4.17 The comparisons of fetal doses in term of the percentage normalized dose difference between TLDs measurement and parameter calculation for pelvic AP examination.....	62
4.18 The comparisons of fetal doses in term of the percentage normalized dose difference between TLDs measurement and parameter calculation for abdomen AP examination.....	65
4.17 The comparisons of fetal doses in term of the percentage normalized dose difference between TLDs measurement and parameter calculation for lumbo-sacral spine AP examination.....	68
4.18 The comparisons of fetal doses in term of the percentage normalized dose difference between TLDs measurement and parameter calculation for lumbo-sacral spine LAT examination.....	71
5.1 The fetal doses from another published works compared with this study....	78

## LIST OF FIGURES

<b>Figure</b>	<b>Page</b>
2.1 Incidence of death and of abnormalities at term following irradiation with 200R at various stages in the prenatal development of mice.....	5
2.2 Dosimetry in a water phantom.....	15
2.3 Schematic diagram showing apparatus for dose measurement using thermoluminescence.....	18
2.4 A simplified energy-level diagram to illustrate thermoluminescent process..	19
2.5 An example of glow curve of LiF (TLD-100) after phosphor has been annealed at 400 °C for 1 hour and read immediately after irradiation to 100R.....	20
2.6 An example of thermoluminescence versus absorbed dose curve for TLD-100 powder.....	21
2.7 Relation of half value layer (HVL) to effective energy.....	22
2.8 Theoretical sensitivity of the thermoluminescence phosphors: (1) CaSO <sub>4</sub> ; (2) CaF <sub>2</sub> ; (3) Al <sub>2</sub> O <sub>3</sub> ; (4) LiF; (5) CaCO <sub>3</sub> ; (6) SiO <sub>2</sub> ; and (7) Li <sub>2</sub> B <sub>4</sub> O <sub>7</sub> .....	23
3.1 The TLD chips, Lithium Fluoride (LiF) from Harshaw Chemical Company (Solon/Harshaw, USA). The TLD-100 chips (left) and the plastic tube for TLD-100 chips (right).....	32
3.2 The personal computer.....	32
3.3 The annealing oven manufactured by Harshaw Bicon.....	33
3.4 The Harshaw model 5500 automatic TLD reader.....	34
3.5 The RANDO phantom.....	35
3.6 Victoree® model 4000M+.....	36
3.7 The ionization chamber 0.6 cc type NE 2571.....	37
3.8 The Ionex Dosemaster type 2590A.....	37
3.9 The water phantom.....	38

<b>Figure</b>	<b>Page</b>
3.10 ELDORADO 78 cobalt-60 teletherapy machine.....	39
3.11 Toshiba x-ray machine model KXO-80G/DT-BTH/DST-100A.....	39
3.12 Beam quality of Toshiba x-ray machine model KXO-80G/DT-BTH/DST-100A.....	41
3.13 The setup of thermoluminescent dosimeter for linearity dose response.....	42
3.14 The location of TLDs in RANDO phantom.....	43
3.15 The pelvis slabs inserted with TLD chips were irradiated by Toshiba x-ray machine. The field size setting (left) and the set up of pelvic examination (right).....	44

## LIST OF ABBREVIATIONS

<b>Abbreviation</b>	<b>Terms</b>
AAPM	American Association of Physicists in Medicine
AEC	Automatic exposure control
$Al_2O_3$	Aluminum oxide
AP	Antero-posterior projection
BSF	Backscatter factor
BG	Background
$CaCO_3$	Calcium carbonate
$CaF_2$	Calcium fluoride
$CaSO_4$	Calcium sulphate
cc	Cubic centimeter
CF	The correction factor
cGy	Centigray
$^{60}Co$	Cobalt-60
CR	Computed radiography
CT	Computed tomography
$^{137}Cs$	Cesium-137
CsI	Cesium Iodide
$^{\circ}C$	Degree celcius
C/kg	Coulomb per kilogram
DAP	Dose area product
DR	Digital radiography
ECC	Element correction coefficient

<b>Abbreviation</b>	<b>Terms</b>
ESD	Entrance skin dose
FID	Focus to image plate distance
FSD	Focus to surface distance
Gd <sub>2</sub> O <sub>2</sub> S	Gadolinium di-oxysulfide
Gy	Gray
HVL	Half value layer
IAEA	International Atomic Energy Agency
ICRP	International Commission on Radiological Protection
ICRU	International Commission on Radiation Units and Measurements
Inv.	Inverse square correction factor
keV	Kiloelectron volt
k <sub>u</sub>	The radiation quality correction factor
kVp	Kilovoltage peak
k <sub>w</sub>	The kerma to water
LAT	Lateral projection
Li <sub>2</sub> B <sub>4</sub> O <sub>7</sub>	Lithium borate
LiF	Lithium fluoride
mA	Milliampere
mAs	Milliampere-second
MDD	Minimum detectable dose
MeV	Megaelectron volt
mGy	Milligray
mm	Millimeter



<b>Abbreviation</b>	<b>Terms</b>
mm Al	Millimeter aluminum
$M_u$	The meter reading
MV	Megavolt
mR	Milliroentgen
nC	Nanocoulomb
$N_{D,w}$	Absorbed dose to water calibration factor
NE	Nuclear Enterprise
$N_k$	Air kerma calibration factor of an ionizing chamber
$N_x$	Exposure calibration factor of an ionizing chamber
NRPB	National Radiological Protection Board
PACS	Picture Archiving and Communication System
PMT	Photomultiplier tube
PSL	Photostimulable luminescence
$P_u$	Factor to allow for of non-water equivalent of the ionization chamber, when in the use's beam
$Q_{ci}$	The correction charge integral
QC	Quality control
$Q_i$	The charge integral value
$r$	The correlation coefficient
RCF	The reader calibration factor
RSNA	Radiological Society of North America
SCD	Source to chamber distance
SD	Standard deviation
SID	Source to image distance

Abbreviation	Terms
SSDL	The secondary standard dosimetry laboratory
Sv	Sievert
TLD	The thermoluminescent dosimeter
TTP	The time temperature profile
CV	The coefficient of variation
W/e	The mean energy expended in air per ion pair formed and per electron charge
Z	The atomic number
$Z_{\text{eff}}$	The effective atomic number
$\rho$	The density
$\mu_{\text{en}}/\rho$	Mass energy absorption coefficient
$\mu_{\text{tr}}/\rho$	Mass energy transfer coefficient
$\mu\text{Gy}$	Microgray
$\mu\text{Sv}$	Microsievert

สถาบันวิทยบริการ  
จุฬาลงกรณ์มหาวิทยาลัย

# CHAPTER 1

## INTRODUCTION

### 1.1 Background and rationale

Thousands of pregnant women are exposed to ionizing radiation each year. Lack of knowledge is responsible for great anxiety and probably unnecessary termination of pregnancies. For most patients, radiation exposure is medically appropriate and the radiation risk is minimal [1].

The computed radiography (CR) system has many advantages over conventional radiography [2]. The advent of computed radiography the dose to patients is higher than screen-film radiography and overexposure is quite common [3]. The doses for computed radiography were higher than the doses for the other two modalities (conventional screen-film radiography and direct digital radiography) [4]. In the case of examinations involving the abdominal, lumbo-sacral spine and pelvis doses to the embryo may be considerably higher in comparison with extra-abdominal examinations. The women who underwent diagnostic x-ray procedures and were later discovered to have been pregnant at the time of radiological examination were increased. These pregnant patients who found in clinical practice were either accidentally or because of clinical urgency [5]. The computed radiography has an important role in diagnostic imaging, because of its ease of use and fast processing. However, many people found that the patient radiation dose is highly increased to support multi-resolution results [1]. So, it may cause some effects to the fetus in pregnant woman, especially in the first trimester, the new born baby may be in malformation situation causing the termination. So if the fetal dose in specific examination could be estimated, the physician would have a reasonable decision making. The published works purposed method to estimate the fetal dose of conventional radiography by calculating from many measurement parameters [2-5]. By this method, physician could know a result in a short time. However, the CR replaced the conventional radiography the accuracy of calculation dose should be confirmed.

In this study, the fetal dose in RANDO phantom irradiated by CR system for abdomen, pelvic and lumbo-sacral spine examinations were measured using TLDs and calculated using exposure parameters. The measured and calculated results were shown at the fetus site, the correlation were evaluated.

### 1.2 Research objectives

1.2.1 To measure the fetal dose with TLDs in RANDO phantom irradiated by computed radiography which simulated in the first trimester of pregnancy.

1.2.2. To study the correlation between the measured and calculated fetal dose in RANDO phantom.

# CHAPTER 2

## REVIEW OF RELATED LITERATURES

### 2.1 Theory

#### 2.1.1 Radiation effects in utero [6, 7, 8]

Developing organisms are highly dynamic systems that are characterized by rapid cell proliferation, migration, and differentiation. Thus, the developing embryo is extremely sensitive to ionizing radiation, as would be expected based on Bergonie and Tribondeau's laws of radiosensitivity. The response after exposure to ionizing radiation depends on a number of factors including (a) total dose, (b) dose rate, (c) radiation quality, and (d) the stage of development at the time of exposure. Together, these factors determine the type and extent of the damage that would be of concern after an exposure, among which are prenatal or neonatal death, congenital abnormalities, growth impairment, reduced intelligence, genetic aberrations, and an increase in risk of cancer.

##### 2.1.1.1 Radiation effects and gestation

The gestation period can be divided into three stages: a relatively short preimplantation stage, followed by an extended period of major organogenesis, and finally the fetal growth stage, during which differentiation is complete and growth mainly occurs. Each of these stages is characterized by different response to radiation exposure, owing principally to the relative radiosensitivities of the tissues at the time of exposure.

##### (a). Preimplantation

The preimplantation stage begins with the union of the sperm and egg and continues through day 9 in humans, when the zygote becomes embedded in the uterine wall. During this period, the two pronuclei fuse, cleave, and form the morula and blastula.

The conceptus (the terms embryo, fetus, unborn child, conceptus and others have been proposed for various stages of development of child) is extremely sensitive during the preimplantation stage and radiation damage can result in prenatal death. During this period the incidence of congenital abnormalities is low, although not completely absent. Embryos exhibit the so called all or nothing response, in which, if prenatal death dose not occur, the damaged cells are repaired or replaced to the extent that there are unlikely to be visible signs of abnormalities even though radiation may have killed several cells.

Several factors, including repair capability, lack of cellular differentiation, and the relatively hypoxic state of the embryo, are thought to contribute to its resistance to radiation induced abnormalities. During the first few divisions, the cells are undifferentiated and lack predetermination for a particular organ system. If radiation exposure were to kill some cells at this stage, the remaining cells could continue the embryonic development without gross malformations because

they are indeterminate. However, chromosomal damage at this point may be passed on and expressed at some later time. When cells are no longer indeterminate, loss of even a few cells may lead to anomalies, growth retardation, or prenatal death. The most sensitive times of exposure in humans are at 12 hours after conception, when the two pronuclei fuse to the one cell stage and again at 30 and 60 hours when the first two divisions occur.

Chromosomal aberrations from radiation exposure at the one cell stage could result in loss of a chromosome in subsequent cell divisions that would then be uniform throughout the embryo. Most chromosomal loss at this early stage is lethal. Loss of a sex chromosome in female embryos may produce Turner's syndrome.

The woman may not know she is pregnant during the preimplantation period, the time at which the conceptus is at greatest risk of lethal effects. Animal experiments have demonstrated an increase in the spontaneous abortion rate after doses as low as 50 to 100 mGy (5 to 10 rad) delivered during the preimplantation period. After implantation, doses in excess of 250 mGy (25 rad) are required to induce prenatal death. The spontaneous abortion rate has been reported to be between 30% and 50%.

#### (b). Organogenesis

Embryonic malformations occur more frequently during the period of major organogenesis (2<sup>nd</sup> to 8<sup>th</sup> week after conception). The initial differentiation of cells to form certain organ systems typically occurs on a specific gestational day. For example, neuroblasts (stem cells of the CNS) appear on the 18<sup>th</sup> gestational day, the forebrain and eyes begin to form on day 20, and primitive germ cells are evident on day 21. Each organ system is not at equal risk during the entire period of major organogenesis. In general, the greatest probability of a malformation in a specific organ system (the so called critical period) exists when the radiation exposure is received during the period of peak differentiation of that system.

The response of each organ to the induction of radiation induced malformation is unique. Such factors as gestational age; radiation quantity, quality, and dose rate; oxygen tension; the cell type undergoing differentiation and its relationship to surrounding tissues; and other factors influence the outcome.

#### (c). Fetal growth stage

The fetal growth stage in humans begins after the end of major organogenesis (day 45) and continues until term. During this period the incidence of radiation-induced prenatal death and congenital anomalies is, for the most part, negligible. Anomalies of the nervous system and sense organs are the primary radiation-induced abnormalities observed during this period, which coincides with their relative growth and development. Much of the damage induced at the fetal growth stage may not be manifested until later in life as behavioral alterations or reduced intelligence (e.g., IQ).

### 2.1.1.2 Effect on the conceptus

Some possible consequences of ionizing radiations for conceptuses and their progeny are:

- If only a few cells are involved, immunologic mechanisms may recognize the aberrant ones, destroy them, and replace them with healthy cells.
- If the cells are not replaced, growth impairment of organs may result without function damage. The child might not achieve his/her full growth potential, but is otherwise normal.
- Damage to the cells may interrupt some crucial stage of development from which recovery is not possible, resulting in a deformity. This is most critical during incipient organ development when damage to a few cells can disrupt and permanently affect later development. In the vast majority of cases, the likelihood of a diagnostic examination inducing such an effect is extremely small or nonexistent, the likelihood depends on many factors, the two most important of which are gestation age and dose.
- Some somatic defects may occur that are too subtle to be noticed.
- Genetic changes in a cell may cause development of a neoplasm, which will remain unexpressed for many years.
- Heritable changes in the reproductive organs may occur that could, theoretically, affect the progeny of the conceptus but not the conceptus itself.

Radiation included effects on a conceptus are frequently separated into two categories: stochastic and deterministic. Stochastic effects are assumed to be monoclonal in origin, i.e., changes in a single cell, most importantly in the genome, maybe sufficient to cause the effect. For stochastic effects, only the probability that the effect will be induced increase with dose, not the severity of the effect. The examples of such effects include neoplasm and heritable effect. For deterministic effect, many cells must be adversely affected. This will not occur unless the exposure to the radiation is above a certain threshold dose. For deterministic effects, the probability of including the effect and the severity of the effect increase only after the threshold dose is exceeded. An example of a deterministic effect is malfunction. Therefore, the likelihood of including an effect will always depend on the dose delivered, but how the likelihood increase with increasing dose depends on the type of effect and several other factors.

The reader should be aware that these concepts of radiation effects are used to describe effect as scientists currently understand them. It may be possible that effect exist that do not fit nicely into either of these two categories. For example, it may be possible that some cancers will be more aggressive and more intractable to treatment as dose increases; i.e., the severity of the cancer might increase with dose. Other variation of effect that might not fit neatly into this categorization might exist, but none are known at this time.

The sensitivity of a conceptus to radiation depends on the degree of mitotic activity of the cells, the magnitude of and the delivery rate of the radiation, and the maturity of the developing offspring.

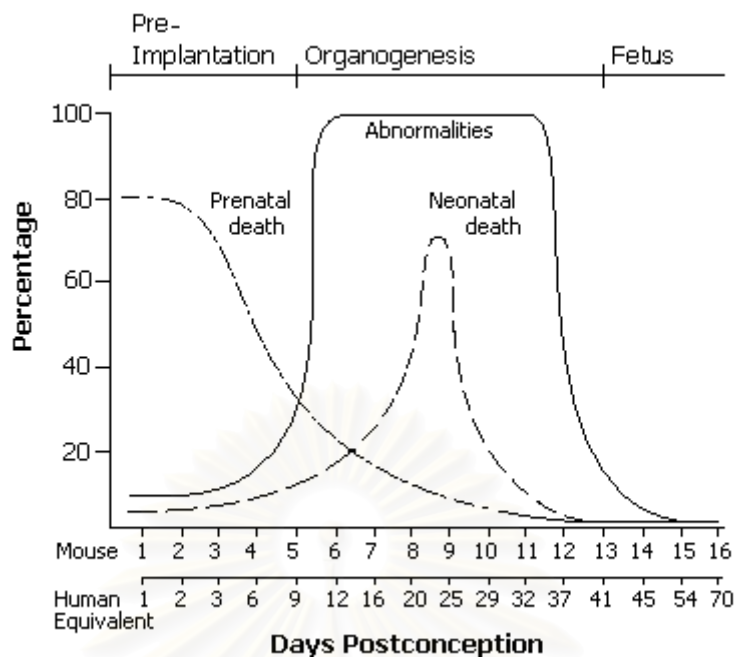


**Figure 2.1** Incidence of death and of abnormalities at term following irradiation with 200R at various stages in the prenatal development of mice. The lower scale correlates conception age for humans. (Russel LB, Russel WL. An analysis of the changing radiation response of the developing mouse embryo. *J Cell Physiol [Suppl 1]* 43:103, 1954. [Reprinted by permission of Wiley-Liss, Inc., a subsidiary of John Wiley & Sons, Inc. © 1954 by Wiley-Liss, Inc.]

Russell and Russell (1954), Brent and Gorson (1972), and Rugh (1964) demonstrated a correlation between conception age and radiation-induced malfunctions in mice and rates (Figure 2.1). These experiments were carried out at dose levels considerably higher than those used in diagnostic radiology. They were designed to induce effects so that they could be correlated with gestation time. Resorption usually resulted when the radiation was delivered prior to implantation. Prenatal death in the rodents could be induced at these doses when delivered during organogenesis, but with decreasing incidence as development progressed. The critical period for induced malfunctions occurred during organogenesis. Malfunction was much reduced when the radiation was delivered during the fetal stage (after organogenesis). Rugh (1964) demonstrated that specific radiation-induced malfunctions are correlated with a critical period of prenatal development of that organ.

#### 2.1.1.2 Depth of the conceptus

Conceptus dose is dependent on conceptus depth because tissues between the surface of the patient and the pregnant uterus attenuate the x-rays beam. The common assumption that the uterus lies half the AP distance inside the pelvis is not correct. Regozzino and coworkers (1986) demonstrated in 16 randomly selected patients that the conceptus depth from the anterior surface in early pregnancy is about 30% of the AP thickness. Significant differences exist between the central and actual depth (Table 2.1). Furthermore, the uterus is not always in a forward position; it has a

retroverted orientation in about 20% of all normal women (Parsons and Sommers, 1978)

**Table 2.1** Conceptus depth in anteverted uteri.

Patient AP thickness	Central depth	Actual conceptus depth from anterior surface	Reference
19 cm <sup>a</sup>	9 cm <sup>a</sup>	6 cm <sup>a</sup>	Regozzino & coworkers (1986)
26 cm	13 cm	6 cm	Wagner & coworkers (1983)
20 cm	10 cm	3.8 cm (Partially full bladder) 6.7 cm (Full bladder)	Regozzino & coworkers (1981)

<sup>a</sup> Average value of 16 early pregnancies.

The importance of this is illustrated by comparing result for conceptus dose from data of Gray and associates (1981) and Rosenstein (1976a, 1976b). Gray and associates measured uterus dose in a simulated human and assumed the uterus to be 12.0 cm from the anterior surface. Rosenstein calculated conceptus dose using a mathematical model assuming the depth to be 8.0 cm. For similar lower abdominal AP radiographic conditions, the uterine dose per entrance exposure in the two cases differed by a factor of 2.0. This disparity is explained in part by using the data of Harrison (1981).

#### 2.1.1.3 Risk related to gestational age

Early gestation/first trimester, at this point, the rate of fetal growth is very rapid and the fetus, as an organism, is at its most radiation sensitive stage if fetal demise is taken as an end point. The incidence of fetal wastage consequential to radiation exposure at this stage of gestation is not know, since (a) many women were never aware they were pregnant at the time of the exposure or miscarriage, and (b) the background rate of miscarriage is believed to be high (25 – 50 percent of conceptions).

Second trimester, during this period, the overall growth rate of the fetus has slowed. However, the major organ systems are beginning to differentiate. From a standpoint of future development, the fetus is in its most sensitive stage. The incidence of gross congenital malfunctions and mental retardation are dose related and appear to have thresholds; i.e. dose below which the incidence above background is not elevated.

Third trimester, irradiation during this period may deplete cell populations at very high doses (over 50 rem), but will not result in gross organ malfunction.

#### 2.1.1.4 Risk related to radiation dose

The risk of deleterious effects increases with increasing dose. The nature of this dependence, i.e. the shapes of the dose-response curves for humans in the low-dose range (under 50 rem), is controversial. For some prenatal irradiation effect, there is epidemiological basis for the existence of threshold doses. For other,



such as childhood cancer induction, the existence of a threshold is not clear cut. Despite these uncertainties in the dose effect relationship, some broad generalizations based on fetal dose ranges may be made.

Fetal dose less than 1,000 millirem, there is no evidence supporting the increased incidence of any deleterious developmental effect on the fetus at diagnostic doses within this range.

Fetal dose between 1,000 millirem and 10,000 millirem, the additional risk of gross congenital malfunctions, mental retardation, intrauterine growth retardation and childhood cancer is believed to be low compared to the baseline risk. However, the lower limits (in term of statistical confidence interval around mean) for threshold doses for some studies, especially those related to cancer induction, fall within this range.

Fetal dose exceed than 10,000 millirem, the lower limits (in term of statistical confidence interval) for threshold doses for effects such as mental retardation and diminished IQ and school performance fall within this range. Overall, exposure at levels exceeding 10 rem could be expected to result in a dose related increased risk for deleterious effect. For example, the lower limit (95% confidence interval) for threshold for mental retardation is about 15 rem, which an expectation value of about 30 rem.

#### 2.1.1.5 Counseling the pregnant patient exposed to ionizing radiation

Due to the complexity of the issues surrounding fetal irradiation, there is no standard or predetermined advice that can be given to the expectant patient. However, it is possible to assist the patient in assessing the implications of the exposure if a systematic evaluation of the risk is performed. According to Dr. Robert Brent, the following parameters should be considered in the evaluation.

- Gestational age at the time of exposure
- Menstrual history
- History of previous pregnancies, including a history of congenital malfunctions
- Other potentially harmful environmental factors (malnutrition, smoking, alcohol / drug, etc)
- Maternal / paternal age
- Calculation of fetal exposure using dose reconstruction techniques
- Attitude of the mother toward the pregnancy

In any event, it is important not to defer medically necessary studies with anticipated fetal doses of less than 5,000 millirem based solely on a concern for causing adverse fetal effects.

### 2.1.2 Ionizing radiations [6, 8]

#### 2.1.2.1 Exposure and air kerma

X-ray and gamma rays cause ionization as they pass through air. The number of ions created is dependent on the number and energy of x-ray or gamma rays passing through it. For diagnostic energies, exposure is the amount of ionic

charge created per unit mass of air by x or gamma radiation. In SI units, exposure is measured as coulombs per kilogram of air. Another common unit of exposure is the roentgen (R). One roentgen of exposure produces 0.26 millicoulombs per kilogram of air. Such an exposure produces over 2 billion ion pairs per cubic centimeter of exposed air at standard temperature and pressure. Diagnostic exposures are usually measured in mC/kg of air or in milliroentgens.

Kerma is the kinetic energy released in matter by an ionizing radiation. Air kerma (K) is the kerma in air and is directly related to exposure.

$$K_{air} (mGy) = 3.396 \times 10^4 X (C / kg) \quad \dots (2.1)$$

$$K_{air} (mGy) = 8.76 X (R) \quad \dots (2.2)$$

Note that the units of kerma, mGy, are the same as the units of absorbed dose, as discussed later. Air kerma is a quantity that is less frequently used in the United States than in other countries.

#### 2.1.2.2 Absorbed dose

X-rays ionize atoms and molecules in human tissues through the deposition of energy. This ionization is the first step in a series of events that may lead to a biologic effect. Absorbed dose is a measure of energy deposited per unit mass and provides a means to gauge the potential for biologic effects. Absorbed dose is measured in units of gray (Gy) or milligray (mGy). One gray is equivalent to an energy deposition of 1 joule per kilogram (J/kg) of tissue. The outdated unit of absorbed dose is the rad, which equals 0.01 Gy. Absorbed dose rate is the amount of energy deposited in a given period of time and is typically measured in units of milligrays per minutes or hours.

Entrance skin dose (ESD) is a measure of the radiation dose absorbed by the skin where the x-ray beam enters the patient. ESD can be measured directly with thermoluminescent dosimeters or computed from measurements made with an ionization chamber. Kerma (kinetic energy released in matter) is defined as the amount of energy transferred from the incident x-rays to charged particles per unit mass in the medium of interest. Kerma includes any energy subsequently given up as photons (ie, bremsstrahlung), but excludes any further energy transfer to other charged particles. Exposure, a somewhat outdated concept, represents the amount of energy initially transferred from the incident x-ray to charged particles per unit mass of air. Exposure excludes any further energy loss by the charged particles that are subsequently given up as photons or to other charged particles.

The unit of air kerma is the same as the unit for absorbed dose (ie, gray or milligray), whereas the unit of exposure is the roentgen (R). Tissue dose is the product of kerma or exposure and a conversion factor known as the f-factor. For the range of energies encountered in diagnostic radiology, the f-factor is approximately 1.06 for air kerma and 0.93 for exposure. The kerma value retains its units, whereas exposure is converted into rads. To determine a true absorbed dose from the factors just described also requires inclusion of the backscatter, which is the factor by which the radiation dose is increased by radiation scattered back from the body. Use of the backscatter factor in calculations of ESD accounts for the radiation scattered back to

the surface of the patient. Backscatter factors depend partially on the energy and field size of the x-ray beam, but they are typically in the range of 1.3-1.4.

Organ dose refers to the radiation absorbed dose delivered to the organs of a patient during a radiologic examination. Specific organs of interest include, but are not limited to, active bone marrow, thyroid, breasts, gonads, and the lens of the eye. Dose to the embryo or fetus may also occur during diagnostic procedures, and knowledge of conceptus dose is critical to responsible patient management.

### 2.1.2.3 The energy and number of x-ray

Since the energy of x-rays determine how easily they penetrate the patient, it is important to understand how various radiographic factors influence x-ray energy.

X-rays are produced inside a glass vacuum tube that houses a hot cathode and an anode. When high voltage is applied across the anode and cathode, electrons are stripped from the filament of the cathode and accelerated toward the anode. These electrons achieve high speeds and, upon collision with the anode, x-rays with a wide range of energies are produced. The spectrum of x-rays energies and temporal characteristics of the applied kilovoltage, as well as by the materials placed between the anode and the patient.

The peak kilovoltage (kVp) across the x-rays tube generally varies from 60 kVp to 150 kVp for diagnostic x-rays. For mammography, lower kVp techniques are used, usually around 25 kVp. Waveform refers to the time dependent form in which the voltage is supplied to the x-rays tube. This may be a single phase waveform, three-phase waveform or mid- or high-frequency waveforms. Single phase is the type used in homes, and three phase and high frequency waveforms are commonly employed in industry. Each produce x-rays with slightly different x-rays energy spectra.

The materials between the anode and the patient are referred to as the filtration and include the glass of the x-rays tube and additional material, usually sheets of aluminum. Other materials may also be present. The total filtration is normally specified as an aluminum equivalent, which is the amount of aluminum that, when placed in front of the x-rays, would reduce their intensity to the same level as do the actual materials present. The equivalent quality normally ranges from 0.5 mm to 4.5 mm of aluminum. Calculating conceptus dose at the wrong kVp, waveform, or filtration contributes to the inaccuracy of calculation.

The intensity of x-rays used to image the patient is determined by kVp, waveform, and filtration as well as other important factors. These other factors include the distance of the patient from the x-rays source, the sensitivity of the image-recording device (usually film), the patient's size, and the materials placed between the patient and the film, such as the table and grid (a device to help improve contrast on the radiograph).

X-rays intensity varies inversely with the square of the distance from the source. This is due to the fact that x-rays fan out in an expanding sphere as they move away from their production point. This phenomenon is referred to as the inverse-square law.

#### 2.1.2.4 Factors affecting dose in digital radiography

Digital radiography is divided into the categories of computed radiography and direct radiography. Computed radiography refers to imaging systems that use photostimulable phosphor (PSP) plates, which are placed in a cassette similar to screen-film combinations, to capture the latent image. The user inserts the plate into a processor, where it is read, or processed, by a laser that scans the entire surface area and produces an image that may be displayed on a monitor for viewing. Direct radiography refers to imaging systems in which the x-ray beam impinges directly on an image receptor that translates the information into an image, which is then displayed on a monitor without an intermediate step by the operator.

Patient dose in computed radiography is affected by all the factors listed for conventional radiography, as well as other considerations. Typical computed radiography systems operate at a speed equivalent to an approximately 200 speed screen-film combination. However, these systems permit a much wider range of exposures for producing acceptable diagnostic images than do conventional screen-film systems. This wide range, or latitude, may allow the operator to use lower peak kilovoltages and tube currents, since the images can be manipulated to adjust contrast and brightness after the image data have been obtained (ie, postprocessing). However, if very low kilovoltages and tube currents are used, substantial levels of noise can be introduced into the image. Overexposures in the traditional film-processing sense are not really possible. Excessively high kilovoltage and tube currents should not be routinely used just to avoid retakes due to possible noise.

#### 2.1.3 Computed radiography [7]

Computed radiography (CR) is a marketing term for photostimulable phosphor detector (PSP) system. Phosphors used in screen-film radiography, such as  $Gd_2O_2S$  emit light promptly (virtually instantaneously) when struck by an x-ray beam. When x-rays are absorbed by photostimulable phosphors, some light is also promptly emitted, but much of the absorbed x-ray energy is trapped in the PSP screen and can be read out later. For this reason, PSP screens are also called storage phosphors or image plates. CR was introduced in the 1970s, saw increasing use in the late 1980s, and was in wide use at the turn of the century as many departments installed PACS, often in concert with the development of the electronic medical record.

CR imaging plates are made of BaFBr and BaFI. Because of this mixture, the material is often just called barium fluorohalide. A CR plate is a flexible screen that is enclosed in cassette similar to a screen-film cassette. One imaging plate is used for each exposure. The imaging plate is exposed in a procedure identical to screen-film radiography, and the CR cassette is then brought to a CR reader unit. The cassette is placed in the readout unit, and several processing steps then take place:

1. The cassette is moved into the reader unit and the imaging plate is mechanically removed from the cassette.
2. The imaging plate is translated across a moving stage and scanned by a laser beam.
3. The laser light stimulates the emission of trapped energy in the imaging plate, and visible light is released from the plate.

4. The light released from the plate is collected by a fiber optic light guide and strikes a photomultiplier tube (PMT), where it produces an electronic signal.
5. The electronic signal is digitized and stored.
6. The plate is then exposed to bright white light to erase any residual trapped energy.
7. The imaging plate is then returned to the cassette and is ready for reuse.

The digital image that is generated by the CR reader is stored temporarily on a local hard disk. Many CR systems are joined (“docked”) directly to laser printers that make film hard copies of the digital images. CR systems often serve as entry points into a PACS, and in such cases the digital radiographic image is sent to the PACS system for interpretation by the radiologist and long-term archiving.

#### 2.1.4 In utero exposure in diagnostic radiology [8]

Whenever a patient of childbearing age needs a radiologic procedure, certain patient safety measures should be taken. If the patient is or could reasonably be pregnant, the examination should not be performed unless the need is great. If the examination must be performed, the following precautions should be used: (a) the patient’s abdomen should be shielded if the type of examination permits, (b) fluoroscopy time should be limited to an absolute minimum, and (c) the number of radiographs or scans should be reduced to as few as necessary.

Once an exposure of a pregnant patient has taken place, fetal dose can be estimated to determine what, if any, additional risk may be present for the developing fetus and if any future action should be taken.

#### 2.1.5 Factors affecting fetal dose in diagnostic radiology [8]

**Direct (inside field of view) exposure-** If a fetus is located within the field of view of a particular examination, such as studies of the abdomen, pelvis, and lumbar spine; it is exposed directly to primary beam radiation. This situation typically results in the highest fetal doses. In these instances, a shield is usually of limited value because it cannot cover the area being imaged.

**Indirect (outside field of view) exposure-** When a fetus is positioned outside the field of view, such as during examinations of the skull and extremities, the bulk of the exposure received is from indirect scattered radiation from the maternal tissues. This situation usually results in lower fetal doses than incurred during a direct exposure. The actual dose varies depending on the distance between the fetus and the primary x-ray field. Unfortunately, a shield has limited value in this case as well because most of the fetal dose results from internal scatter in the mother.

#### 2.1.6 Fetal dose estimation in diagnostic radiology [8]

To provide a reasonable estimation of fetal dose, one must know the output intensity (measured in exposure or air kerma) of the x-ray equipment for radiographic exposure and entrance exposure (or air kerma rate) for fluoroscopic exposures, along with the conditions of the examination. The half-value layer is also used to determine beam penetrability. Information about the conditions of the procedure includes the

location and number of views taken and the radiographic exposure factors. For fluoroscopic procedures, the beam-on time and the number of digital or cassette spot images taken, with the related exposure factors, are needed. The required information about the patient includes the fetal age at the time of exposure, the patient's size or thickness, and the depth of the fetus. It is also important to know the orientation of the patient in relation to the x-ray tube.

**Direct (inside field of view) exposure-** Once the facts about the examination are known, calculations are performed by using measured values of exposure or air kerma, along with the specific technique factors used, to obtain a maternal entrance exposure. This entrance exposure is then used to calculate the dose at the depth of the fetus by using either published depth-dose or tissue-air ratio tables. This procedure is applicable to both radiographic and fluoroscopic exposures.

**Indirect (outside field of view) exposure-** The calculation method used for indirect exposures differs somewhat from that employed for direct exposures. The maternal entrance exposure is determined on the basis of the same information, and then published scatter factors are applied to account for the location of the fetus relative to the location of the examination. The distance between the fetus and the area being imaged is significant factor affecting fetal dose for an indirect exposure.

**Early pregnancy-** Report 54 from the National Council on Radiation Protection and Measurements (NCRP) (Table 2) is particularly useful for calculating fetal doses for many common views for an exposure during early pregnancy. These data include fetal dose from both direct and indirect exposures. The adjustments for depth and distance from the x-ray field are already incorporated in the conversion factors. These factors are based on half-value layer and convert directly from maternal entrance exposure to fetal dose. However, use of this method is limited to average-sized women whose exposure took place early in pregnancy.

**Table 2.2** Estimated doses to the uterus from diagnostic procedures

Examinations	Absorbed dose	
	mrad	mGy
Upper gastrointestinal series	100	1
Cholecystography	100	1
Lumbar spine radiography	400	4
Pelvic radiography	200	2
Hip and femur radiography	300	3
Retrograde pyelography	600	6
Barium enema study	1000	10
Abdominal (KUB) radiography	250	2.5
Hysterosalpingography	1000	10
CT		
Head	~0	~0
Chest	16	16
Abdomen	3000	30

Some procedures have relatively low maternal exposures and are located at sufficient distance from the fetus that they result in very little, sometimes immeasurable, fetal exposure. Skull and other head examinations; cervical spine, chest and extremity examinations; and mammography fall into this category. Table

2.2 provides estimated doses to the uterus from typical diagnostic procedures. However, any procedure that incorporates fluoroscopy can vary greatly from these values.

In 1977, NCRP Report 54 recommended: “The risk [of abnormality] is considered to be negligible at 5 rad (50 mGy) or less when compared to other risks of pregnancy, and the risk of malformations is substantially increased above control levels only at doses above 15 rad (150 mGy). Therefore exposure of the fetus to radiation arising from diagnostic procedures would very rarely be cause by itself, for terminating a pregnancy”. Table 2.3 presents recommendations for continuing a pregnancy after radiation exposure as a function of gestational age and dose.

**Table 2.3** Continuing a pregnancy after radiation exposure as a function of gestational age and dose

Gestational age	Fetal absorbed dose		
	<5 rad (<50 mGy)	5-15 rad (50-150 mGy)	>15 rad (>150 mGy)
<14 d (<2 wk)	Recommended	Recommended	Recommended
14-56 d (2-8 wk)	Recommended	Maybe consider termination (in presence of other severe risks)	Maybe consider termination (in presence of other risks)
57-105 d (8-15 wk)	Recommended	Maybe consider termination (in presence of other risks)	Higher risk conditions exist, but termination is not necessarily recommended
>105 days (15 wk to term)	Recommended	Recommended	Recommended

When a patient undergoes diagnostic x-ray procedures and subsequently finds that she is pregnant, the immediate concern is about abnormalities in the developing fetus. Animal data suggest that doses of 5-50 rad (50-100 mGy) received before embryonic implantation may result in prenatal death. Small head size (microcephaly) has been the primary anomaly observed in children of survivors of the nuclear bombing of Hiroshima and Nagasaki, who sustained in utero radiation exposure. The most sensitive period for this effect is 2-15 weeks after conception. In fetuses who receive in utero radiation exposure during the latter half of this period (ie, at 8-15 weeks), severe mental retardation and intellectual deficits are also of concern at doses as low as 10 rad (100 mGy). However, the doses received during radiologic procedures are typically orders of magnitude lower than those delivered to experimental rats and mice and nuclear bombing survivors. Table 2.4 presents the effects of prenatal exposure as a function of gestational age.

Radiation-induced childhood malignancy caused by in utero radiation exposure is also a concern. Data suggest that a fetus exposed in utero to 1 rad (10 mGy) during the 1<sup>st</sup> trimester would be 3.5 times more likely to develop childhood

cancer. In the unexposed population, the frequency of childhood cancer is one in 1500 or 0.07%. Because the natural frequency is so low, 3.5 times that value is still quite low ( $3.5 \times 0.07\% = 0.25\%$ ), which leaves a high probability of 99.75% that the child exposed in utero will not develop childhood cancer. However, there is substantial uncertainty and a fair amount of controversy surrounding risk factors such as these. Other publications contain much more information on this subject matter.

**Table 2.4** Effects of radiation exposure on prenatal development

Gestational stage	Days after conception	Fetal dose		Observed effect
		rad	mGy	
Preimplantation	0-14	5-10	50-100	Animal data suggest possibility of prenatal death
Major organogenesis	8-56	20-25	200-250	Animal and NBS data suggest that this is the most sensitive stage for growth retardation
	14-105			NBS data indicate small head size; those exposed before 8 wk did not display any intellectual deficit even with small head; most sensitive time for induction of childhood cancer
Rapid neuron development and migration	56-105	>10	>100	Small head size, seizures, decline in IQ points: 25 points/100 rad (1 Gy)
After organogenesis and rapid neuron development	105 to term	>10	>100	Associated with increased frequency of childhood cancer
		>50	>500	Severe mental retardation observed at 16-25 wk

When used under properly controlled conditions, radiation is a safe and indispensable tool for medical diagnoses. Proper radiation safety management should ensure that practitioners are knowledgeable about typical patient doses that are imparted in each type of radiologic examination and about the factors that affect these doses. By understanding the factors that affect patient doses, practitioners can help keep doses as low as possible while still creating diagnostic quality images.

### 2.1.7 Absorbed dose calibration [9]

#### 2.1.7.1 Medium energy x-rays: 100 kVp to 300 kVp

The primary standard dosimetry laboratory (PSDL) generally has air kerma and exposure standards for several x-ray energy regions. Therefore it is possible at the second standard dosimetry laboratory (SSDL) to transfer calibrations



to the user's chamber in term of exposure  $N_x (=X_c/M_c)$  and air kerma  $N_k (=k_{air,c}/M_c)$ . The relationship between these two calibration factors is:

$$N_k = N_x \frac{W}{e} \frac{1}{(1-g)} \quad \dots (2.3)$$

The method for the determination of absorbed dose in a water phantom using an exposure or air kerma calibrated ionization chamber will differ somewhat for medium energy x-rays from that at high energy radiation. The main reason is that none of the electrons generated in the water phantom will reach the air cavity. (A 200 keV electron will have a maximum range in graphite less than 0.3 mm, i.e. less than the thickness of most mainly chamber walls.) Electrons producing ionization inside the air cavity are therefore mainly generated in the chamber walls. (A few electrons are also generated in the air of the cavity.)

$$K_{air} = M_u N_k k_u \quad \dots (2.4)$$

The absorbed dose is to be determined by the user in uniform water phantom at the point P (Figure 2.2). An ionization chamber is placed with its center P' at the point. A measurement is carried out giving the meter reading ( $M_u$ ). The air kerma is obtained at a point P' in the center of air cavity inside the water phantom as the chamber is calibrated to indicate the air kerma free in air, i.e. as if the chamber was not present. This means that we obtain the air kerma at the center (P'') of an air cavity of a size defined by the outer wall surfaces. Correction factors for attenuation in the chamber walls and non-air equivalence of the walls are thus already included in the calibration factor  $N_k$ . The radiation quality correction factor ( $k_u$ ) is required because the ratio  $K_{air}/M_u$  may be sensitive to the difference in spectral distribution of the radiation field used for the calibration free in air and that in the phantom at the position of the detector. For most practical situation  $k_u$  can be taken as unity, as it is recommended to use reference instruments for which the change in response (i.e. meter reading to air kerma) with energy is small (less than  $\pm 2\%$  in the range of half value layers from 2 mm Al to 3 mm Cu, i.e. from approximately 70 kVp to 250 kVp x-ray tube potential).

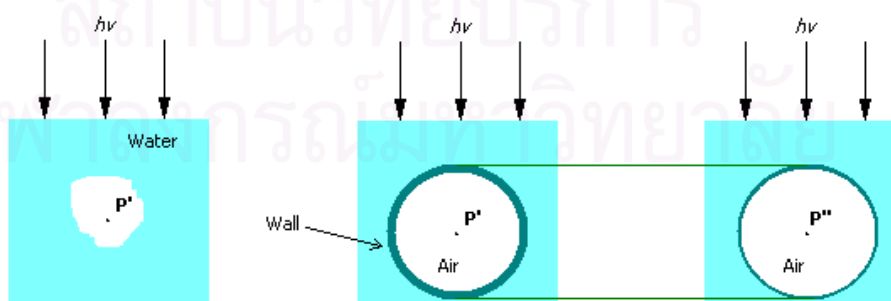


**Figure 2.2** Dosimetry in a water phantom

The water kerma is then obtained from

$$\frac{K_w}{K_{air}} = \left( \frac{\overline{\mu_{tr}}}{\rho} \right)_{w,air} \quad \dots (2.5)$$

For conventional x-ray the energy transfer to bremsstrahlung from generated electrons is almost negligible, i.e.  $g = 0$  and therefore  $(\mu_{tr} / \rho) = (\mu_{en} / \rho)$ , and furthermore  $K_w \approx D_w$ . Equation 2.5 and 2.6 give

$$D_w = M_u N_k k_u \left( \frac{\overline{\mu_{en}}}{\rho} \right)_{w,air} p_u \quad \dots (2.6)$$

The perturbation correction factor ( $p_u$ ) is here introduced explicitly because the equation without this factor would give the absorbed dose to small mass of water at the center P'' of the cavity. In the formalism recommended by ICRU in its Report 23 a 'displacement correction' incorporated in the conversion coefficient (F) but in the medium energy x-ray region no detailed information was available at the time. The perturbation correction factor ( $p_u$ ) corrects for the replacement of water by air and the chamber wall material. The values of perturbation correction factor ( $p_u$ ) derived from measurement of absorbed dose in the phantom by means of an extrapolation chamber and by means of thimble ionization chambers calibrated to indicated air kerma. Monte Carlo calculations by Schneider and Grosswendt support the values. Recent calorimeter work leads to similar result, suggesting that much previous and present dosimetry with medium energy x-rays in phantom is in error. Therefore, use of the formalism described here may produce deviations from the results obtained by produces neglecting perturbation correction. Absorbed dose values derived by the present formalism will therefore be a few percent higher in the upper energy range with a maximum of up to about 10% at 100 kVp.

#### 2.1.7.2 Low energy x-rays: 10 kVp to 100 kVp

The main dosimetric task in this photon energy range is the determination of the absorbed dose at the surface of a phantom. The determination, using a plane-parallel chamber, can either be based on a calibration at the surface of a phantom, method (a), or (when the former method is not available) on a calibration carried out free in air, method (b).

(a). Primary standards based on extrapolation ionization chamber techniques have been established recently. They allow direct calibration of the user's ionization chamber indicating absorbed dose to water at the surface of a water phantom.

As the photon fluence decreases very rapidly within the first few millimeter of depth in the phantom, only plane-parallel ionization chambers with small electrode distances and very thin entrance foils are suitable. These design features do not allow the user of the chamber inside a water phantom and therefore a solid phantom must be used. The calibration factor  $N_{D,w}$  is defined as

$$D_w = M_u N_{D,w} \quad \dots (2.7)$$

Where  $D_w$  is the water absorbed dose at the surface of a water phantom as measured with a primary standard, and  $M_u$  is the reading of the instrument placed at the surface of a solid phantom, at the same distance from source. It should be noted that an ionization chamber calibrated free in air should not be used on the surface of a phantom unless a correction factor which takes into account the scattering contribution from phantom is known and applied.

(b). The chamber may be calibrated in terms of air kerma free in air. A calibration factor ( $N_k$ ) is then available. No extra phantom is used for the measurement but the ionization chamber may be embedded in some material which then has to be regarded as part of the chamber. The inner surface of the entrance foil is the effective point of measurement. This is brought to reference point. The absorbed dose to water at that reference point at the surface of phantom in the absence of the ionization chamber is the given by

$$D_w = M_u N_k B k_u \left( \frac{\overline{\mu_{en}}}{\rho} \right)_{w,air} \quad \dots (2.8)$$

Where, B represents for the reference field size. The term  $(\overline{\mu_{en}} / \rho)_{w,air}$  is the ratio of the average mass absorption coefficient of water to that of air averaged over the spectral energy fluence distribution at the surface of the phantom. Values of this ration as a function of the beam quality expressed as half value thickness. The factor  $k_u$  corrects for the difference in spectral distribution of the radiation field used for the calculation and that at surface of the phantom. For most practical situations this factor should be very close to unity.

#### 2.1.8 Thermoluminescent dosimetry (TLD) [10, 11]

In recent years many applications of thermoluminescent dosimeter have been reported in the literature, and many applications have gone unreported. There are hundreds of thermoluminescent dosimeter readers in operation in various laboratories around the world.

Many of dosimetry problems arising in radiation dosimetry can be resolved by using thermoluminescent dosimeter. The small size, good energy dependence, good sensitivity and large useful dose range of thermoluminescent dosimeter are key advantages, as the direct measurement of dose is possible under conditions in which other forms of dosimetry are not practical; measurement of the dose from the primary beam during fluoroscopy is convenient since the dosimeter do not interfere with the study.

There are several solid state systems available for the dosimetry of ionizing radiation. However, none of the system provider absolute measurement-each needs calibration in a known radiation field before it can be used for the determination of absorbed dose.

There are two types of solid state dosimeters: (a) integrating type dosimeters (thermoluminescent crystal, radiophotoluminescent glasses, optical density type dosimeters such as glass and film), and (b) electrical conductivity dosimeters (semiconductor junction detectors, induced conductivity in insulating materials). Of these, the most widely used systems for the measurement of absorbed dose are the thermoluminescent dosimeter, diode and film, which are described.

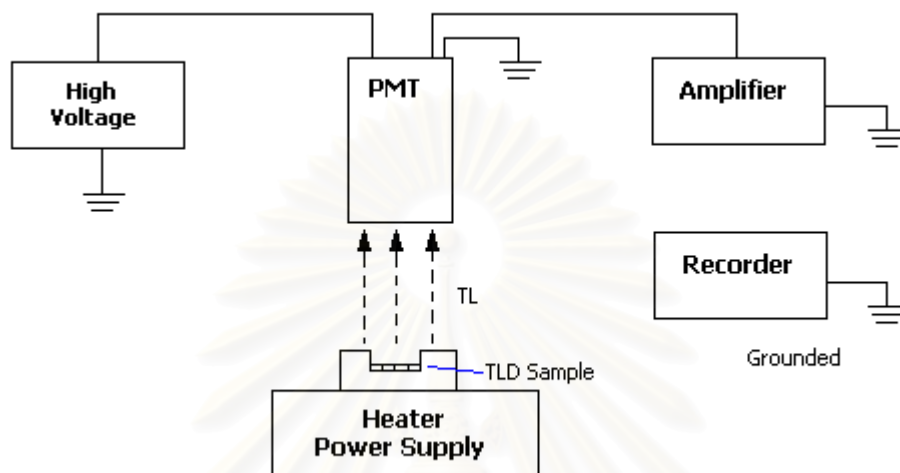


**Figure 2.3** Schematic diagram showing apparatus for dose measurement using thermoluminescence

Many crystalline materials exhibit the phenomenon of thermoluminescence used in thermoluminescent dosimeter. When, such as a crystal is irradiated, a very minute fraction of the absorbed energy is stored in the crystal lattice. Some of this energy can be recovered later as visible light if the material is heated. This phenomenon of release of visible photons by thermal mean is known as thermoluminescence.

The arrangement for measuring the thermoluminescence output is shown schematically in Figure 2.3. The radiation material is placed in a heater cup or planchet, where it is heated for a reproducible heating cycle. The emitted light is measured by a photomultiplier tube (PMT) which converts light into an electrical current. The current is then amplified and measured by a recorder or a counter.

There are several thermoluminescence phosphors available but the most noteworthy are lithium fluoride (LiF), lithium borate ( $\text{Li}_2\text{B}_4\text{O}_7$ ), and calcium fluoride ( $\text{CaF}_2$ ). Of these phosphors, LiF is most extensively studied and most frequently used for clinical dosimetry. LiF in its purest form exhibits relatively little thermoluminescence. But the presence of a trace amount of impurities (e.g., magnesium) provides the radiation-induced thermoluminescence. These impurities give rise to imperfections in the lattice structure of LiF and appear to be necessary for the appearance of the thermoluminescence phenomenon.

### 2.1.8.1 Simplified theory of thermoluminescent dosimetry

The chemical and physical theory of thermoluminescent dosimeter is not exactly known, but simple models have been proposed to explain the phenomenon qualitatively. Figure 2.4 show an energy-level diagram of an inorganic crystal exhibiting thermoluminescence by ionizing radiation.

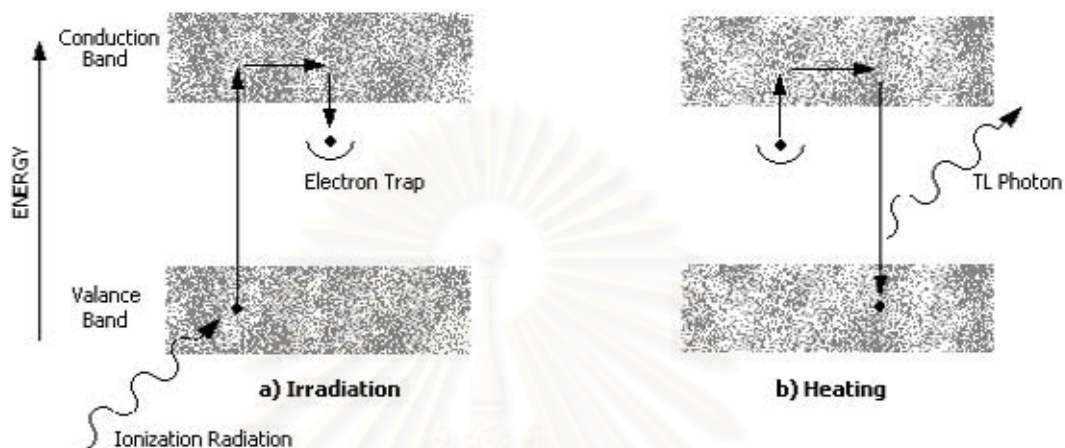


**Figure 2.4** A simplified energy-level diagram to illustrate thermoluminescent process

In an individual atom, electron occupies discrete energy levels. In a crystal lattice, on the other hand, electronic energy levels are perturbed by mutual interactions between atoms and give rise to energy bands the “allow” energy bands and the forbidden energy bands. In addition, the presence of impurities in the crystal creates energy trap in the forbidden region, providing metastable state for the electron. When the material is irradiate, some of the electron in the valance band. The vacancy thus created in the valance band is called a positive hole. The electron and the hole move independently through their respective hole. The electron and the hole move independently through their respective bands until they recombine (electron returning to the ground state) or until they fall into a trap (metastable state). If there is instantaneous emission of light owing to these transitions, the phenomenon is called fluorescence. If an electron in the trap requires energy to get out of the trap and fall into the valance band, the emission of light in this case is called phosphorescence (delayed fluorescence). If phosphorescence at room temperature is very slow, but can be speed up significantly with a moderate amount of heating ( $\sim 300\text{ }^{\circ}\text{C}$ ), the phenomenon is called thermoluminescence.

A plot of thermoluminescence against temperature is called ‘glow curve’ (Figure 2.5). As the temperature of the thermoluminescence material exposed to radiation is increased, the probability of releasing trapped electrons increases. The light emitted first increases, reach a maximum value, and fall again to zero. Because most phosphors contain a number of traps at various energy levels in the forbidden band, the glow curve may consist of a number of glow peaks as show in Figure 2.4. The different peaks correspond to different ‘trapped’ energy levels.

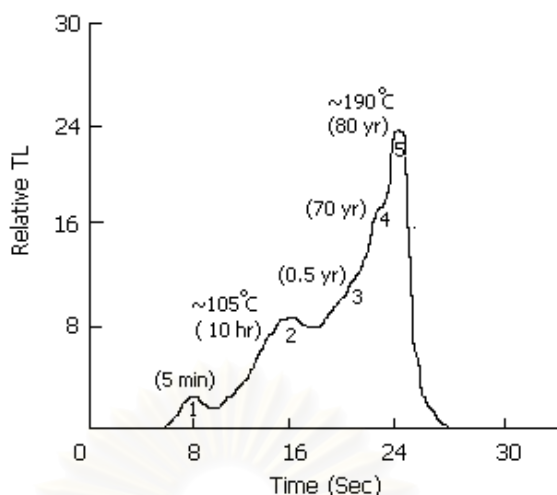


**Figure 2.5** An example of glow curve of LiF (TLD-100) after phosphor has been annealed at 400 °C for 1 hour and read immediately after irradiation to 100R

#### 2.1.8.2 Lithium fluoride

Lithium fluoride has an effective atomic number of 8.2 compared with 7.4 for soft-tissue. This makes this material very suitable for clinical dosimetry. The dose absorbed in LiF can be converted to dose in muscle by considerations similar to those discussed earlier. For example, under electronic equilibrium conditions, the ratio of absorbed dose in the two media will be the same as the ratio of their mass energy absorption coefficient. If the dimensions of the dosimeter are smaller than the ranges of the electron crossing the dosimeter, then the Bragg-gray relationship can also be used. The ratio of absorbed doses in the two media will be the same as the ratio of mass stopping power. The applicability of the Bragg-gray cavity theory to thermoluminescent dosimeter has been discussed by several authors.

#### 2.1.8.3 Practical consideration

As stated previously, the thermoluminescent dosimeter must be calibrated before it can be used for measuring an unknown dose. Because the response of the thermoluminescent dosimeter materials is affected by their previous radiation history and thermal history, the material must be suitably annealed to remove residual effect. The standard pre-irradiation annealing procedure for LiF is 1 hour of heating at 400 °C and then 24 hour at 80 °C. The slow heating, namely 24 hour at 80 °C, remove peak 1 and 2 of the glow curve by decreasing the ‘trapping efficiency’. Peak 1 and 2 can also be eliminated by post-irradiation annealing for 10 minute at 100 °C. The need for eliminating peak 1 and 2 arise from the fact that the magnitude of these peaks decreases relatively fast with time after irradiation. By removing these peaks by annealing, the glow curve becomes more stable and therefore predictable.

The dose response curve for TLD-100 is shown in Figure 2.6. The curve is generally linear up to  $10^3$  cGy but beyond this it becomes supraliner. The response curve, however, depends on many conditions that have to be standardized to achieve reasonable accuracy with thermoluminescent dosimeter. The calibration

should be done with the same thermoluminescent dosimeter reader, in approximately the same quality beam and to approximately the same absorbed dose level.

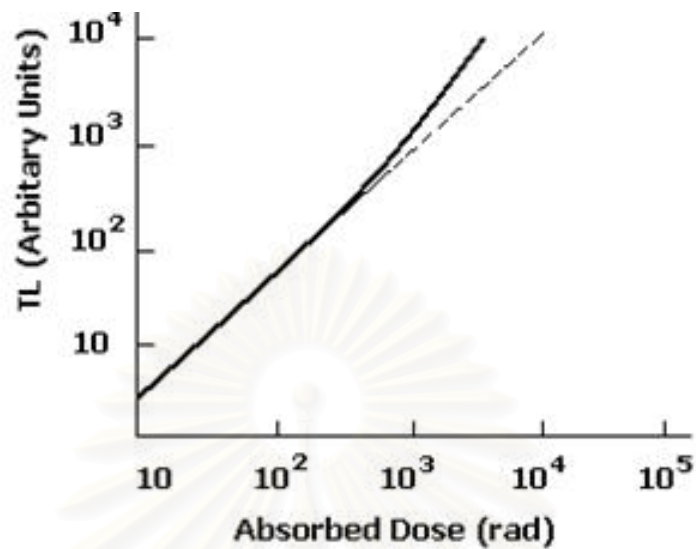


**Figure 2.6** An example of thermoluminescence versus absorbed dose curve for TLD-100 powder (schematic)

The thermoluminescent dosimeter response is defined as thermoluminescence output per unit absorbed dose in the phosphor. Figure 2.7 gives the energy response curve for LiF (TLD-100) for photon energies below megavoltage range. The studies of energy response for photons above <sup>60</sup>Co and high energy electrons have yielded somewhat conflicting results.

When considerable care is used, precision of approximately 3% may be obtained using thermoluminescent dosimeter powder or extruded material. Although not as precise as the ion chamber, thermoluminescent dosimeter's main advantage is in measuring dose in regions where ion chamber cannot be used. For example, thermoluminescent dosimeter is extremely useful for patient dosimetry by direct insertion into tissue or body cavities. Since thermoluminescent dosimeter material is available in many forms and sizes, it can be used for special dosimetry situation such as for measuring dose distribution in the build-up region, around brachytherapy source, and for personal dose monitoring.

#### 2.1.8.4 Energy response

The photoelectric absorption process is usually the predominant absorption process at low (< 100 keV) photon energies. This interaction, which involves the innermost electron, is dependent on the nuclear charge of the atom, the atomic number (Z). Consequently, radiation detectors with high atomic number's show a greatly enhanced response at the low photon energies. The energy response of a detector at a particular photon energy may be defined as the response of the detector at that photon energy relative to its response at some reference energy (usually 1-3 MeV) where the photoelectric absorption process is largely in operation. The

dosimeter is said to have a good energy response if its response per roentgen shows little change with photon energy, the energy response is poor if this charge is charge. Detectors with an effective atomic number approximately that of air ( $Z = 7.64$ ) show a good energy response while those with an effective atomic number much different from 7.64 show a poor energy response.

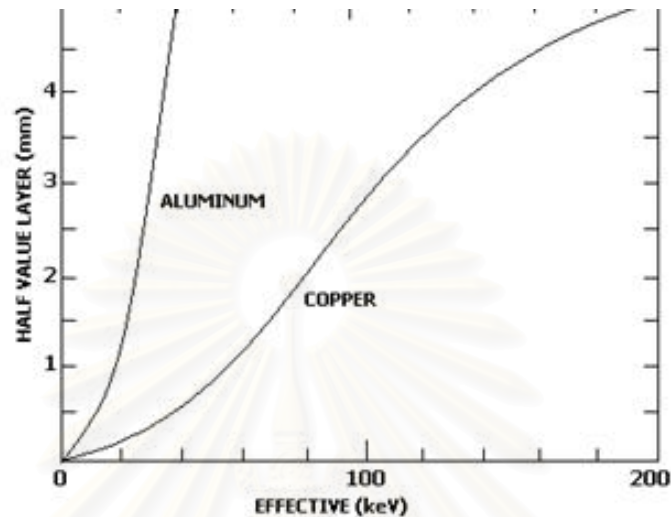


**Figure 2.7** Relation of half value layer (HVL) to effective energy

One recurring problem in dealing with energy response is the precise statement of x-ray beam quality. If the radiation source is a monoenergetic gamma-ray emitter (for example,  $^{137}\text{Cs}$ ) then the beam quality can be expressed simply and accurately as the monoenergetic photon energy (662 keV). On the other hand, if the radiation source used is an x-ray generator that produces a spectrum of photon energies up to the maximum accelerating voltage, then specification of the beam quality is much more difficult. Beam quality may be expressed in terms of 'effective keV' defined as that monoenergetic photon energy which has the same half value layer as dose the x-ray beam in question. Conversion from the measured half value layer to effective energy (keV) can be made from Figure 2.7. Effective energy (keV) determined in this manner is not a highly precise statement of quality for example, two x-ray beams generated at different accelerating voltages and with different filtrations can have identical half value layer (and consequently the same effective energy). It is often valuable to specify the first and second half value layer as well as the accelerating voltage and the amount of filtration.

There are two ways to determine energy response curves for thermoluminescence phosphors by using experimentally determined values based on calculated values from available absorption coefficients for the various photon energies. Experimentally measured values are usually more appropriate when correcting for the energy responses in various experimental irradiations. Figure 2.8 show energy responses curve which were calculated by comparing the absorption coefficient of the various thermoluminescence phosphors with the energy deposited in tissue. Energy response is usually related to the exposure in air rather than to the dose in tissue.



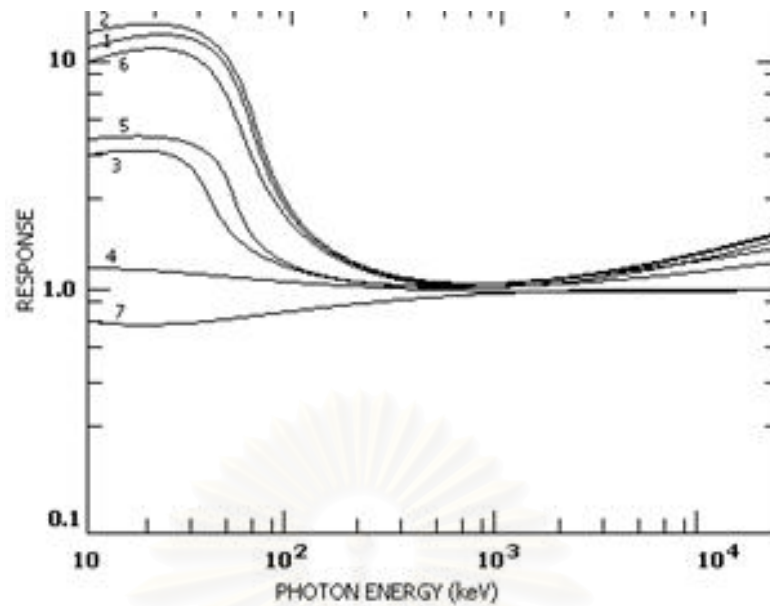


**Figure 2.8** Theoretical sensitivity of the thermoluminescence phosphors: (1)  $\text{CaSO}_4$ ; (2)  $\text{CaF}_2$ ; (3)  $\text{Al}_2\text{O}_3$ ; (4)  $\text{LiF}$ ; (5)  $\text{CaCO}_3$ ; (6)  $\text{SiO}_2$ ; and (7)  $\text{Li}_2\text{B}_4\text{O}_7$

#### 2.1.9 Calibration of thermoluminescent dosimeter [12]

The purpose of calibrating a thermoluminescent dosimeter instrument is to produce consistent and accurate reading in dosimetrically meaningful units. The calibration process involves the following 2 steps.

##### 2.1.9.1 Generate calibration dosimeter

In this process, an element correction coefficient (ECC) is generated by using a set of dosimeters, typically 1-2% of the total population to be calibration dosimeter. They are identified and segregated from the field dosimeter.

All dosimeter are annealed to clear them all residual exposure. Duration time between annealing and exposing should be the same for all dosimeters. After being exposed to the known radiation dose, the charge integral value ( $Q_i$ ) in nanocoulomb (nC) of each dosimeter (i) is read out and recorded. Then the average charge integral ( $\bar{Q}$ ) of all dosimeters is calculated and the element correction coefficient ( $\text{ECC}_i$ ) for individual dosimeter i ( $i = 1, 2, 3, \dots, n$ ) is computed by dividing the average charge integral by the individual charge ( $Q_i$ ) as:

$$\text{ECC}_i = \frac{\bar{Q}}{Q_i} \quad \dots (2.9)$$

##### 2.1.9.2 Calibration of thermoluminescent dosimeter reader

A group of dosimeter about 1-2% of dosimeters in (a) which have  $\text{ECC}_i$  value close to 1 are chosen to be calibration dosimeters. The calibration dosimeters are exposed to know amount of radiation dose (D) in grays and read by

thermoluminescent dosimeter reader. As  $Q_i$  is the reading for the dosimeter I, the corrected charge integral  $Q_{ci}$  of the dosimeter is calculated by:

$$Q_{ci} = Q_i \times ECC_i \quad \dots (2.10)$$

Then the reader calibration factor (RCF) is calculated from the equation:

$$RCF = \frac{\overline{Q_c}}{D} \quad \dots (2.11)$$

When  $Q_c$  is the average corrected charge integral and calculated by:

$$\overline{Q_c} = \frac{1}{n} \left( \sum_{i=1}^n Q_{ci} \right) \quad \dots (2.12)$$

### 2.1.9.3 Calibration of dosimeter

The rest of the dosimeter [number of the dosimeters in (a) – number of dosimeters in (b)] are used as field dosimeters. They are exposed by the known radiation dose of the L grays and read by thermoluminescent dosimeter reader. The calibration value of element correction coefficient for individual dosimeter ( $ECC_{ci}$ ) is then calculated by:

$$ECC_{ci} = \frac{(RCF \times L)}{Q_i} \quad \dots (2.13)$$

### 2.1.10 Determination of unknown radiation dose

The field dosimeters in 3.3.4 (c) are used to measure unknown radiation dose. The unknown dose D in grays is calculated by using  $ECC_{ci}$  from the equation:

$$D = \frac{(Q_i \times ECC_{ci})}{RCF} \quad \dots (2.14)$$

When  $Q_i$  is the reading of the individual field dosimeter i of any user defined length.

### 2.1.11 Uncertainty of measurement [13,14]

An uncertainty is evaluated by statistical analysis of a series of observations, it is known as a Type A evaluation.

A type A evaluation will normally be used to obtain a value for the repeatability or randomness of a measurement process. For some measurements, the random component of uncertainty may not be significant in relation to other contributions to uncertainty. It is nevertheless desirable for any measurement process that the relative importance of random effects be established. When there is a significant spread in a sample of measurement results, the arithmetic mean or average

of the results should be calculated. If there are  $n$  independent repeated values for a quantity  $Q$  then the mean value  $\bar{q}$  is give by

$$\bar{q} = \frac{1}{n} \sum_{j=1}^n q_j = \frac{q_1 + q_2 + q_3 \dots q_n}{n} \quad \dots (2.15)$$

The spread in the results gives an indication of the repeatability of the measurement process, which depends on various factors, including the apparatus used, the method, and sometimes on the person making the measurement. A good description of this spread of values is the standard deviation  $\sigma$  of the  $n$  values that comprise the sample, which is given by

$$\sigma = \sqrt{\frac{1}{n} \sum_{j=1}^n (q_j - \bar{q})^2} \quad \dots (2.16)$$

This expression yields the standard deviation  $\sigma$  of the particular set of values sampled. However, these are not the only values that could have been sampled. If the process is repeated, another set of values, with different values of  $\bar{q}$  and  $\sigma$ , will be obtained.

For the large values of  $n$ , these mean values approach the central limit of a distribution of all possible values. This probability distribution can often be assumed to have the normal from.

As it is impractical to capture all values that are available, it is necessary to make an estimate of the value of  $\sigma$  that would be obtained were this possible. Similarly, the mean value obtained is less likely to be the same as that which would be obtained if a very large number of measurements could be taken, therefore an estimate has to be made of the possible error from the “true” mean.

From the equation 2.14 gives the standard deviation for the sample actually selected, rather than of the whole population of possible samples. However, from the results of a single sample of measurements, an estimate,  $s(q_j)$ , can be made of the standard deviation  $\sigma$  of the whole population of possible values of the measured from the relation.

$$s(q_j) = \sqrt{\frac{1}{n-1} \sum_{j=1}^n (q_j - \bar{q})^2} \quad \dots (2.17)$$

The mean value  $\bar{q}$  will be derived from a finite number  $n$  of samples and therefore its value will not be the exact mean that would have been obtained if an infinite number of samples could have been taken. The mean value itself therefore has uncertainty. This uncertainty is referred to as the experimental standard deviation of the mean. It is obtained from the estimated standard deviation of the population by the expression:

$$s(\bar{q}) = \frac{s(q_j)}{\sqrt{n}} \quad \dots (2.18)$$

The standard uncertainty is then the standard deviation of the mean. This is known as the *standard uncertainty* and is given the symbol  $u_i(x)$ .

$$u_i(x) = s(\bar{q}) \quad \dots (2.19)$$

Once the standard uncertainties  $x_i$  and the sensitivity coefficients  $c_i$  have been evaluated, the uncertainties have to be combined in order to give a single value of uncertainty to be associated with the estimate  $y$  of the measurement  $Y$ . This is known as the *combined standard uncertainty* and is given the symbol  $u_c(y)$ .

The combined standard uncertainty is calculated as follow:

$$u_c(y) = \sqrt{\sum_{i=1}^N c_i^2 u^2(x_i)} = \sqrt{\sum_{i=1}^N u_i^2(y)} \quad \dots (2.20)$$

The GUM recognizes the need for providing a high level of confidence – referred to herein as *coverage probability* - associated with an uncertainty and uses the term *expanded uncertainty*,  $U$ , which is obtained by multiplying the combined standard uncertainty by a coverage factor. The coverage factor is given the symbol  $k$ , thus the expanded uncertainty is given by

$$U = k u_c(y) \quad \dots (2.21)$$

In accordance with generally accepted international practice, it is recommended that a coverage factor of  $k=2$  is use to calculate the expanded uncertainty. This value of  $k$  will give a coverage probability of approximately 95%, assuming a normal distribution.

Note: A coverage factor of  $k = 2$  actually provides a coverage probability of 95.45% for a normal distribution. For convenience this is approximated to 95% which would relate to a coverage factor of  $k = 1.96$ . However, the difference is not generally significant since, in practice, the coverage probability is usually based on conservative assumptions and approximations to the true probability distributions.

## 2.2 Related literatures

Osei E K and Faulkner K, [15] studied the radiation absorbed dose to the embryo/fetus which was estimated from acknowledge of technique factors and examination details using normalized uterine dose published by the National Radiological Protection Brard (NRPB). Doses to the embryo/fetus varied between less than 0.01  $\mu$ Gy and 117 mGy, depending on the examination. Gestation ages ranged between 2 and 24 weeks.

Osei E K and Faulkner K, [16] studied the fetal size that was estimated from the depth from mother's anterior surface to the mid-line of the abdomen using ultrasound scan in 215 pregnant women. The fetal position from the anterior surface of the mother's abdomen is shorter for posterior placenta and empty bladder volume, but longer for anterior placenta and full bladder volume. The fetal size at 0-14 weeks was found to be about 5.9 cm to 6.8 cm. Mean fetal depth observed for all bladder volumes over the period 8-25 weeks was damaged to the developing brain has been observed to in mental retardation.

Ragozzino M W, et al. [17] studied the average fetal depth in utero from the anterior maternal skull and abdomen was measured by ultrasound in 97 pregnant women, found at 0-14 weeks which had the fetal depth about  $6.1 \pm 1.1$  cm and the maternal anteroposterior (AP) thickness about  $19.5 \pm 1.5$  cm.

Unlubay D and Bilaloglu P, [18] studied the dose received which depends on mAs, but other parameters are necessary for calculation (film source distance, kV, filtration). To prevent accidental irradiation of the fetus, women must receive information about radiation effects, and the physician must choose a nonirradiating technique. Termination of pregnancy is an individual decision affected by many fator. Fetal doses below 50 mGy should not be considered a reason for terminating pregnancy. For a low dose procedure such as a chest X-ray, the only information that may be needed is verbal assurance that the risk is judged to be low. When fetal doses are above 1 mGy and above, more detailed explanation is given.

Tung C J and Tsai H Y, [19] studied the national survey of patient doses for diagnostic radiology in the Republic of China. They performed a pilot study for this survey to develop a protocol of the dose assessments. Entrance skin doses and organ (including ovary, testicle and uterus) doses were measured by thermoluminescent dosimeters and calculated by means of Monte Carlo simulations for several diagnostic procedures. They derived a formula and used the RadComp software for the computation of entrance skin doses. This formula involves several factors, such as kVp, mAs, the focus-to-skin-distance and aluminum filtration. RadComp software was applied to obtain free-air entrance exposures which were converted to entrance skin doses by considering the backscattering radiation from the body. Organ doses were measured using a RANDO phantom and calculated using a mathematical phantom for several diagnostic examinations. Genetically significant doses were calculated from ovary and testicle doses for the evaluation of hereditary effects. Embryo/fetal doses were determined from the uterine doses by considering the increase in uterus size with gestational age. They found that the patient doses studied in this work were all below the reference doses recommended by the U.K.

Bradley B, Fleck A and Osei E K, [20] studied the pregnant patient who has received a radiological examination involving ionizing radiation. The dose to the fetus should be assessed based on the patient's treatment plan. A major source of uncertainty in the estimation of fetal absorbed dose is the influence of fetal size and position as these changes with gestational age. Various studies of fetal dose during pregnancy have appeared in the literature. Whilst these papers contain many useful data for estimating fetal dose, they usually contain limited data regarding the depth and size of the fetus within the maternal uterus. They have investigated doses to the fetus from radiation therapy of the breast of a pregnant patient using an anthropomorphic phantom. Normalized data for estimating fetal doses that takes into account the fetal size (gestational age: 8-20 weeks post-conception) and the depth within the maternal abdomen (4-16 cm) for different treatment techniques have been provided. The data indicate that fetal dose is dependent on both depth within the maternal abdomen and gestational age, and hence these factors should always be considered when estimating fetal dose.

Damilakis J, et al. [21] studied the thermoluminescent dosimeter used for dose measurements in anthropomorphic phantoms which was simulated the pregnancy at the three trimesters of gestation. The effect of chest thickness on conceptus dose and risk was studied by adding slabs of lucite on the anterior and posterior surface of the phantom chest. The conceptus risk for radiation-induced childhood fatal cancer and hereditary effects was calculated based on appropriate risk factors. The average AP chest dimension ( $d_a$ ) was estimated for 51 women of childbearing age from chest CT examinations. The value of  $d_a$  was estimated to be 22.3 cm (17.4-27.2 cm). The calculated maximum conceptus dose was  $107 \times 10^{-3}$  mGy for AP chest radiographs performed during the third trimester of pregnancy with maternal chest thickness of 27.2 cm. This calculation was based on dose data obtained from measurements in the phantoms and  $d_a$  estimated from the patient group. The corresponding average excess of childhood cancer was 10.7 per million patients. The risk for hereditary effects was 1.1 per million births. Radiation dose for a conceptus increases exponentially as chest thickness increases. The conceptus dose at the third trimester is higher than that of the second and first trimesters. The results of the current study suggest that chest radiographs carried out in women at any time during gestation will result in a negligible increase in risk of radiation-induced harmful effects to the unborn child. After a properly performed maternal chest X-ray, there is no need for individual conceptus dose estimations.

Damilakis J, et al. [22] studied the maximum embryo dose during intravenous urography (IVU) examinations, when inadvertent irradiation of a pregnant woman occurs, and to investigate the variation of doses received from different institutions. Doses at average embryo depth from IVU examinations have been measured in four institutions, using a RANDO phantom and thermoluminescent crystals. In order to estimate the maximum range of embryo doses, radiologists were asked to carry out the examinations with the same technique as in female patients with acute ureteral obstruction. The range of doses estimated at embryo depth for the institutions participating in this study was 5.77 to 35.2 mGy. The considerable interhospital variation found in dose can be explained by different equipment and technique used. A simple method of estimating embryo dose from pelvic radiographs reported previously was found to be also applicable to IVU examinations. Absorbed dose at 6 cm, the average embryo depth, was found significantly less than 50 mGy.

Aldrich J E, et al. [23] studied the surface doses to patients during abdomen, chest and pelvic radiography were measured over a period of 3 years, during which time computed radiography (CR) and digital radiography (DR) systems were introduced to replace film-screen systems. For film-screen and CR the surface doses were measured with thermoluminescent dosimeters. For DR the surface doses were calculated from the dose-area product (DAP) meter readings. Published diagnostic reference levels were used as target values in this optimization. Initially, CR doses were the same as or higher than for film-screen, and the doses were lower of DR compared to film-screen.

Compagnone G, et al. [24] studied the radiation dose to patient undergoing standard radiographic examinations using conventional screen-film radiography, computed radiography and direct digital radiography; entrance surface dose and effective dose were calculated for six standard patient exposure parameters for the three imaging modalities. It was found that doses for computed radiography (all examinations) were higher than the doses for the other two modalities; effective doses for direct digital radiography were ~29% and ~43% lower than those for screen-film radiography and computed radiography, respectively. The image quality met the criteria in the European guidelines for all modalities.



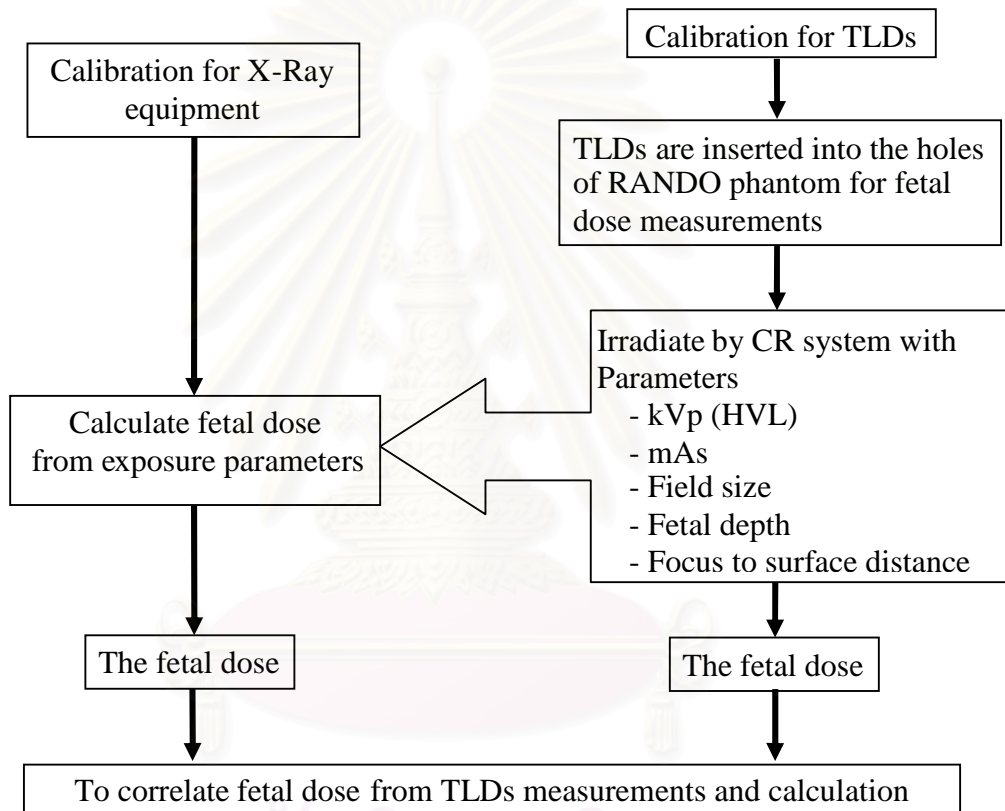
# CHAPTER 3

## RESEARCH METHODOLOGY

### 3.1 Research design

The study is the observational study.

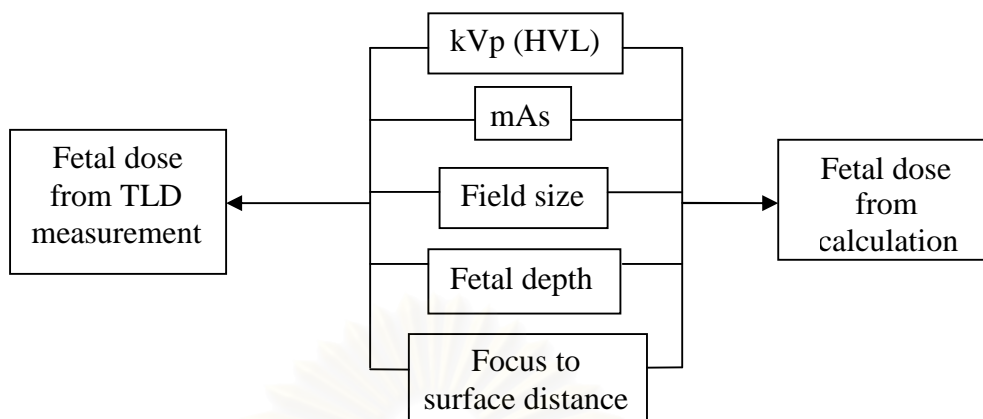
### 3.2 Research design model



สถาบันวิทยบริการ  
จุฬาลงกรณ์มหาวิทยาลัย



### 3.3 Conceptual framework



### 3.4 Key word

- Fetal dose
- Computed radiography
- Thermoluminescent dosimeters
- RANDO phantom

### 3.5 Research questions

#### 3.5.1 Primary question

What are the fetal doses in RANDO phantom during abdominal, pelvis and lumbo-sacral spine radiographic procedures in computed radiography?

#### 3.5.2 Secondary question

What are the correlations between measured and calculated fetal dose in RANDO phantom?

สถาบันวิทยบริการ  
จุฬาลงกรณ์มหาวิทยาลัย

### 3.6 Material

#### 3.6.1 Thermoluminescent dosimeter, Lithium Fluoride (TLD-100) [11, 23]

The TLD chips used for this study are Lithium Fluoride (LiF), it is shown in Figure 3.1(a) from Harshaw Chemical Company, Solon/Harshaw, USA. The crystals doped with magnesium and titanium (LiF:Mg, Ti) with the natural isotope mixture of lithium (TLD-100). They have a nominal density of  $2.64 \text{ g/cm}^3$  and effective atomic number  $Z_{\text{eff}}$  of 8.2 that sufficiently close to tissue. All chips have the surface area of  $3.2 \times 3.2 \text{ mm}^2$ , a thickness of 0.89 mm, and the area of  $10.16 \pm 0.12 \text{ mm}^2$ .

Three pieces of thermoluminescent dosimeter chips were loaded in the plastic tubes, shown in Figure 3.1(b). These tubes will be irradiated for thermoluminescent dosimeter characteristics study and fetal dose measurement.

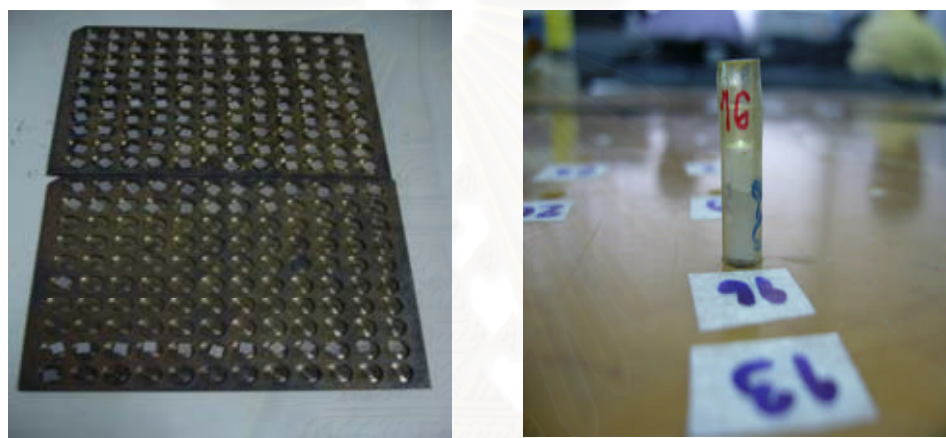


**Figure 3.1** The TLD chips, Lithium Fluoride (LiF) from Harshaw Chemical Company (Solon/Harshaw, USA). The TLD-100 chips (left) and the plastic tube for TLD-100 chips (right).

#### 3.6.2 Thermoluminescent dosimetry system [24, 25]

The thermoluminescent dosimetry system consists of

3.6.2.1 Personal computer to control the Automatic TLD reader system 5500.



**Figure 3.2** The personal computer

3.6.2.2 Vacuum tweezers and mechanically actuated, to assist with the placement of dosimetric materials, it should be used to avoid mechanical tweezers, figures or small scratches, loss of mass or foreign deposits affect light emission.

3.6.2.3 Nitrogen pressure regulators and hoses to feed nitrogen gas into the Harshaw model 5500 reader unit.

3.6.2.4 Annealing oven manufactured by Harshaw Bicon, solon, Ohio, USA.

The annealing oven is controlled by a programmable microprocessor which features two different programs. Reproducible heating procedures for thermoluminescent dosimeters are essential to maintain constant sensitivity and low background readings. The methods for setting program of the annealing oven have two programs.

Program I: Annealing: used for annealing of TLD before irradiation

- Heating to 400 °C (ramp as step as possible)
- Keeping the temperature for 60 minutes
- Cooling to 100 °C (ramp as step as possible)
- Keeping the temperature for 120 minutes
- Cooling down to 45 °C (ramp as step as possible)
- End of program

Program II: Preheating: used before reading by a TLD reader

- Heating to 100 °C (ramp as step as possible)
- Keeping the temperature for 10 minutes
- Cooling down to 45 °C (ramp as step as possible)
- End of program



**Figure 3.3** The annealing oven manufactured by Harshaw Bicon

### 3.6.3 Automatic TLD reader system 5500 [26]

The Harshaw model 5500 automatic TLD reader which is shown in Figure 3.4 manufactured by Harshaw Bicron, Solon, Ohio, USA is a personal computer driven, table-top instrument for thermoluminescent dosimeter (TLD) measurement. It has been designed to economically provide both high performance and high reliability and complies with the latest International Standard Organization (ISO) requirement. This reader is capable of reading 50 dosimeters per loading and accommodates thermoluminescent chips, rods and cubes in a variety of sizes. The flexible design of the controlling software enables the user to configure the workstation for different applications. The software provides real-time monitoring of the instrument's operating conditions and display of the glow curves and response values. The reader uses hot nitrogen gas heating with a closed loop feedback system that produces linearly ramped temperatures accurate within  $\pm 1$  °C to 400 °C. The time temperature profile (TTP) is user-defined in three segments: preheat, acquire and anneal each with independent times and temperatures. Any number of different time temperature profiles may be defined and calibrated. The photomultiplier tube assembly is cooled to constant temperature maintain consistent performance of the photomultiplier tube. Nitrogen is routed through the photomultiplier tube (PMT) chamber to eliminate condensation. The nitrogen supply specification on nitrogen quality pre-purified (99.99%) dry, a pressure of 2 to 4 kg/cm<sup>2</sup>  $\pm 20\%$  and the flow rate capacity must be at least 5.6 liter/min.

The advantages of the hot gas method are as follows:

1. Transfer of heat to the dosimeter is fast.
2. Temperature control is independent on good thermal contact with the tray.
3. Particularly well suited to automatic reader because there is no dependence on the reflectivity of the tray and the mechanical arrangements are simple.



**Figure 3.4** The Harshaw model 5500 automatic TLD reader

### 3.6.4 RANDO phantom [27]

The RANDO phantom which is shown in Figure 3.5 incorporates materials to simulate various body tissue-muscle, bone, lung and air cavities. It is made of tissue equivalent material based on a synthetic isocyanate rubber. The phantom material is processed chemically and physically to achieve a density of  $0.985 \text{ g/cm}^3$  and an effective atomic number of 7.3 based on the International Commission on Radiation Units and Measurement. The phantom is shaped into a human torso and is sectioned transversely into slices of 2.5 cm each containing a matrix of 0.5 cm diameter holes spaced 3 cm apart. The hole grid patterns can be drilled into the sliced sections to enable the insertion of dosimeters.

This study used chest to pelvic part of RANDO phantom or slabs No.12 to 35 for each exposure parameters while TLDs were inserted into the holes of RANDO phantom for fetal dose measurements in slabs No.29 to 31(fetus level section).



**Figure 3.5** The RANDO phantom

### 3.6.5 Dosimeter [28]

#### 2.6.5.1 Victoreen model 4000M+

The Victoreen<sup>®</sup> x-ray test devices, model 4000M+ does it all. Simply place the instrument in the x-ray beam, make one exposure, and it serially displays kVp maximum, kVp average, kVp Effective, dose and time. The model 4000M+ then automatically resets for the next exposure. A CsI photodiode pair provides the kVp measurements through five user selectable filter pairs. This ensures optimum accuracy over the entire diagnostic range with minimum filtration dependence. Exposure measurements are made with a parallel plate ionization chamber located above the filter wheel. Exposure time is measured with quartz crystal accuracy. Plus, a variety of external ion chambers may be connected for even greater flexibility.

The Victoreen model 4000M+ is a self-contained, noninvasive x-ray test device shown in Figure 3.6. In single exposure, it simultaneously measures:

- kVp
- Exposure or air kerma
- Exposure rate or air kerma rate
- Time

The model 4000M+ features a dual sensitivity preamplifier for compatibility with radiographic, fluoroscopic and dental x-ray machine. In addition, it is calibrated for both tungsten anode (W/AI) and molybdenum (Mo/Mo) anode x-ray tubes, making it suitable for screen film mammography applications. Its automatic waveform phase determination and extensive diagnostics minimize the potential for error.

The external ion chamber port accepts a variety of accessory ionization chambers for various applications, including mammography, photo-timer calibration, and input phosphor image intensifier measurements.

The model 4000M+ uses proven technology to compute tube potential with  $\pm 2\%$  accuracy. Five separate, selectable filter pairs ensure optimum accuracy over the maximum range with minimum filtration dependence. A separate internal ionization measures tube output. Time is measured with crystal quartz accuracy. A microprocessor controls the electronics and performs calculations to obtain the displayed results.



**Figure 3.6** Victoreen® model 4000M+

#### 3.6.5.2 Ionization chamber

The secondary standard ionization chamber 0.6 cc graphite guarded stem ion chamber type NE 2571

The system consists of 0.6 cc ionization chamber (guarded stem) type 2571 with thin wall high purity graphite thimble 0.36 mm in thickness and pure aluminum electrode supported by this walled aluminum stem with the build-up thickness 3.87 mm for measuring exposure for 0.3 to 2 MV x-ray or gamma rays from

$^{60}\text{Co}$ . The chamber is connected with dosimeter type 2590 for charge reading. The ionization chamber 0.6 cc type NE 2571 is shown in Figure 3.7.



**Figure 3.7** The ionization chamber 0.6 cc type NE 2571

### 3.6.6 Electrometer

The electrometer used with ionization chamber 0.6 cc type NE 2571 is Ionex Dosemaster type 2590A which is very wide dynamic ranges enable accurate measurements of dose. The units are rad, rem, coulomb per kilogram (C/kg), gray (Gy), sievert (Sv) and coulomb (C) at five digit floating point. Many different types of ionization chambers may be used and many polarizing voltages can be selected to supply the ionization chamber in used. The polarizing voltage range is -1000 to +1000 and setting resolution  $\pm 1$  volt. The Ionex Dosemaster type 2590A is shown in Figure 3.8.



**Figure 3.8** The Ionex Dosemaster type 2590A

### 3.6.7 Water phantom

Basic dose distribution data are usually measured in a water phantom, which closely approximates the radiation absorption and scattering properties of muscle and other soft tissue. Another reason for the choice of water as a phantom material, however, poses some practical problems when used in conjunction with ionization chamber and other detectors that are affected by water, unless they are designed to be waterproof. In most cases, however the detector is encased in a thin plastic (water equivalent) sleeve before immersion into the water phantom. The water phantom is shown in Figure 3.9.

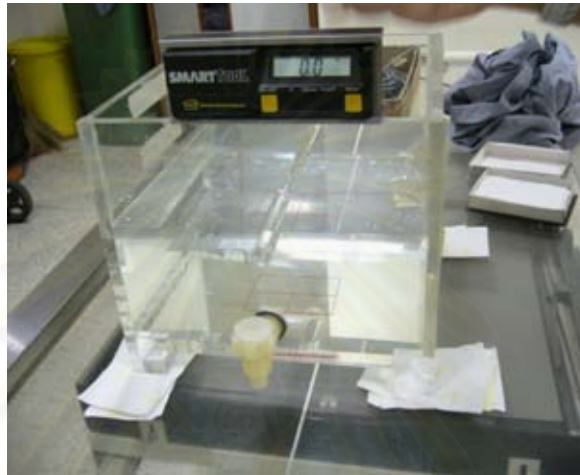


**Figure 3.9** The water phantom

### 3.6.8 Cobalt-60 teletherapy unit

The Cobalt-60 teletherapy unit used in this experimental is ELDORADO 78. The  $^{60}\text{Co}$  source has a half-life of 5.26 years and average gamma energy of 1.25 MeV.

The  $^{60}\text{Co}$  source is produced by irradiating ordinary stable  $^{59}\text{Co}$  with neutrons in a reactor. The nuclear reaction can be represented by  $^{59}\text{Co}(n,\gamma)^{60}\text{Co}$ . The  $^{60}\text{Co}$  source, usually in the form of a solid cylinder, discs, or pallets, is contained inside a stainless-steel capsule and sealed by welding. The double-welded seal is necessary to prevent any leakage of the radioactive material. The ELDORADO 78 Cobalt-60 teletherapy machine is shown in Figure 3.10.

The  $^{60}\text{Co}$  source decays to  $^{60}\text{Ni}$  with the emission of beta particles ( $E_{\text{max}} = 0.32$  MeV) and two photons per disintegration of energies 1.17 and 1.33 MeV. These gamma rays constitute the useful treatment beam. The beta particles are absorbed in the cobalt metal and stainless-steel capsules.

Because of the constant emission of the radiation,  $^{60}\text{Co}$  is used for thermoluminescent dosimeter absorbed dose calibration.





**Figure 3.10** ELDORADO 78 cobalt-60 teletherapy machine

### 3.6.9 Computed radiography system

The x-ray machine, unit of emergency room No.1 manufacturer by Toshiba Medical System model KXO-80G / DT-BTH / DST-100A, with 3 phase generator and a tube with maximum 150 kVp is shown in Figure 3.11. The tube current and exposure time for each radiographic examination were adjusted by automatic exposure control.



**Figure 3.11** Toshiba x-ray machine model KXO-80G/DT-BTH/DST-100A

### 3.7 Method

The study was performed in department of radiology at King Chulalongkorn Memorial Hospital. This study was carried out into seven steps:

- Calibration and quality control of x-ray equipment
- Calibration of thermoluminescent dosimeters (TLDs)
- Preparation of TLDs in RANDO phantom
- Measurement of fetal doses with TLDs
- Calculation of fetal doses by using parameters
- Estimation of uncertainties between TLDs measurement and exposure parameter calculation
- Comparisons and correlation of fetal dose between TLDs measurement and exposure parameter calculation in RANDO phantom

#### 3.7.1 Calibration and quality control of x-ray equipment

This study used AAPM task group No.4 protocol for quality control (QC) of the x-ray machine to evaluate the status of x-ray machine and components, it is shown in appendix. There are a variety of QC tests that should be performed on the tube and collimator to ensure that they are within acceptance parameters.

The term of beam quality (half value layer) is the thickness of an absorber of specified composition required to attenuate the intensity of the beam to half its original value.

The measurements were performed to find the half value layer of Toshiba x-ray machine model KXO-80G/DT-BTH/DST-100A with the kVp changed from 70, 80, 90, 100, the set up is shown in Figure 3.12. The Victoreen 4000M+ meter is being used, this may be done by holding the detachable cap of the Victoreen 4000M+ firmly in a clamp. A field size of small area should be used and radiation scattered from objects in the room should be avoided but the field size should be covered the sensitive volume of the detector. For constant kV and mAs, the measurements should be made with no added aluminum then with enough aluminum thickness to reduce the intensity to be less than one half, and also with aluminum thickness to reduce the intensity to more than one half.



**Figure 3.12** Beam quality of Toshiba x-ray machine model KXO-80G/DT-BTH/DST-100A

### 3.7.2 Calibration of thermoluminescent dosimeters (TLDs) [9, 29, 30]

The Thermoluminescent dosimeters (TLDs), TLD-100 chips with the automatic TL reader of Harshaw model 5500 were used to measure the fetal dose at various points in RANDO phantom. Before using TLDs for the measurement, they should be calibrated to assure that TLDs reading are stable. The TLDs of 150 chips were annealed and irradiated with 10 cGy without evaluation. Then the TLDs were annealed again, the process was repeated for five times. After exited, TLDs were calibrated to determine the ECC and RCF from equation 2.9, 2.11 for each individual dosimeter with gamma rays from ELDORADO 78 Cobalt-60 teletherapy machine of 10 cGy, field size 15x15 cm<sup>2</sup> at the source skin distance of 80 cm.

The calibration of TLDs was evaluated for sensitivity, linearity, energy response and minimum detectable dose of TLD chips.

#### 3.7.2.1 Sensitivity and dose calibration

The sensitivity of each dosimeter was determined by exposing 10 cGy of Co-60 gamma rays to 150 dosimeters, the charge integral value of each dosimeter was read and the element correction coefficient (ECC) was calculated according to equation 2.7. The dosimeters that have the element correction coefficient values between 0.8 and 1.2 were selected for using in this study. In addition the dosimeters of element correction coefficient values varied by  $\pm 1\%$  (0.99 to 1.01) were chosen for absorbed dose calibration. The absorbed dose of 10 cGy of <sup>60</sup>Co gamma rays from ELDORADO 78 Cobalt-60 teletherapy were irradiated to these dosimeters, the average value of charge integral reading was used as a factor to convert charge to absorbed dose. This is a reader calibration factor (RCF) value; the equation is according to equation 2.11.

### 3.7.2.2 Linearity

The Toshiba x-ray machine model KXO-80G/DT-BTH/DST-100A was calibrated for absorbed dose values of 70, 80, 90 and 100 kVp at 320 mA. The 0.6 cc NE 2571 connected to Ionex Dosemaster 2590A was inserted into the water phantom at 2.0 depths, the focus to skin distance was 62 cm and the field size was 9 x 9 cm<sup>2</sup>. The setup is shown in Figure 3.13. The exposure times were selected to give the dose range between 0 and 60 mGy. The absorbed dose was calculated according to equation 2.6. The calibration was performed for all kVp used according to an International Code of Practice: IAEA TRS 277 [9]. For <sup>60</sup>Co machine the calibration was performed at 80 cm source to surface distance, 10 cm depth and 10 x 10 cm field size. Also the calibration of <sup>60</sup>Co gamma beams was performed according to IAEA TRS 398 [29].

For the linearity of TLDs response, the dosimeters were irradiated in water phantom at absorbed doses of 70 kVp 2.8 mm Al, 80 kVp 3.31 mm Al, 90 kVp 3.71 mm Al and 100 kVp 4.28 mm Al. Three dosimeters were loaded in the plastic tube which was inserted in the sleeve of water phantom at 2 cm depth. The setup of the measurement was the same as absorbed dose measurement with ionization chamber.



**Figure 3.13** The setup of thermoluminescent dosimeter for linearity dose response

### 3.7.2.3 Energy response

For evaluation of energy response of TLDs, the set up of measurement was the same as linearity procedure. The TLDs were irradiated in water phantom at absorbed dose 50 mGy at 70 kVp, 80 kVp, 90 kVp and 100 kVp of Toshiba x-ray machine model KXO-80G/DT-BTH/DST-100A, Ir-192 (0.38 MeV) and gamma radiation of <sup>60</sup>Co (1.25 MeV).

The response of each beam quality was normalized to <sup>60</sup>Co beams, and then the correction factor for beam energy relative to <sup>60</sup>Co beams was calculated.

### 3.7.2.4 Minimum detectable dose

For evaluation of minimum detectable dose, the variation coefficient (VC) and the background were found, then minimum detectable dose (MDD) is calculated from the equation 3.1.

$$\text{MDD} = 3 \times \text{VC} \times \text{BG} \quad \dots (3.1)$$

Where, VC = variation coefficient, BG = mean background values

### 3.7.3 Preparation of TLDs in RANDO phantom

The RANDO phantom was used in this study instead of real patients. A set up of TLDs in RANDO phantom is shown in Figure 3.14. Three TLDs were positioned in each hole inside the phantom at slabs No. 29, 30 and 31 by placing in plastic tube in holes located at the surface, 3, 6 and 9 cm depth from the anterior surface of phantom for three projections of abdomen AP, pelvis AP and lumbo-sacral spine AP. It was placed in plastic tube in holes located at the surface, 13, 16 and 19 cm depth from the lateral surface of RANDO phantom for the projection of lumbo-sacral spine LAT. Thirty-six TLDs were loaded at each slab. The total TLDs used were 118 TLD chips per one exposure parameter. The total irradiation was 16 times. Then the total of 1888 TLDs reading was observed.

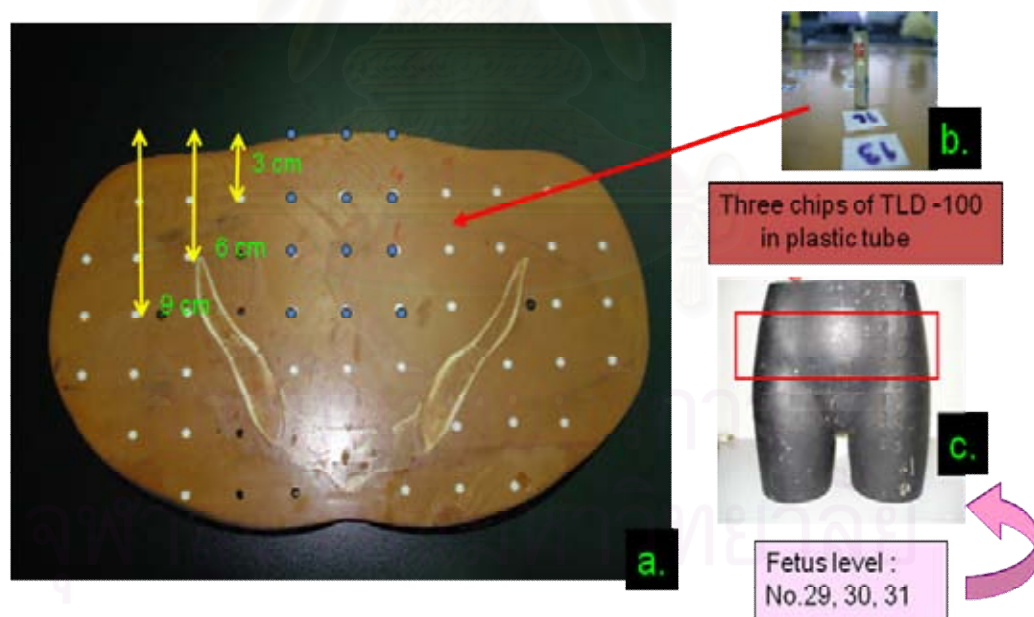


**Figure 3.14** The location of TLDs in RANDO phantom

### 3.7.4 Measurement of fetal doses with TLDs

The TLDs were inserted into RANDO phantom which were irradiated by computed radiography. A set up of each procedure according the parameters is shown in the Table 3.1.

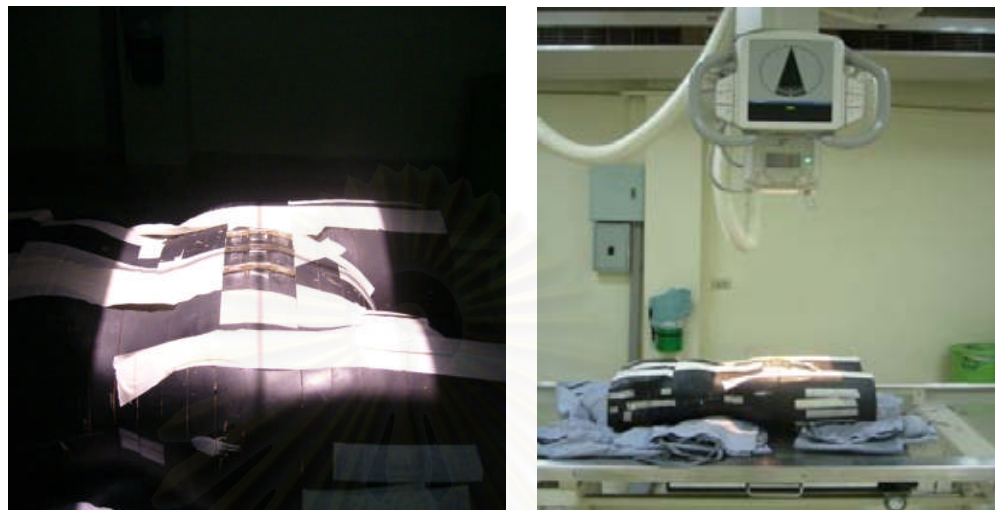


**Figure 3.15** The pelvis slabs inserted with TLD chips were irradiated by Toshiba x-ray machine. The field size setting (left) and the set up of pelvic examination (right)

**Table 3.1** The exposure parameters used for each procedure

Parameter type	Procedures			
	Abdomen AP	Pelvis AP	Lumbo-sacral spine AP	Lumbo-sacral spine LAT
Tube potential (kVp)	70,80,90,100	70,80,90,100	70,80,90,100	70,80,90,100
HVL (70,80,90,100 kVp)				
mAs (AEC)				
Filtration (mm Al)	Fixed	Fixed	Fixed	Fixed
Focus to image plate distance (cm)	100	100	100	100
Focus to surface distance (cm)	Fixed	Fixed	Fixed	Fixed
Field size at focus to image plate distance (cm <sup>2</sup> )	35 x 43	40 x 40	20 x 43	25 x 43
Phantom thickness (cm)	20	20	20	34

### 3.7.5 Calculation of fetal doses by using parameters

The parameters for using calculate the fetal doses that were shown in the Table 3.1. The entrance skin doses (ESDs) were calculated using equation 3.2, where the entrance skin dose (ESDs) is the absorbed dose to the entrance skin of the patient at the central point of the irradiated area (mGy = milligray). Exposure is the dose in air (mR = milliroentgen). The factor 0.00876 converts the exposure in mR to the free air absorbed dose in mGy. The mass attenuation coefficient ( $(\mu/\rho)_{\text{air}}^{\text{tissue}}$ ) is the ratio of the mass energy absorbed dose to a tissue absorbed dose in free air that we used of 1.06 [6,14,19]. The backscatter factor (BSF) is the ratio of the dose on central axis at the depth of maximum dose at the same point in free space.

$$\text{ESD (mGy)} = \text{Exposure (mR)} \times 0.00876 \frac{(\text{mGy})}{\text{mR}} \times (\mu/\rho)_{\text{air}}^{\text{tissue}} \times \text{BSF} \quad \dots (3.2)$$

The fetal doses (FD) were calculated using the following equation 3.3. The percentage depth dose (PDD) is  $(D_d/D_{d_0}) \times 100$ , where  $d$  is any depth and  $d_0$  is reference depth of maximum dose. Then, the correlation of the fetal dose between the measurement and calculation fetal dose in RANDO phantom were evaluated

$$\text{FD (mGy)} = \text{ESD (mGy)} \times \text{PDD}/100 \quad \dots (3.3)$$

### 3.7.6 Estimation of uncertainties between TLDs measurement and exposure parameter calculation.

An uncertainty budget for TLDs measurement can be determined from the relative combined standard uncertainty ( $k=2$ ) which was derived for typical values of uncertainties from various sources such as TLD sensitivity, TLD calibration, TLD energy response, calibration factor of ionization chamber and measuring accuracy of TLD. The uncertainty budget is shown in Table 3.2.

Additional sources of uncertainty arose from exposure parameter calculation which derived from the uncertainty budget such as calibration factor of ionization chamber (Victoreen 4000M+), measurement accuracy or repeatability of x-ray machine, backscatter factor (BSF), percentage depth dose are shown in Table 3.3.

Therefore, the uncertainties were estimated and used to calculate for the error of fetal dose.

**Table 3.2** The uncertainty budget to estimate the relative expanded uncertainty of TLDs measurement.

Source of uncertainty	Standard deviation value ( $\sigma$ )	$n$	Standard deviation of mean	Divisor	%uncertainty
1.TLD sensitivity	$\sigma_1$	1	$\frac{\sigma_1}{\sqrt{1}} = s_1$	1	$\frac{s_1}{1} = u_1$
2.TLD calibration					
-TLDs	$\sigma_2$	1	$\frac{\sigma_2}{\sqrt{1}} = s_2$	1	$\frac{s_2}{1} = u_2$
-Ionization chamber	$\sigma_3$	2	$\frac{\sigma_3}{\sqrt{2}} = s_3$	1	$\frac{s_3}{1} = u_3$
3.TLD energy response	$\sigma_4$	1	$\frac{\sigma_4}{\sqrt{1}} = s_4$	1	$\frac{s_4}{1} = u_4$
4.Calibration factor of ionization chamber	$\sigma_5$	1	$\frac{\sigma_5}{\sqrt{1}} = s_5$	2	$\frac{s_5}{2} = u_5$
5.Measuring accuracy	$\sigma_6$	16	$\frac{\sigma_6}{\sqrt{16}} = s_6$	1	$\frac{s_6}{1} = u_6$
Combined standard uncertainty $u_c(s) = \sqrt{(u_1)^2 + (u_2)^2 + (u_3)^2 + (u_4)^2 + (u_5)^2 + (u_6)^2}$					
Expanded uncertainty, coverage factor $k = 2$ , $U = ku_c(s)$					

Where

- $\sigma_1$  = Standard deviation of TLD sensitivity due to TLD calibration method.
- $\sigma_2$  = Standard deviation of TLD calibration that are the TLDs used due to TLD calibration method.
- $\sigma_3$  = Standard deviation of TLD calibration that are the ionization chamber used due to TLD calibration method.
- $\sigma_4$  = Standard deviation of TLD energy response due to TLD calibration method.
- $\sigma_5$  = Standard deviation of calibration factor of ionization chamber from the calibration certificate for the calibrator.
- $\sigma_6$  = Standard deviation of TLDs measurement in each time of TLDs was irradiated with  $^{60}\text{Co}$ , total 16 times.
- $n$  = The number of measurements contributing to the reported mean value.
- Divisor = The partial derivative or a known sensitivity coefficient.
- $s_1$  to  $s_6$  = The standard deviation of the mean.
- $u_1$  to  $u_6$  = The standard uncertainty
- $u_c(s)$  = The combined standard uncertainty
- $U$  = The expanded uncertainty



**Table 3.3** The uncertainty budget to estimate the relative expanded uncertainty of exposure parameter calculation.

Source of uncertainty	Standard deviation value ( $\sigma$ )	$n$	Standard deviation of mean	Divisor	%uncertainty
1. Calibration factor of ionization chamber (victoreen 4000M+)	$\sigma_1$	1	$\frac{\sigma_1}{\sqrt{1}} = s_1$	2	$\frac{s_1}{2} = u_1$
2. Measurement accuracy					
Repeatability of x-ray machine	$\sigma_2$	4	$\frac{\sigma_2}{\sqrt{4}} = s_2$	1	$\frac{s_2}{1} = u_2$
3. BSF	$\sigma_3$	1	$\frac{\sigma_3}{\sqrt{1}} = s_3$	1	$\frac{s_3}{1} = u_3$
4. Percentage depth dose	$\sigma_4$	1	$\frac{\sigma_4}{\sqrt{1}} = s_4$	1	$\frac{s_4}{1} = u_4$
Combined standard uncertainty $u_c(s) = \sqrt{(u_1)^2 + (u_2)^2 + (u_3)^2 + (u_4)^2}$					
Expanded uncertainty, coverage factor $k = 2$ , $U = ku_c(s)$					

Where

- $\sigma_1$  = Standard deviation of calibration factor of ionization chamber from the calibration certificate for the calibrator.
- $\sigma_2$  = Standard deviation of TLD calibration that are the TLDs used due to TLD calibration method.
- $\sigma_3$  = Standard deviation of backscatter factor.
- $\sigma_4$  = Standard deviation of percentage depth dose.
- $n$  = The number of measurements contributing to the reported mean value.
- Divisor = The partial derivative or a known sensitivity coefficient.
- $s_1$  to  $s_4$  = The standard deviation of the mean.
- $u_1$  to  $u_4$  = The standard uncertainty
- $u_c(s)$  = The combined standard uncertainty
- $U$  = The expanded uncertainty

### 3.7.7 Comparison of radiation doses from TLDs measurement and exposure parameter calculation

The radiation doses from TLDs measurement and parameter calculation of all examinations were normalized to the reference points at surface of RANDO phantom to evaluate for the dose difference. The percentage normalized dose differences of fetal dose between TLDs measurement and parameter calculation is expressed from the equation 3.4 as

$$\% \text{Normalized dose diff.} = \frac{[\text{TLDs measured dose} - \text{calculated dose}]}{\text{TLDs measured dose at surface}} \times 100 \quad \dots (3.4)$$

### 3.7.8 Correlation of fetal dose between TLDs measurement and exposure parameter calculation.

The graphs were plotted for the doses measured by TLD and the exposure parameter calculation, the correlation coefficient was calculated.

## 3.8 Measurement

Variable: Independent variable = kVp (HVL), mAs, field size, fetal depth  
: Dependent variable = Fetal dose

## 3.9 Data collection

After TLDs have been irradiated, the TLDs were read out on the Harshaw model 5500 automatic TLD reader. Absorbed dose in RANDO phantom were collected by TLDs measurement and exposure parameter calculation which were record in collection data forms.

## 3.10 Data analysis

The fetal doses from TLDs measurement and exposure parameters calculation are continuous data; mean value, standard deviation (SD) and range were analyzed. The table, graphs and scatter diagrams were presented. This study was performed to determine the correlation between measured and calculated fetal dose in RANDO phantom. The statistic evaluation both from the TLDs measurement and exposure parameter calculation by coefficients statistical data analysis and the expanded standard uncertainty were analyzed on Microsoft Office Excel 2003.

## 3.11 Benefit of the study

This study was designed to find the fetal dose in RANDO phantom which simulated in the first trimester of pregnancy by TLDs measurement and calculation. Then the correlation result between measured and calculation can be used as the reference of the methods to calculate fetal dose. Especially, the woman undergoing radiographic examinations in CR system and found that she is a pregnant.

### 3.12 Ethic consideration

This study was performed on the RANDO phantom. However, the ethical was approved by the Ethics Committee, Faculty of Medicine, Chulalongkorn University.



สถาบันวิทยบริการ  
จุฬาลงกรณ์มหาวิทยาลัย

## CHAPTER 4

### RESULTS

#### 4.1 Calibration and quality control of x-ray machine

The result of output measurement of x-ray beams is shown in the Table 4.1. The half value layer were ranged from 2.8 mm Al to 4.28 mm Al for 70 to 100 kVp. The outputs showed the increasing with the kVp, outputs in term of mR/mAs were presented for calculation of entrance skin dose according to equation 3.2.

The quality control of x-ray machine (Appendices) showed the good quality, all the measurements were in the AAPM tolerance.

**Table 4.1** The output measurement of x-ray machine.

kVp	HVL (mm Al)	Output (mR)	Output (mR/mAs)
70	2.8	213.9	8.6
80	3.31	274.7	11.0
90	3.71	348.9	14.0
100	4.28	415.8	16.7

#### 4.2 Calculation of fetal dose with parameters

##### 4.2.1 Parameters for calculation

The output and parameters [6, 17, 30, 31, 32] for calculation of the fetal doses are shown in the Table 4.2 to Table 4.3 and the percentage depth doses [6] are shown in Table 4.4.

**Table 4.2** The parameters for fetal doses calculation.

kVp	HVL (mm Al)	Output (mR/mAs)	Conversion Factor (mGy/mR)	$(\mu_{en} / \rho)_{air}^{tissue}$	BSF field size 35 x 43 cm <sup>2</sup>	BSF field size 20 x 43 cm <sup>2</sup>
70	2.8	8.6	0.00876	1.06	1.34	1.30
80	3.31	11.0	0.00876	1.06	1.39	1.32
90	3.71	14.0	0.00876	1.06	1.43	1.36
100	4.28	16.6	0.00876	1.06	1.45	1.38

**Table 4.3** The exposure parameters of each procedure for fetal doses calculation.

kVp	Pelvis AP			Abdomen AP			Lumbo-sacral spine AP			Lumbo-sacral spine LAT		
	mAs	BSF	Inv.	mAs	BSF	Inv.	mAs	BSF	Inv.	mAs	BSF	Inv.
70	37.7	1.34	0.68	21.7	1.34	0.78	34.8	1.34	0.78	38.0	1.30	1.032
80	23.6	1.39	0.68	12.1	1.39	0.78	16.0	1.39	0.78	13.4	1.32	1.032
90	15.0	1.43	0.68	7.0	1.43	0.78	8.3	1.43	0.78	6.7	1.36	1.032
100	8.6	1.45	0.68	4.4	1.45	0.78	5.7	1.45	0.78	5.1	1.38	1.032

**Table 4.4** The percentage depth dose for fetal doses calculation.

Depth (cm)	Percentage depth dose of each kVp			
	70 kVp	80 kVp	90 kVp	100 kVp
0	100	100	100	100
3	66	68	70	75
6	37	40	45	47
9	21	24	27	29
13	10	12	14	15
16	5.9	7	11	12
19	3.8	5.5	7	9

#### 4.2.2 Calculation of fetal doses from each examination

##### A. Pelvic AP examination

The absorbed doses calculated from exposure parameters for pelvic AP examination at the surface, 3, 6 and 9 cm for 70, 80, 90 and 100 kVp, are shown in Table 4.5. The doses decreased as the kVp increased and reduced with the depth. The surface dose ranged from 1.31 mGy to 2.75 mGy for 100 kVp to 70 kVp at the surface while, at 6.0 cm depth which was the depth of fetus level, the doses ranged from 0.62 mGy to 1.03 mGy.

**Table 4.5** The fetal doses from exposure parameter calculation of pelvic AP examination.

Depth (cm)	Fetal dose (mGy) in each kVp			
	70 kVp	80 kVp	90 kVp	100 kVp
0	2.75	2.28	1.90	1.31
3	1.81	1.55	1.33	0.98
6	1.03	0.91	0.86	0.62
9	0.58	0.55	0.51	0.38

### B. Abdomen AP examination

The absorbed doses calculated from exposure parameters for abdomen AP examination at the surface, 3, 6 and 9 cm for 70, 80, 90 and 100 kVp, are shown in Table 4.6. The surface dose ranged from 0.76 mGy to 1.80 mGy for 100 kVp to 70 kVp at the surface while, at 6.0 cm depth which was the depth of fetus level, the doses ranged from 0.36 mGy to 0.67 mGy.

**Table 4.6** The fetal doses from exposure parameter calculation of abdomen AP examination.

Depth (cm)	Fetal dose (mGy) in each kVp			
	70 kVp	80 kVp	90 kVp	100 kVp
0	1.80	1.33	1.01	0.76
3	1.19	0.91	0.71	0.57
6	0.67	0.53	0.45	0.36
9	0.38	0.32	0.27	0.22

### C. Lumbo-sacral spine AP examination

The absorbed doses calculated from exposure parameters for lumbo-sacral spine AP examination at the surface, 3, 6 and 9 cm for 70, 80, 90 and 100 kVp, are shown in Table 4.7. The surface dose ranged from 0.94 mGy to 2.80 mGy for 100 kVp to 70 kVp at the surface while, at 6.0 cm depth which was the depth of fetus level, the doses ranged from 0.44 mGy to 1.05 mGy.

**Table 4.7** The fetal doses from exposure parameter calculation of lumbo-sacral spine AP examination.

Depth (cm)	Fetal dose (mGy) in each kVp			
	70 kVp	80 kVp	90 kVp	100 kVp
0	2.80	1.67	1.14	0.94
3	1.85	1.14	0.80	0.71
6	1.05	0.67	0.51	0.44
9	0.59	0.40	0.31	0.27

### D. Lumbo-sacral spine LAT examination

Absorbed doses measured at the surface, 13, 16 and 19 cm for lumbo-sacral spine LAT examination for 70, 80, 90 and 100 kVp, are shown in Table 4.8. The surface doses ranged from 1.12 mGy to 4.07 mGy for 100 kVp to 70 kVp at the surface, at the fetus level the doses ranged from 0.13 mGy to 0.24 mGy.

**Table 4.8** The fetal doses from exposure parameter calculation of lumbo-sacral spine LAT examination.

Depth (cm)	Fetal dose (mGy) in each kVp			
	70 kVp	80 kVp	90 kVp	100 kVp
0	4.07	1.86	1.22	1.12
13	0.41	0.22	0.17	0.17
16	0.24	0.13	0.13	0.13
19	0.15	0.10	0.09	0.10

### 4.3 Thermoluminescent dosimeters calibration

#### 4.3.1 Sensitivity of TLD-100 chips

The relative sensitivity of these TLD chips was determined and individual calibration factors were calibrated. The sensitivity or element correction coefficient (ECC) of individual TLD chips ranged from 0.924 to 1.072 for TLD chips in this study. Only the TLD chips which had the sensitivity factor close to 1.0 (0.99 to 1.01) was selected to be used in the calibration of reader calibration factor (RCF) by equation 2.11.

#### 4.3.2 Linearity of TLD-100 chips

The linearity of TLD-100 chips response was studied by irradiated in water phantom at absorbed dose of known dose at 70 kVp, 80 kVp, 90 kVp, 100 kVp, Ir-192 (0.38 MeV) and  $^{60}\text{Co}$  (1.25 MeV).

The charges corrected by the sensitivity were plotted with the absorbed dose ranged from 0.3 to 100 mGy. They are shown in Figure 4.1, 4.2, 4.3, 4.4, 4.5 and 4.6 for 70 kVp, 80 kVp, 90 kVp, 100 kVp, Ir-192 (0.38 MeV) and  $^{60}\text{Co}$  (1.25 MeV), respectively. All the graphs showed linear relationship between responses of TLDs and absorbed dose with the correlation coefficient of 0.9992-1.0000.

สถาบันวิทยบริการ  
จุฬาลงกรณ์มหาวิทยาลัย

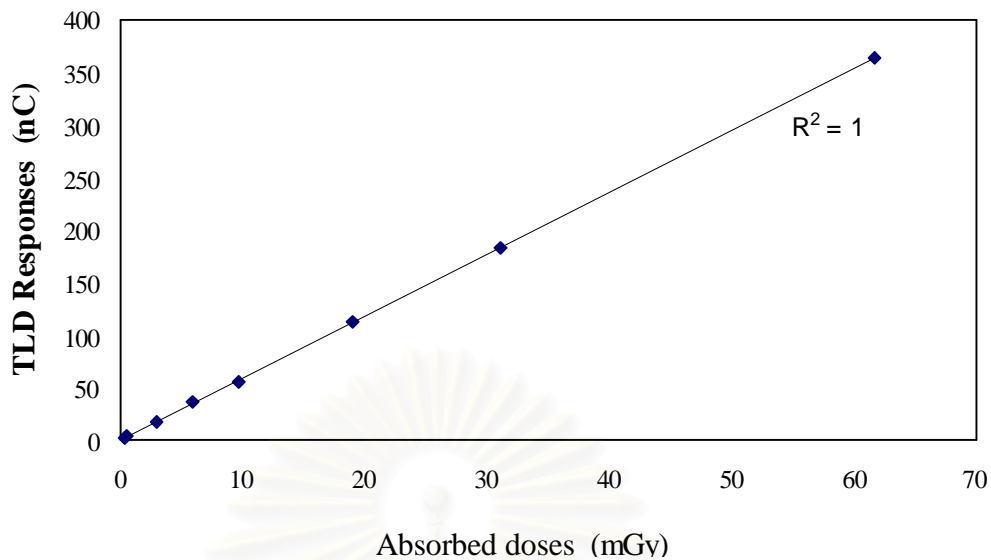


**Figure 4.1** Responses of LiF TLD-100 chips when irradiated at various doses for 70 kVp, 2.8 mm Al HVL.

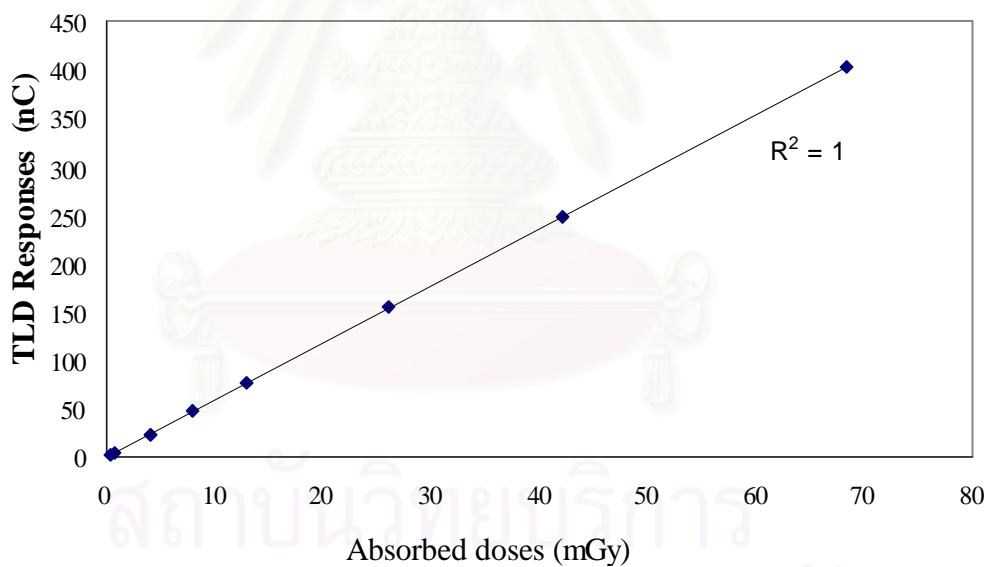


**Figure 4.2** Responses of LiF TLD-100 chips when irradiated at various doses for 80 kVp, 3.31 mm Al HVL.



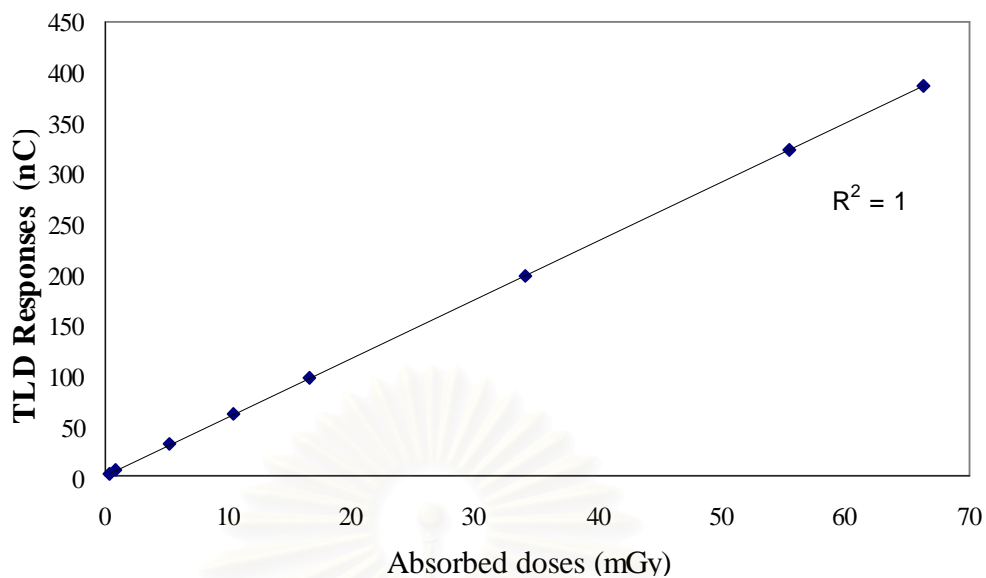


**Figure 4.3** Responses of LiF TLD-100 chips when irradiated at various doses for 90 kVp, 3.71 mm Al HVL.

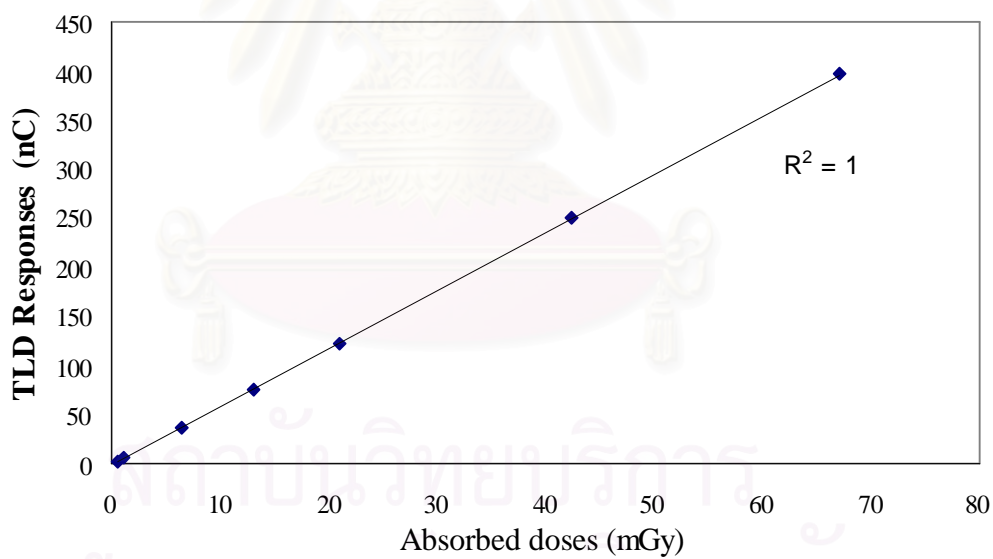


**Figure 4.4** Responses of LiF TLD-100 chips when irradiated at various doses for 100 kVp, 4.28 mm Al HVL.

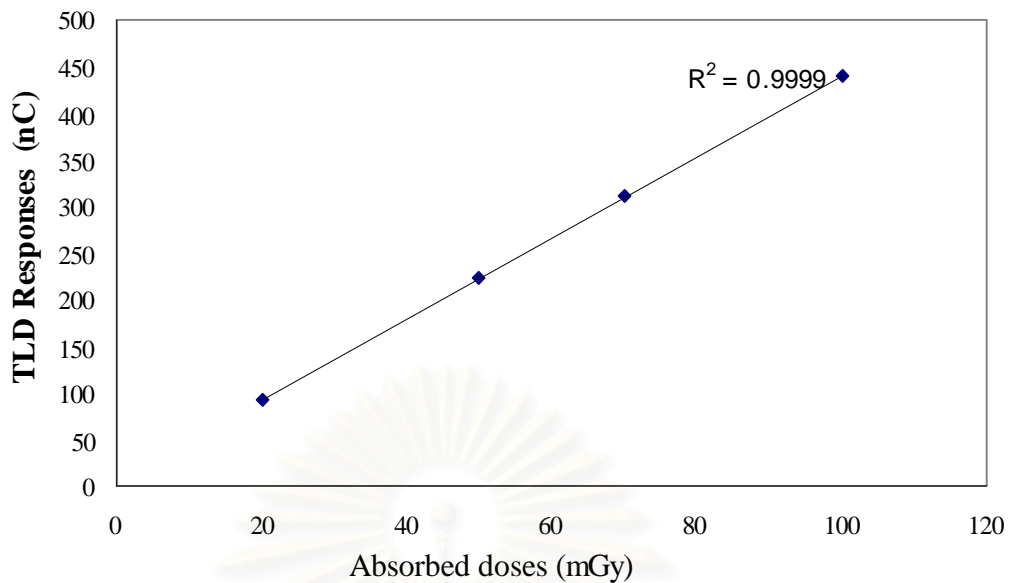


**Figure 4.5** Responses of LiF TLD-100 chips when irradiated at various doses for Ir-192 (0.38 MeV), 27 mm Al HVL.

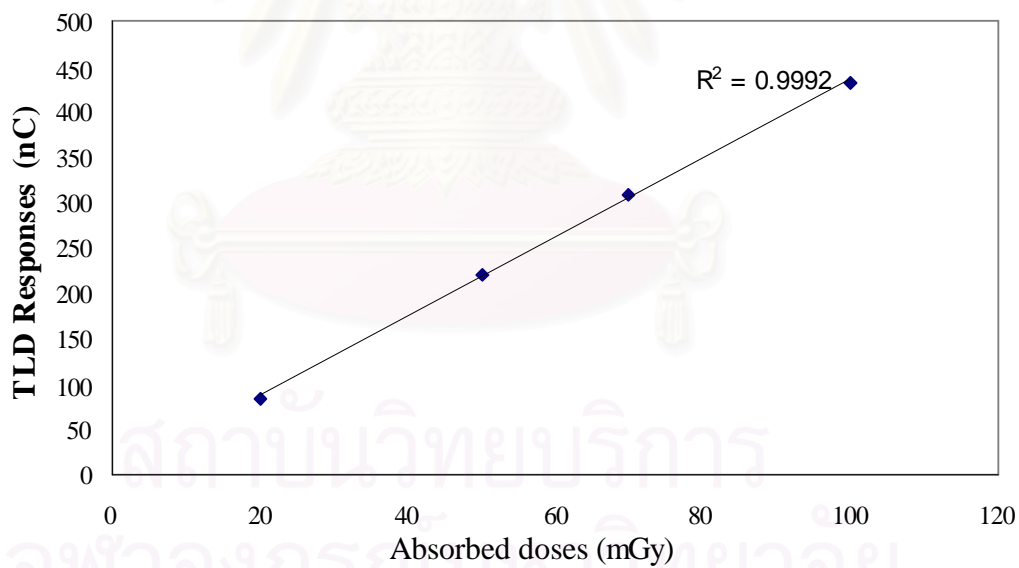


**Figure 4.6** Responses of LiF TLD-100 chips when irradiated at various doses for  $^{60}\text{Co}$  (1.25 MeV), 45 mm Al HVL.

### 4.3.3 Energy response of TLD-100 chips

The energy response of TLD chips in kilovoltage relative to  $^{60}\text{Co}$  gamma rays at absorbed dose of 50 mGy is shown in Table 4.9 and Figure 4.7, the half value layer and the effective energy for each beam were presented. The correction factor (CF) of energy response relative to  $^{60}\text{Co}$  for TLD chips used in CR x-ray beams are calculated, they are the reciprocal of the response. The factors ranged from 0.7363 to 0.7469 for half value layer of 2.8 to 4.28 mm Al which are the range of the quality of beams used in CR x-ray machine.

**Table 4.9** The energy response of TLD-100 chips in kilovoltage relative to  $^{60}\text{Co}$  gamma rays at absorbed dose of 50 mGy.

kVp	Effective energy (MeV)	HVL (mm Al)	TLD reading (nC)	Ratio of kilovoltage response relative to $^{60}\text{Co}$	CF
70	0.033	2.80	295.18	1.358	0.7363
80	0.035	3.31	294.27	1.354	0.7386
90	0.037	3.71	291.37	1.341	0.7459
100	0.04	4.28	291.00	1.339	0.7469
Ir-192	0.38	27.0	223.38	1.023	0.9730
Co-60	1.25	45.0	217.34	1.000	1.0000

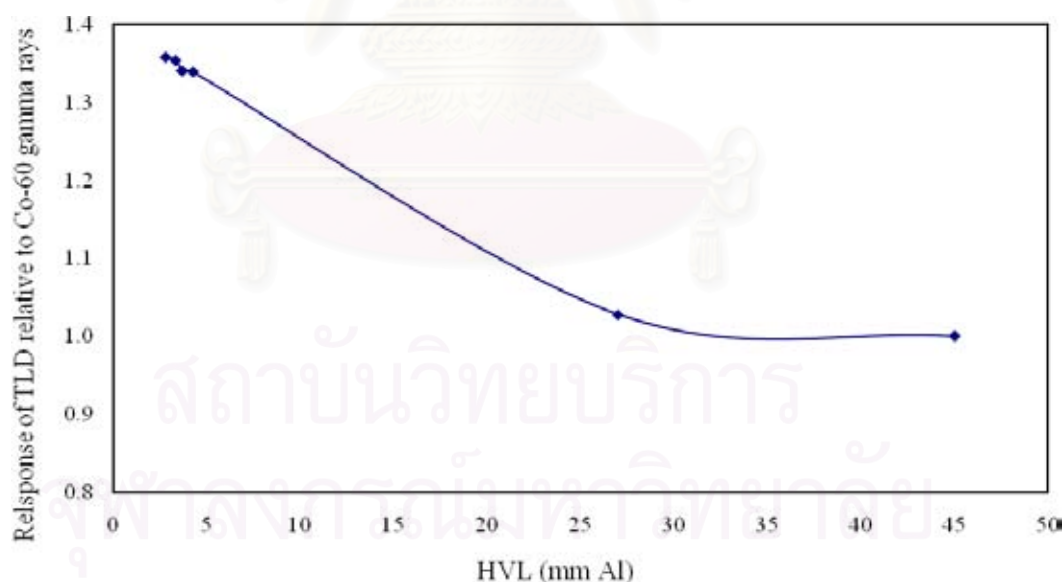


**Figure 4.7** Energy responses of LiF TLD-100 chips when irradiated in water phantom normalized to  $^{60}\text{Co}$  gamma rays at the absorbed dose of 50 mGy.

#### 4.3.4 Minimum detectable dose

The characteristics of thermoluminescent dosimeter which are including variation coefficient (VC) of some dose values, background and minimum detectable dose are reported in Table 4.10. In this study the minimum detectable dose of TLD-100 chips ranged from 0.005 to 0.022 mGy with the mean value of 0.013.

**Table 4.10** The minimum detectable dose.

Times	The minimum detectable dose of TLDs			
	Mean background values (mGy)	Standard deviation (SD)	Variation coefficient (VC)	Minimum detectable dose (MDD) (mGy)
1	0.058	0.007	0.126	0.022
2	0.031	0.004	0.123	0.011
3	0.032	0.004	0.165	0.016
4	0.026	0.003	0.116	0.009
5	0.031	0.005	0.150	0.014
6	0.024	0.003	0.123	0.009
7	0.035	0.004	0.103	0.011
8	0.036	0.003	0.105	0.009
9	0.037	0.005	0.131	0.014
10	0.034	0.005	0.149	0.015
11	0.062	0.007	0.111	0.021
12	0.026	0.004	0.162	0.012
13	0.033	0.005	0.141	0.014
14	0.048	0.005	0.112	0.016
15	0.033	0.005	0.141	0.014
16	0.027	0.002	0.069	0.005

#### 4.4 Measurement of fetal doses in RANDO phantom

##### 4.4.1 Pelvic AP examination

The absorbed doses measured at the surface, 3, 6 and 9 cm for pelvic AP examination for 70, 80, 90 and 100 kVp, are shown in Table 4.11. The doses also decreased as the kVp increased and reduced with the depth as the result from the parameter calculation. The surface dose ranged from 1.52 mGy to 3.14 mGy for 100 kVp to 70 kVp at the surface while, at 6.0 cm depth which was the depth of fetal level, the doses ranged from 0.83 mGy to 1.39 mGy.

**Table 4.11** The fetal doses in RANDO phantom from TLDs measurement of pelvic AP examination.

Mean fetal dose (mGy) from TLDs measurements in each depth and various kVp				
Depth (cm)	70 kVp	80 kVp	90 kVp	100 kVp
0	3.14	2.63	2.22	1.52
3	2.26	1.97	1.74	1.22
6	1.39	1.26	1.14	0.83
9	0.80	0.76	0.71	0.52

#### 4.4.2 Abdomen AP examination

The absorbed doses measured at the surface, 3, 6 and 9 cm for abdomen AP examination for 70, 80, 90 and 100 kVp, are shown in Table 4.12. The surface doses ranged from 0.99 mGy to 2.03 mGy for 100 kVp to 70 kVp at the surface while, at 6.0 cm depth which was the depth of fetal site, the doses ranged from 0.55 mGy to 0.87 mGy. The surface and fetal doses at various depths were lower than the pelvic examination due to the difference of exposure techniques and also the fetal site was about 5 cm far from the center of the beam, while in pelvic examination the fetal site was at the center of the beam.

**Table 4.12** The fetal doses in RANDO phantom from TLDs measurement of abdomen AP examination.

Mean fetal dose (mGy) from TLDs measurements in each depth and various kVp				
Depth (cm)	70 kVp	80 kVp	90 kVp	100 kVp
0	2.03	1.67	1.25	0.99
3	1.42	1.21	0.94	0.78
6	0.87	0.76	0.62	0.55
9	0.49	0.44	0.38	0.36

#### 4.4.3 Lumbo-sacral spine AP examination

The absorbed doses measured at the surface, 3, 6 and 9 cm for lumbo-sacral spine AP examination for 70, 80, 90 and 100 kVp, are shown in Table 4.13. The surface dose ranged from 0.98 mGy to 2.88 mGy for 100 kVp to 70 kVp at the surface, while at 6.0 cm depth which was the depth of fetal site, the doses ranged from 0.46 mGy to 1.1 mGy. The doses at the surface and at various depths showed lower value than pelvic AP examination and abdomen AP examination, this is due to the fetal site was about 8 cm far from the center of the beams.

**Table 4.13** The fetal doses in RANDO phantom from TLDs measurement of lumbo-sacral spine AP examination.

Mean fetal dose (mGy) from TLDs measurements in each depth and various kVp				
Depth (cm)	70 kVp	80 kVp	90 kVp	100 kVp
0	2.88	1.77	1.18	0.98
3	1.90	1.26	0.87	0.73
6	1.10	0.77	0.54	0.46
9	0.61	0.46	0.33	0.28

#### 4.4.4 Lumbo-sacral spine LAT examination

The absorbed doses measured at the surface, 13, 16 and 19 cm for lumbo-sacral spine LAT examination for 70, 80, 90 and 100 kVp, are shown in Table 4.14. The surface doses ranged from 1.38 mGy to 3.74 mGy for 100 kVp to 70 kVp at the surface, the doses were higher than the other procedures because the focus to surface distance has shorter distance than pelvic AP, abdomen AP and lumbo-sacral spine AP examination. The fetal depth was 16.0 cm, it was deeper than the AP field so the doses reduced and ranged from 0.15 mGy to 0.2 mGy.

**Table 4.14** The fetal doses in RANDO phantom from TLDs measurement of lumbo-sacral spine LAT examination.

Mean fetal dose (mGy) from TLDs measurements in each depth and various kVp				
Depth (cm)	70 kVp	80 kVp	90 kVp	100 kVp
0	3.74	2.43	1.47	1.38
13	0.33	0.26	0.22	0.21
16	0.20	0.17	0.15	0.15
19	0.12	0.12	0.11	0.10

#### 4.5 Estimation of uncertainties for TLDs measurement and exposure parameter calculation

The uncertainties were estimated to determine the error of fetal dose from TLDs measurement method and exposure parameter calculation method, they are shown in Table 4.14 and Table 4.15, respectively. The uncertainty of TLDs measurement equals to 9.42% with 95% confidence level. The uncertainty of exposure parameter calculation equals to 8.14% with 95% confidence level.

**Table 4.15** The uncertainty budget to estimate the relative expanded uncertainty of TLDs measurement.

Source of uncertainty	Standard deviation value ( $\sigma$ )	$n$	Standard deviation of mean	Divisor	%uncertainty
1.TLD sensitivity	4.29	1	4.29	1	4.29
2.TLD calibration					
-TLDs	1.72	1	1.72	1	1.72
-Ionization chamber	0.10	2	0.07	1	0.07
3.TLD energy response	0.61	1	0.61	1	0.61
4.Calibration factor of ionization chamber	0.60	1	0.60	2	0.30
5.Measuring accuracy	2.44	16	16	1	0.61
Combined standard uncertainty					
$u_c(s) = \sqrt{(4.29)^2 + (1.72)^2 + (0.07)^2 + (0.61)^2 + (0.30)^2 + (0.61)^2} = 4.71\%$					
Expanded uncertainty, coverage factor $k = 2$ , $U = 2 \times 4.71 = 9.42\%$					

**Table 4.16** The uncertainty budget to estimate the relative expanded uncertainty of exposure parameter calculation.

Source of uncertainty	Standard deviation value ( $\sigma$ )	$n$	Standard deviation of mean	Divisor	%uncertainty
1.Calibration factor of ionization chamber (victoreen 4000M+)	4	1	4	2	2.0
2.Measurement accuracy					
Repeatability of x-ray machine	0.55	4	0.28	1	0.28
3.BSF (Harrison,1982)[38]			2.5	1	2.5
4.Percentage depth dose			2.5	1	2.5
Combined standard uncertainty $u_c(s) = \sqrt{(2.0)^2 + (0.28)^2 + (2.5)^2 + (2.5)^2} = 4.07\%$					
Expanded uncertainty, coverage factor $k = 2$ , $U = 2 \times 4.54 = 8.14\%$					

## 4.6 Comparison of fetal doses from TLDs measurement and exposure parameter calculation

### 4.6.1 The fetal doses from pelvic AP examination

The comparisons of absorbed doses from TLDs measurement and parameter calculation of pelvic AP examination together with the percentage normalized dose differences are shown in Table 4.17, the graphs were plotted with the uncertainty of each data point and are shown in Figure 4.8, Figure 4.9, Figure 4.10 and Figure 4.11 for 70 kVp, 80 kVp, 90 kVp and 100 kVp, respectively. The graphs showed the correlation coefficient of 0.992 to 0.997 for TLDs measurement and 0.978 to 0.993 for parameter calculation.

All of the TLD values showed higher doses than the calculation. The difference tended to decreased as the depth increased. The percentage differences of doses for all kVp studied ranged from 12.42% to 14.41%, 14.33% to 18.47%, 11.46% to 13.81% and 7.01% to 9.21% for surface, 3, 6 and 9 cm, respectively. The differences were agreeable for various kVp at the fixed depth.

**Table 4.17** The comparisons of fetal doses in term of the percentage normalized dose difference between TLDs measurement and parameter calculation for pelvic AP examination.

Fetal dose (mGy) from TLDs measurement and parameter calculation and %normalized dose diff.												
Depth (cm)	70 kVp			80 kVp			90 kVp			100 kVp		
	TLDs	Cal.	%Diff	TLDs	Cal.	%Diff.	TLDs	Cal.	%Diff.	TLDs	Cal.	%Diff.
0	3.14	2.75	12.42	2.63	2.28	13.31	2.22	1.90	14.41	1.52	1.31	13.83
3	2.26	1.81	14.33	1.97	1.55	15.97	1.74	1.33	18.47	1.22	0.98	15.79
6	1.39	1.03	11.46	1.26	0.91	13.31	1.14	0.86	12.61	0.83	0.62	13.81
9	0.80	0.58	7.01	0.76	0.55	7.98	0.71	0.51	9.01	0.52	0.38	9.21



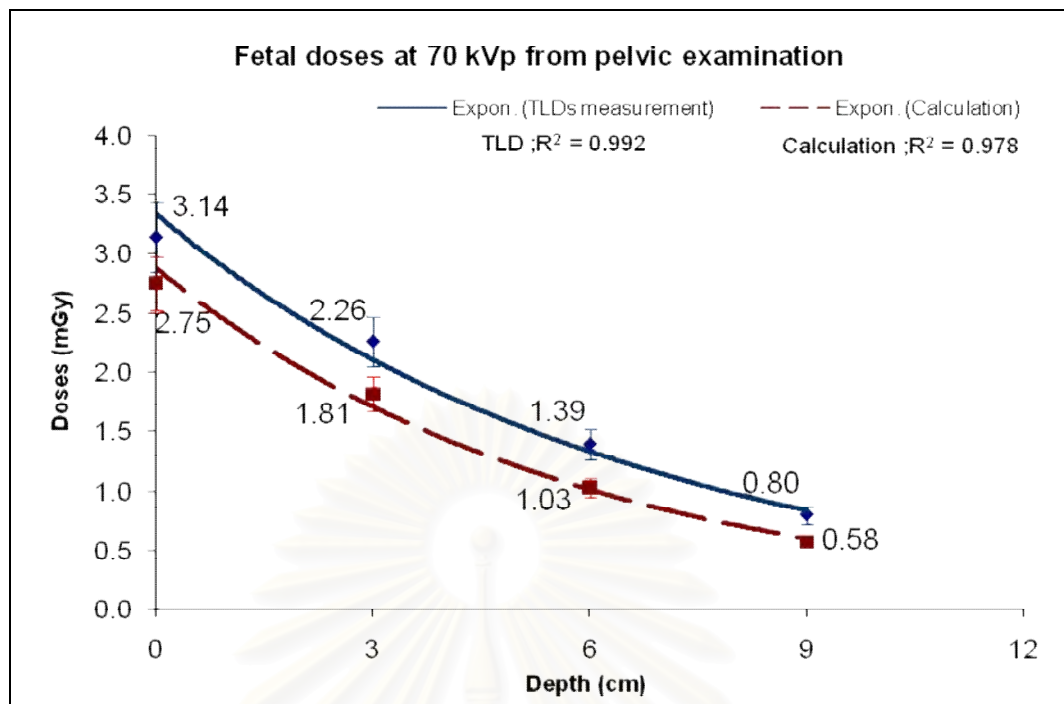


**Figure 4.8** Fetal doses of TLDs measurement and parameter calculation in RANDO phantom of pelvic AP examination at 70 kVp, the error bars showed the uncertainty of 9.42% for measurement and 8.14% for calculation.

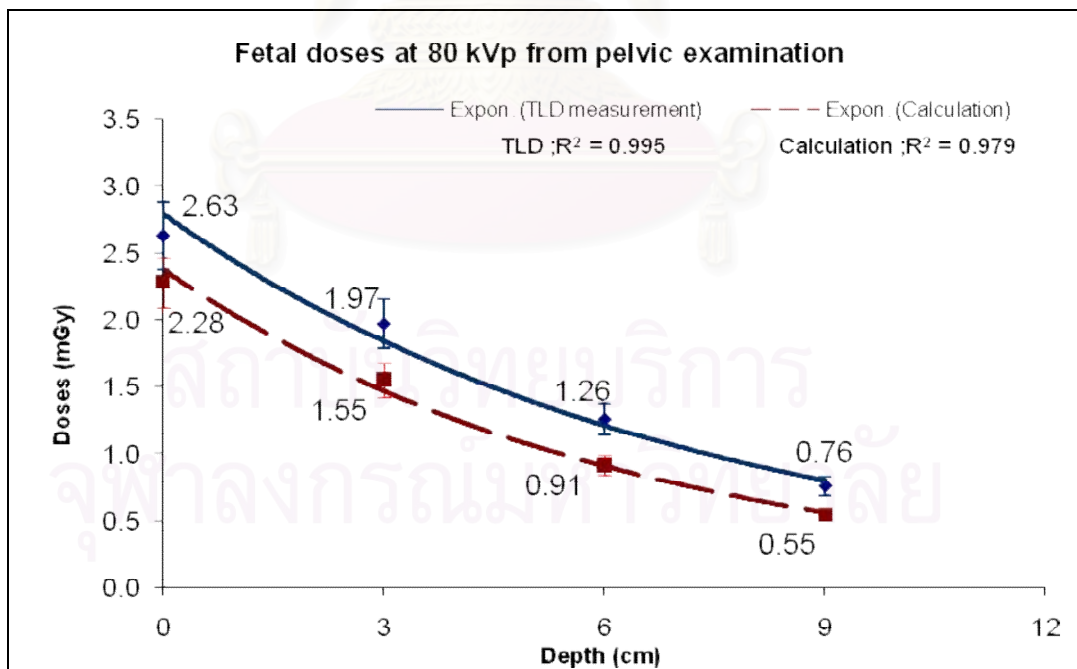


**Figure 4.9** Fetal doses of TLDs measurement and parameter calculation in RANDO phantom of pelvic AP examination at 80 kVp, the error bars showed the uncertainty of 9.42% for measurement and 8.14% for calculation.

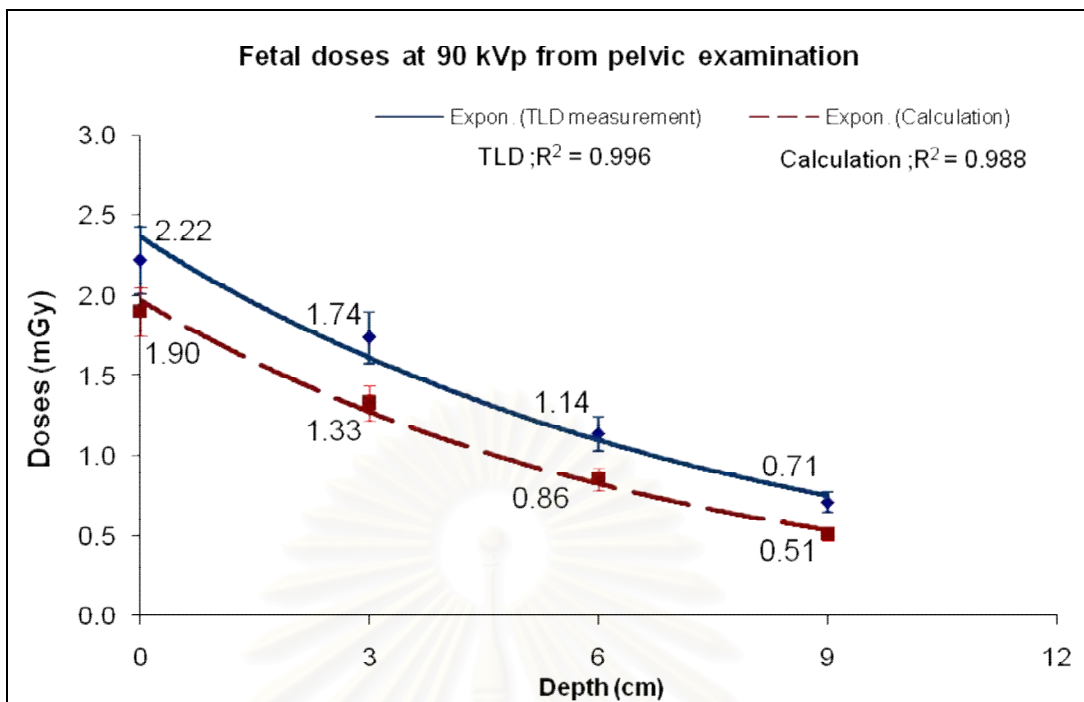


**Figure 4.10** Fetal doses of TLDs measurement and parameter calculation in RANDO phantom of pelvic AP examination at 90 kVp, the error bars showed the uncertainty of 9.42% for measurement and 8.14% for calculation.

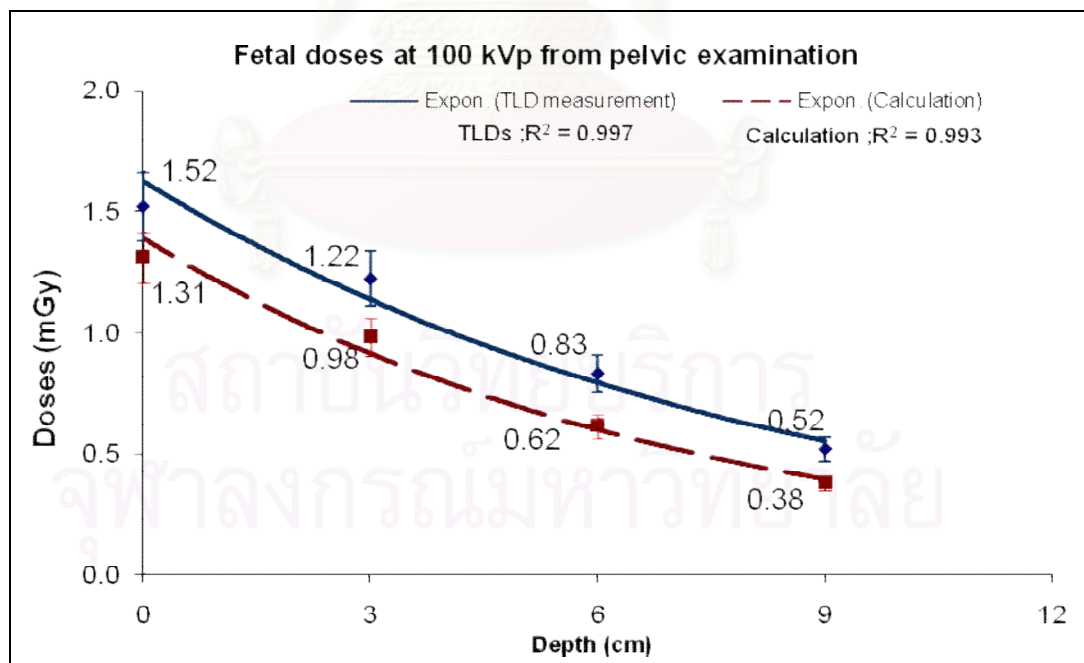


**Figure 4.11** Fetal doses of TLDs measurement and parameter calculation in RANDO phantom of pelvic AP examination at 100 kVp, the error bars showed the uncertainty of 9.42% for measurement and 8.14% for calculation.

#### 4.6.2 The fetal doses from abdomen AP examination

The comparisons of absorbed doses from TLDs measurement and parameter calculation of abdomen AP examination together with the percentage normalized dose differences are shown in Table 4.18, the graphs were plotted with the uncertainty of each data point and are shown in Figure 4.12, Figure 4.13, Figure 4.14 and Figure 4.15 for 70 kVp, 80 kVp, 90 kVp and 100 kVp, respectively. The graphs showed the correlation coefficient of 0.989 to 0.988 for TLDs measurement and 0.978 to 0.993 for parameter calculation.

All of the TLD values also showed higher doses than the calculation. The difference tended to decreased as the depth increased. However, the percentage normalized dose differences showed large variation when varying kVp for each fixed depth which was contrary to the result of pelvic examination. The percentage differences of normalized doses for all kVp studied ranged from 11.33% to 23.23%, 11.33% to 21.21%, 9.85% to 19.19% and 5.41% to 14.14% for surface, 3, 6 and 9 cm, respectively.

**Table 4.18** The comparisons of fetal doses in term of the percentage normalized dose differences between TLDs measurement and exposure parameter calculation for abdomen AP examination.

Fetal dose (mGy) from TLDs measurement and parameter calculations and %normalized dose diff.												
Depth (cm)	70 kVp			80 kVp			90 kVp			100 kVp		
	TLDs	Cal.	%Diff	TLDs	Cal.	%Diff.	TLDs	Cal.	%Diff.	TLDs	Cal.	%Diff.
0	2.03	1.80	11.33	1.67	1.33	20.36	1.25	1.01	19.2	0.99	0.76	23.23
3	1.42	1.19	11.33	1.21	0.91	17.96	0.94	0.71	18.4	0.78	0.57	21.21
6	0.87	0.67	9.85	0.76	0.53	13.77	0.62	0.45	13.6	0.55	0.36	19.19
9	0.49	0.38	5.41	0.44	0.32	7.18	0.38	0.27	8.8	0.36	0.22	14.14

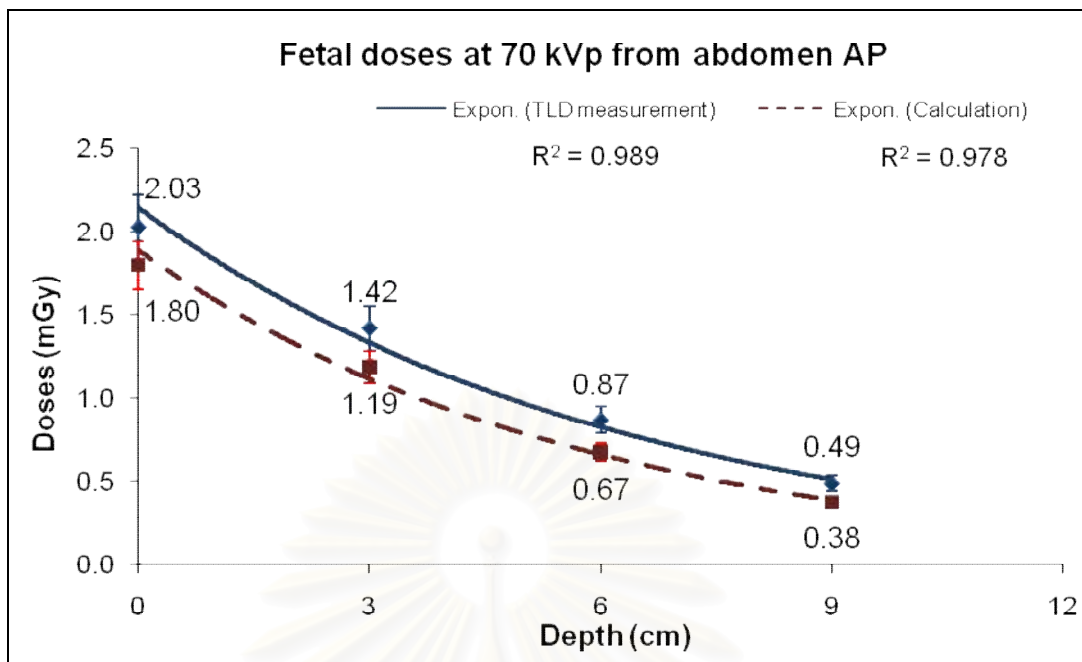


**Figure 4.12** Fetal doses of TLDs measurement and parameter calculation in RANDO phantom of abdomen AP examination at 70 kVp, the error bars showed the uncertainty of 9.42% for measurement and 8.14% for calculation.

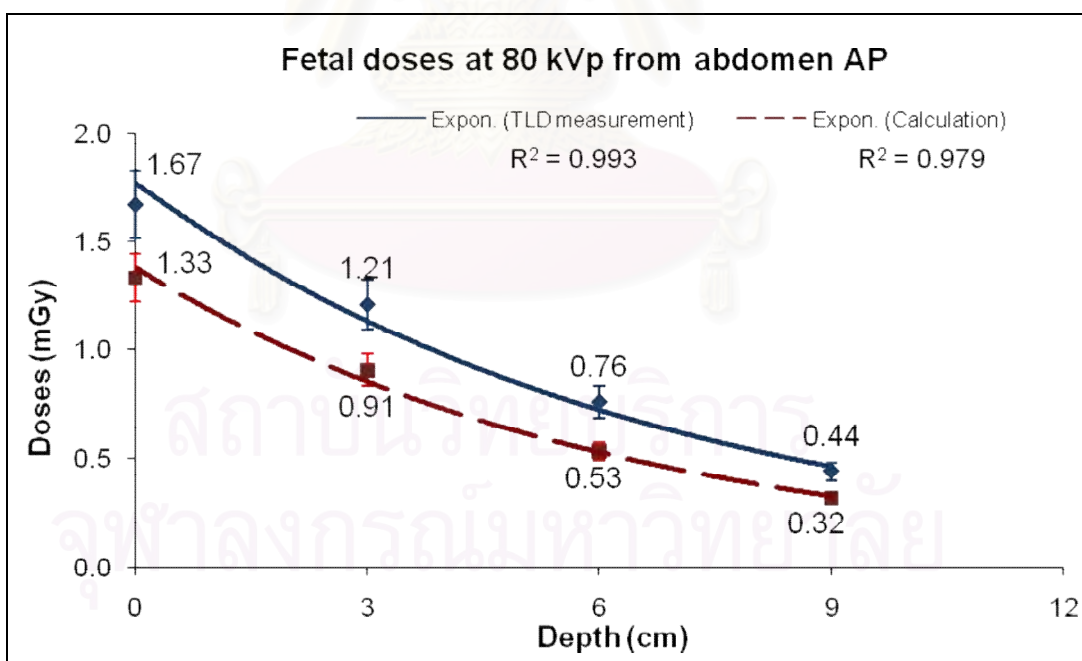


**Figure 4.13** Fetal doses of TLDs measurement and parameter calculation in RANDO phantom of abdomen AP examination at 80 kVp, the error bars showed the uncertainty of 9.42% for measurement and 8.14% for calculation.

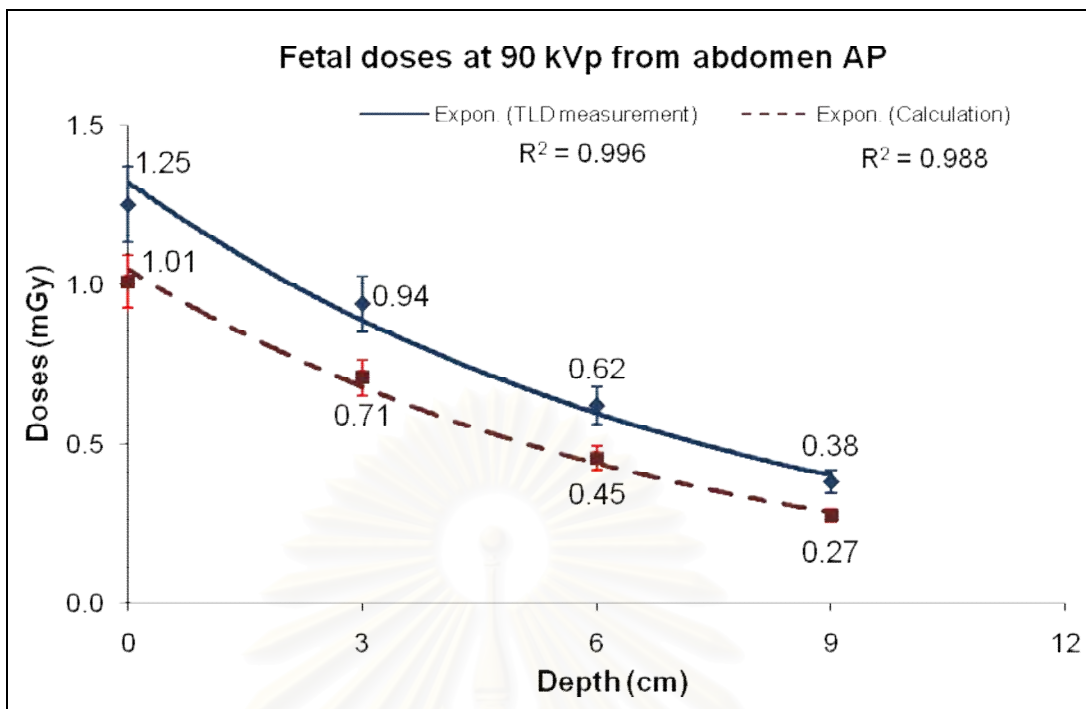


**Figure 4.14** Fetal doses of TLDs measurement and parameter calculation in RANDO phantom of abdomen AP examination at 90 kVp, the error bars showed the uncertainty of 9.42% for measurement and 8.14% for calculation.

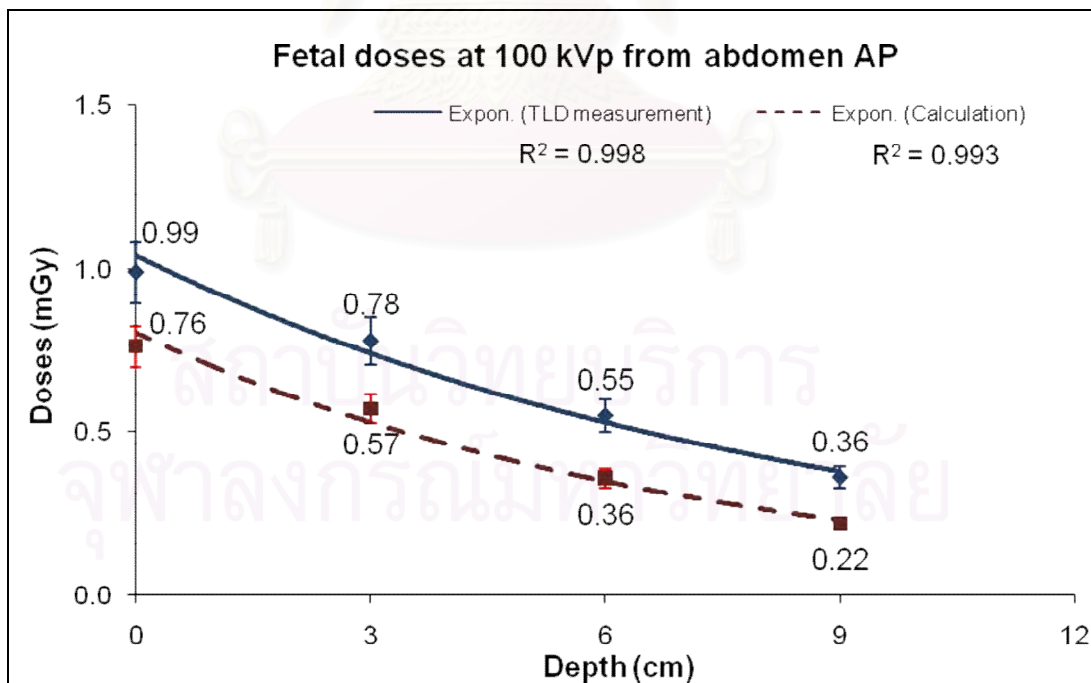


**Figure 4.15** Fetal doses of TLDs measurement and parameter calculation in RANDO phantom of abdomen AP examination at 100 kVp, the error bars showed the uncertainty of 9.42% for measurement and 8.14% for calculation.

#### 4.6.3 The fetal doses from lumbo-sacral spine AP examination

The comparisons of absorbed doses from TLDs measurement and parameter calculation of lumbo-sacral spine AP examination together with the percentage normalized dose differences are shown in Table 4.19, the graphs were plotted with the uncertainty of each data point and are shown in Figure 4.16, Figure 4.17, Figure 4.18 and Figure 4.19 for 70 kVp, 80 kVp, 90 kVp and 100 kVp, respectively. The graphs showed the correlation coefficient of 0.979 to 0.989 for TLDs measurement and 0.978 to 0.994 for parameter calculation.

All of the TLD measurement value showed the higher value than calculation. The percentage differences of normalized doses for all kVp studied ranged from 2.77% to 5.65%, 1.74% to 6.78%, 1.74% to 5.65% and 0.69% to 3.39% for surface, 3, 6 and 9 cm, respectively.

**Table 4.19** The comparisons of fetal doses in term of the percentage normalized dose differences between TLDs measurement and parameter calculation for lumbo-sacral spine AP examination.

Fetal dose (mGy) from TLDs measurement and parameter calculation and %normalized dose diff.												
Depth (cm)	70 kVp			80 kVp			90 kVp			100 kVp		
	TLDs	Cal.	%Diff	TLDs	Cal.	%Diff.	TLDs	Cal.	%Diff.	TLDs	Cal.	%Diff.
0	2.88	2.80	2.77	1.77	1.67	5.65	1.18	1.14	3.39	0.98	0.94	4.08
3	1.90	1.85	1.74	1.26	1.14	6.78	0.87	0.80	5.93	0.73	0.71	2.04
6	1.10	1.05	1.74	0.77	0.67	5.65	0.54	0.51	2.54	0.46	0.44	2.04
9	0.61	0.59	0.69	0.46	0.40	3.39	0.33	0.31	1.69	0.28	0.27	1.02

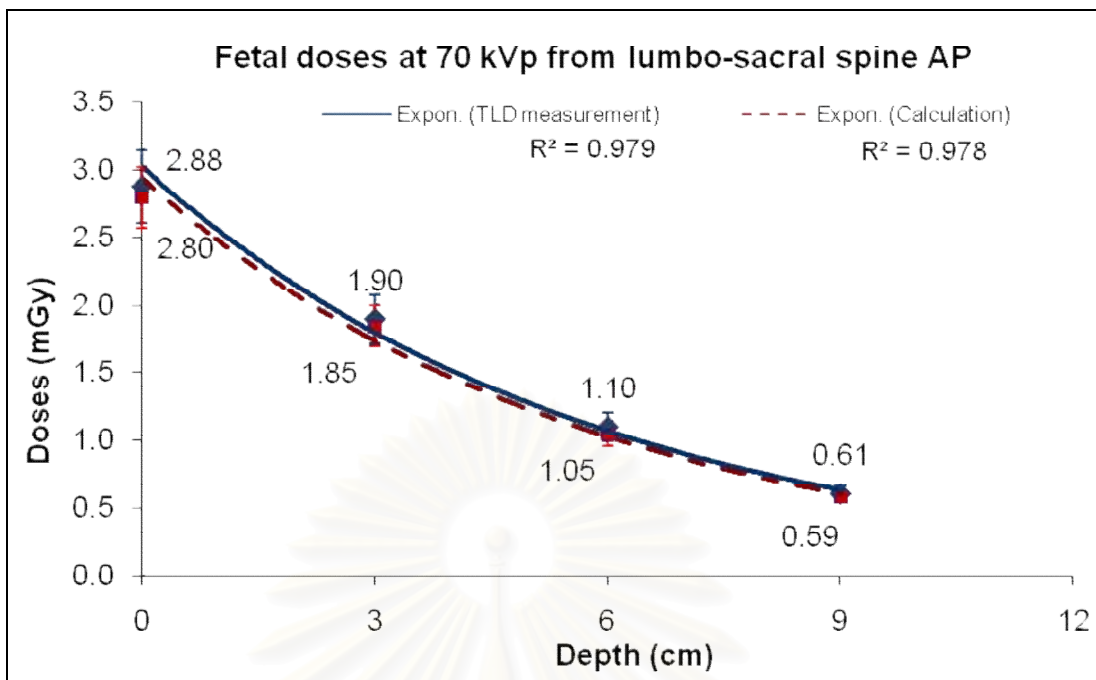


**Figure 4.16** Fetal doses of TLDs measurement and parameter calculation in RANDO phantom of lumbo-sacral spine AP examination at 70 kVp, the error bars showed the uncertainty of 9.42% for measurement and 8.14% for calculation.

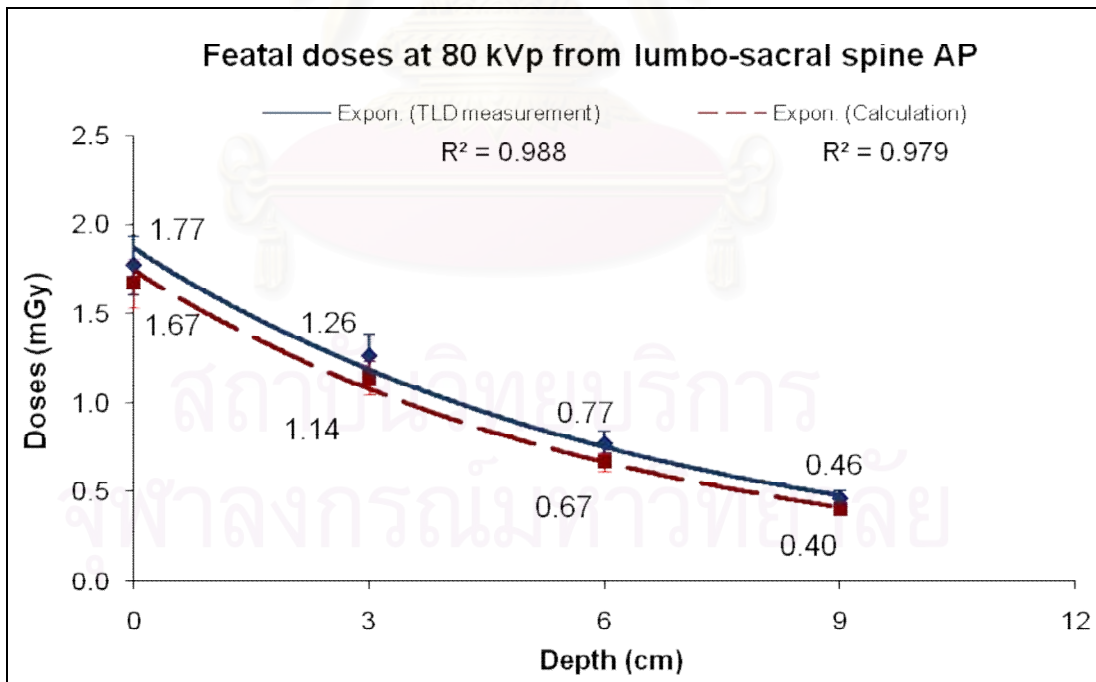


**Figure 4.17** Fetal doses of TLDs measurement and parameter calculation in RANDO phantom of lumbo-sacral spine AP examination at 80 kVp, the error bars showed the uncertainty of 9.42% for measurement and 8.14% for calculation.

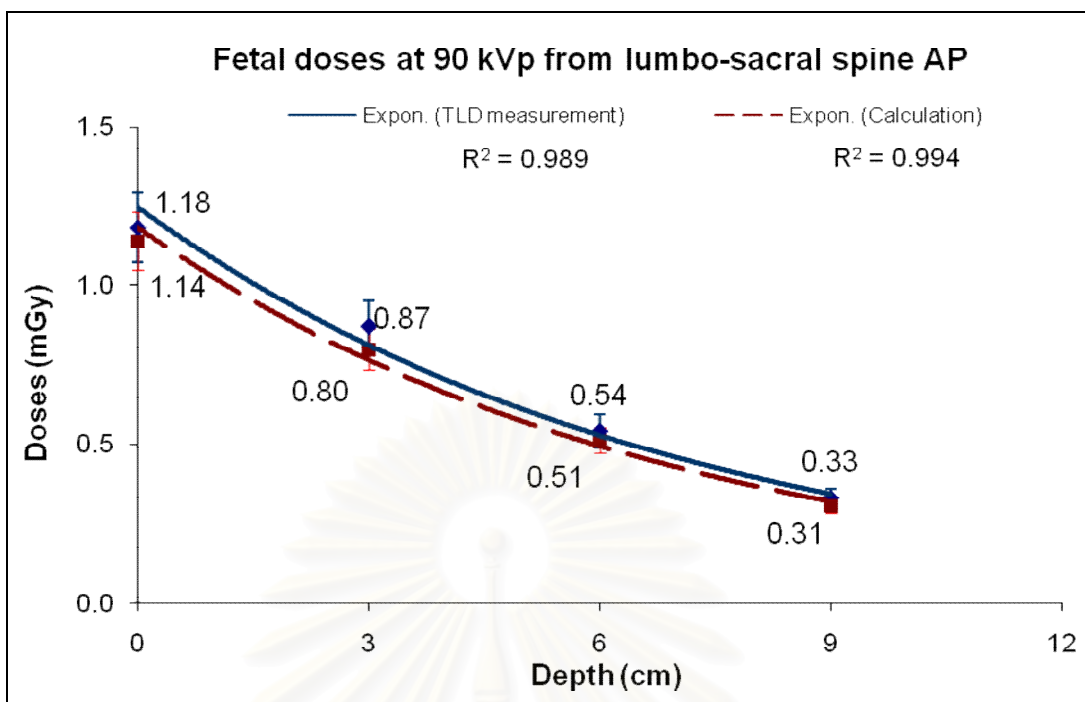


**Figure 4.18** Fetal doses of TLDs measurement and parameter calculation in RANDO phantom of lumbo-sacral spine AP examination at 90 kVp, the error bars showed the uncertainty of 9.42% for measurement and 8.14% for calculation.

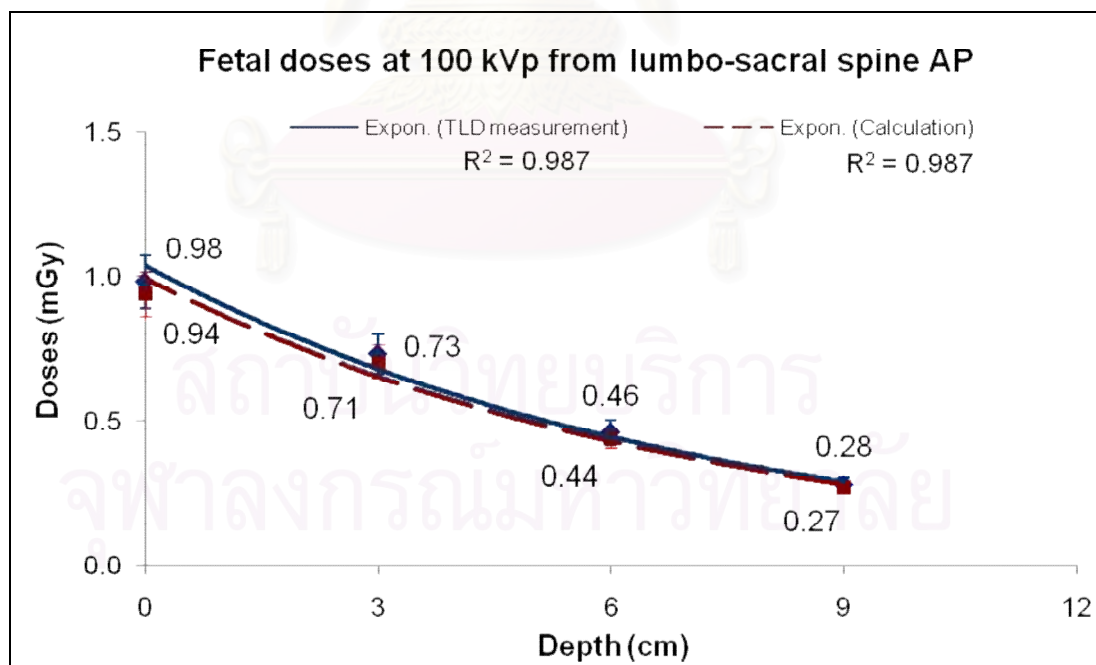


**Figure 4.19** Fetal doses of TLDs measurement and parameter calculation in RANDO phantom of lumbo-sacral spine AP examination at 100 kVp, the error bars showed the uncertainty of 9.42% for measurement and 8.14% for calculation.



#### 4.6.4 The fetal doses from lumbo-sacral spine LAT examination

The comparisons of absorbed doses from TLDs measurement and parameter calculation of lumbo-sacral spine AP examination together with the percentage normalized dose differences are shown in Table 4.20, the graphs were plotted with the uncertainty of each data point and are shown in Figure 4.20, Figure 4.21, Figure 4.22 and Figure 4.23 for 70 kVp, 80 kVp, 90 kVp and 100 kVp, respectively. The graphs showed the correlation coefficient of 0.979 to 0.989 for TLDs measurement and 0.978 to 0.994 for parameter calculation.

Most of the TLDs measurement value was higher than calculation, only some measurement showed lower values. The percentage differences of normalized doses for all kVp studied ranged from 0.34% to 1.02%, 0.35% to 1.02%, 0.00% to 3.95% and 0.00% to 2.26% for surface, 13, 16 and 19 cm, respectively. The surface dose showed large variation when varying kVp, but the doses at the deeper depth was low so the difference when varying kVp for fixed depth became low.

**Table 4.20** The comparisons of fetal doses in term of the percentage normalized dose difference between TLDs measurement and exposure parameter calculation for lumbo-sacral spine LAT examination.

Fetal dose (mGy) from TLDs measurement and parameter calculation and %normalized dose diff.												
Depth (cm)	70 kVp			80 kVp			90 kVp			100 kVp		
	TLDs	Cal.	%Diff	TLDs	Cal.	%Diff.	TLDs	Cal.	%Diff.	TLDs	Cal.	%Diff.
0	3.74	4.07	-9.62	2.43	1.86	23.46	1.47	1.22	17.01	1.38	1.12	18.84
13	0.33	0.41	-2.14	0.26	0.22	1.65	0.22	0.17	3.40	0.21	0.17	2.90
16	0.20	0.24	-1.07	0.17	0.13	1.65	0.15	0.13	1.40	0.15	0.13	1.45
19	0.12	0.15	-0.8	0.12	0.10	0.82	0.11	0.09	1.36	0.10	0.10	0

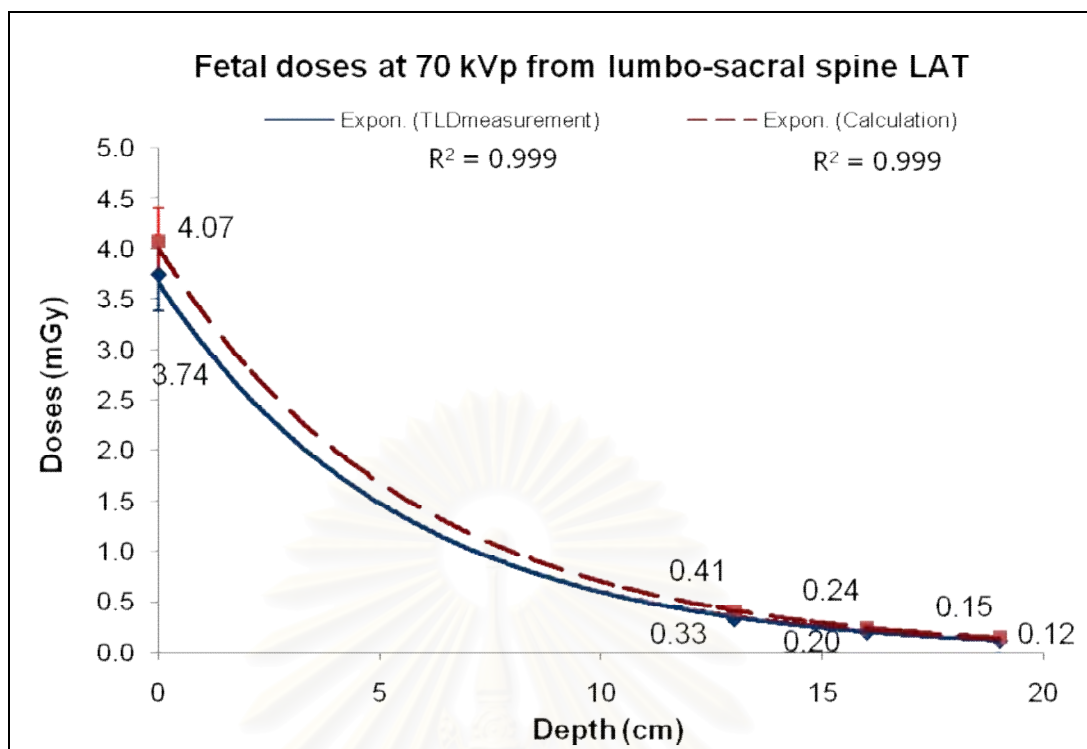


**Figure 4.20** Fetal doses of TLDs measurement and parameter calculation in RANDO phantom of lumbo-sacral spine LAT examination at 70 kVp, the error bars showed the uncertainty of 9.42% for measurement and 8.14% for calculation.

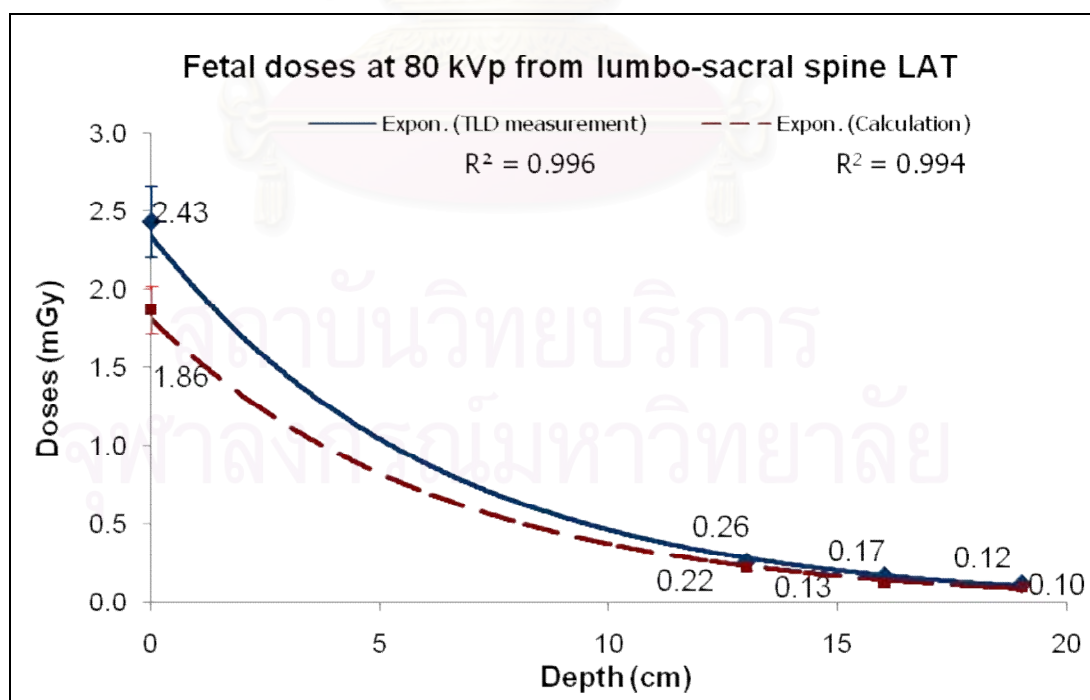


**Figure 4.21** Fetal doses of TLDs measurement and parameter calculation in RANDO phantom of lumbo-sacral spine LAT examination at 80 kVp, the error bars showed the uncertainty of 9.42% for measurement and 8.14% for calculation.

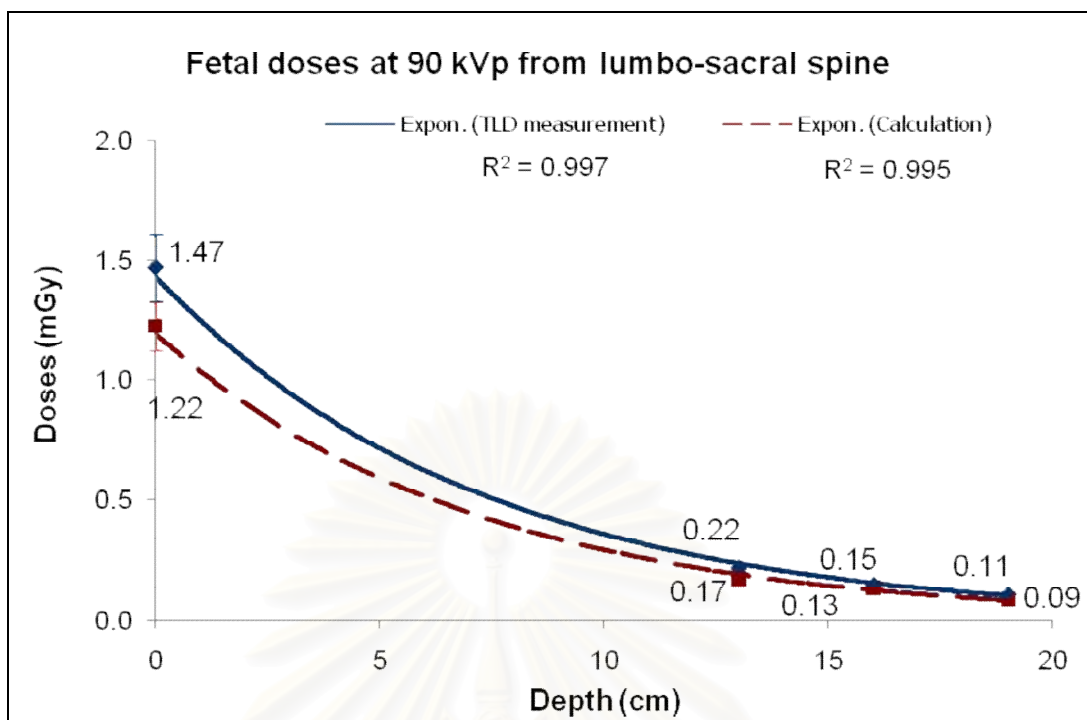


**Figure 4.22** Fetal doses of TLDs measurement and parameter calculation in RANDO phantom of lumbo-sacral spine LAT examination at 90 kVp, the error bars showed the uncertainty of 9.42% for measurement and 8.14% for calculation.

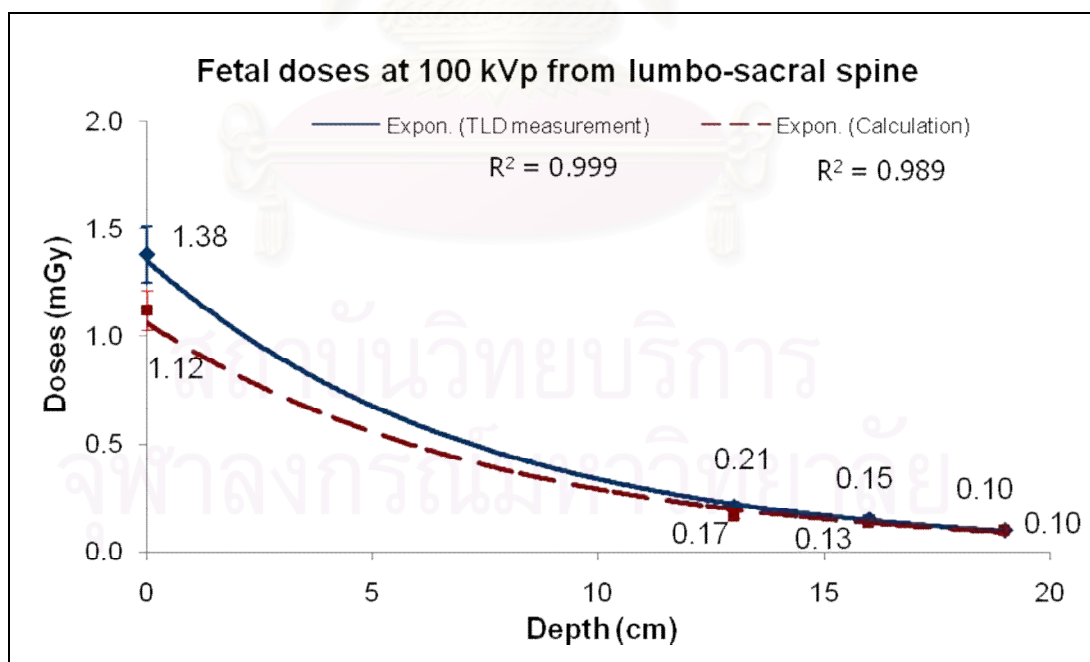


**Figure 4.23** Fetal doses of TLDs measurement and parameter calculation in RANDO phantom of lumbo-sacral spine LAT examination at 100 kVp, the error bars showed the uncertainty of 9.42% for measurement and 8.14% for calculation.

## 4.7 Correlation of fetal doses between TLDs measurement and exposure parameter calculation

4.7.1 Correlation of fetal doses between TLDs measurement and parameter calculation for various depths.

The absorbed doses obtained from TLDs measurements and parameter calculations were plotted in a wide range of doses at various depths for all procedures and kVp used, they are shown in Figure 4.24. The curve showed good correlation between TLD measurement and calculation with the correlation coefficient of 0.967.

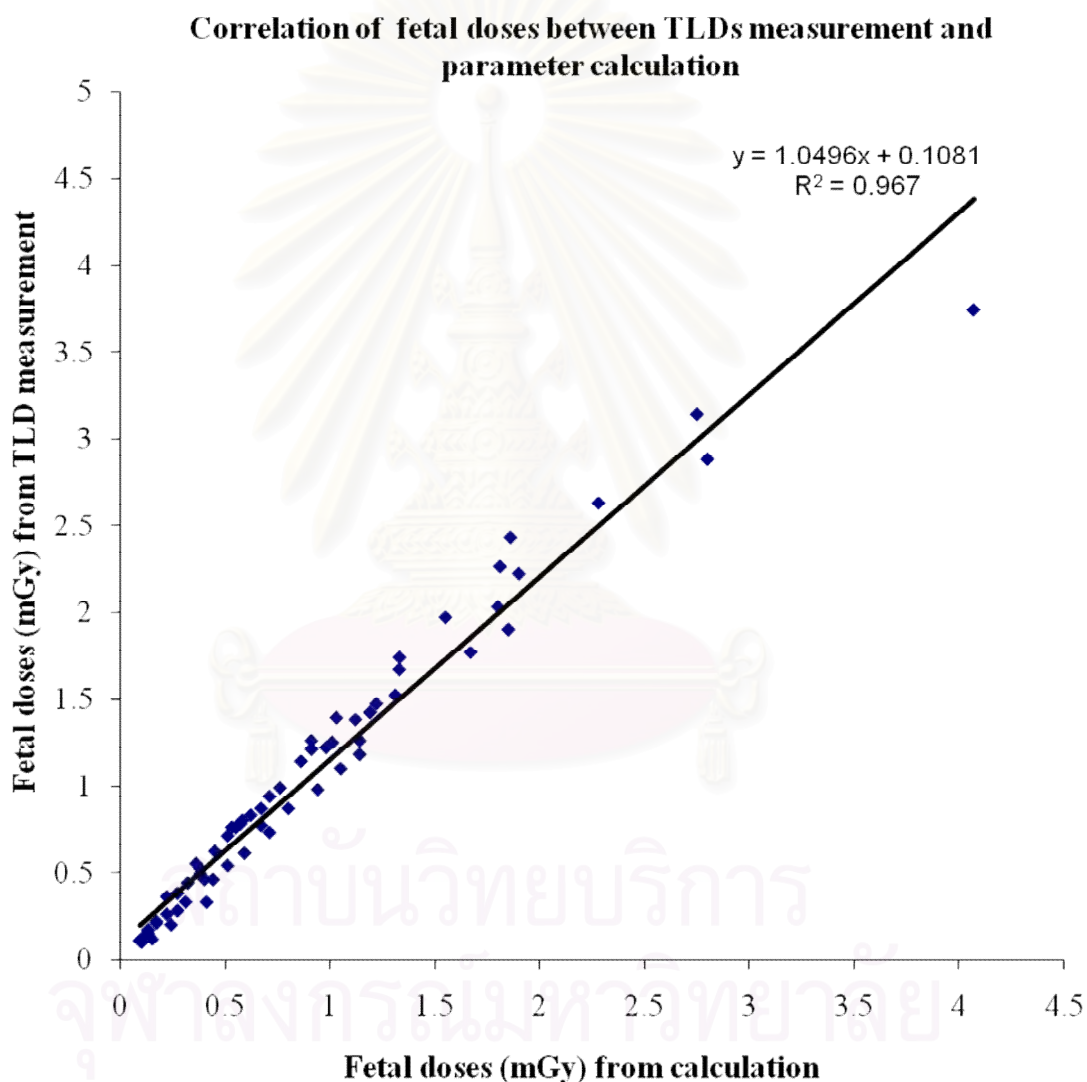


**Figure 4.24** Correlation of fetal doses between TLDs measurement and parameter calculation for various depths.

#### 4.7.2 Correlation of fetal doses at fetal level

The fetal doses obtained from TLDs measurement and parameter calculation at the fetal level were plotted for all procedures and kVp used, they are shown in Figure 4.25. The curve showed acceptable correlation between TLDs measurement and parameter calculation with the correlation coefficient of 0.938.

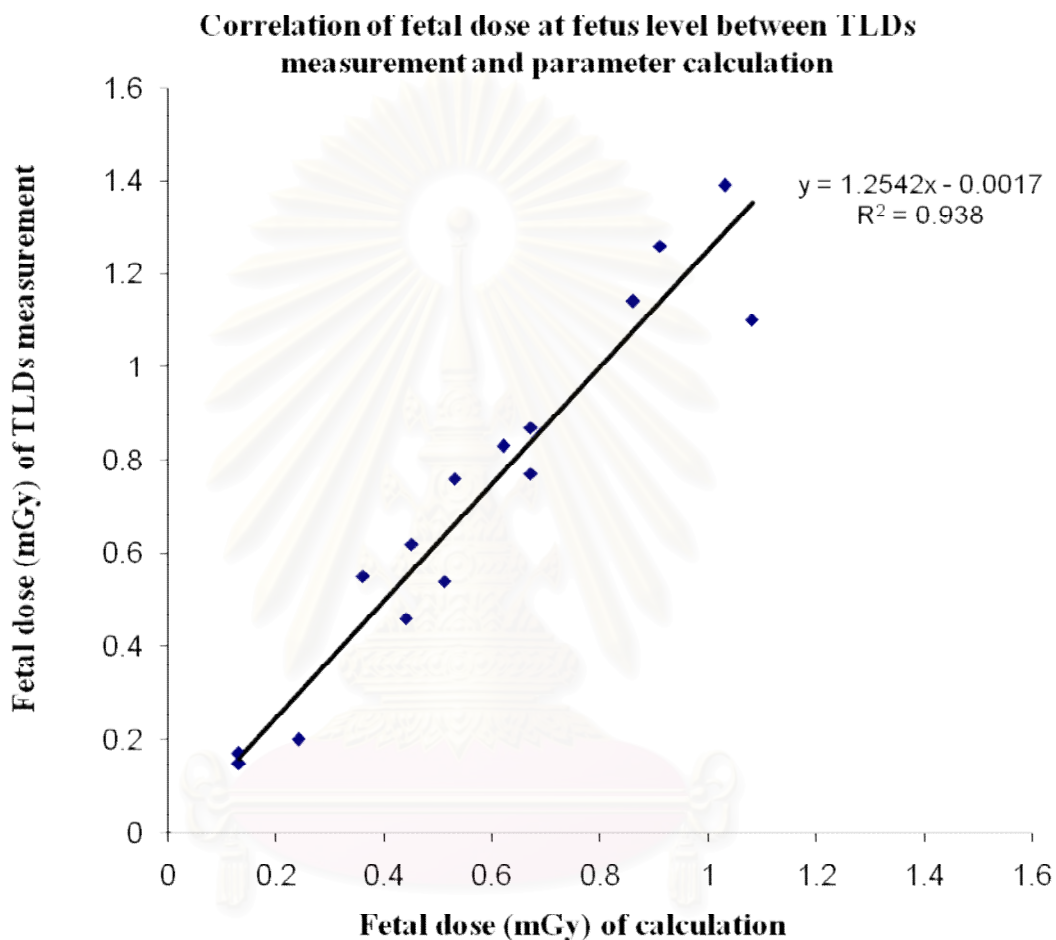


**Figure 4.25** Correlation of fetal doses at fetus level between TLDs measurement and parameter calculation.

# CHAPTER 5

## DISCUSSION AND CONCLUSION

### 5.1 Discussion

The increasing use of ionizing radiation in hospitals has made medical exposure an important source of radiation in the population dose. Diagnostic x-ray examinations are carried out in pregnant patients in clinical practice either accidentally or because of clinical urgency. The risk is dependent on the gestational age and the amount of radiation dose absorbed by the conceptus. Under normal operating conditions, conceptus dose from extra-abdominal examination are lower than 1 mGy [5]. In the case of examination involving the abdomen or pelvis, dose to the embryo may be considerably higher in comparison with extra-abdominal examination. So estimation of the risk to the conceptus is importance. The determination of the equivalent dose to the fetus is interest as a basis for risk estimate. The quick method is to estimate the fetal dose from the exposure parameters. To confirm the actual dose to the fetus, the measurement in the phantom should be performed. For computed radiography that replaced the conventional radiography contributed more dose to the patients are obtained, so it is the reason that this study was undertaken in computed radiography for pelvis, abdomen and lumbo-sacral spine examination.

#### 5.1.1 Calibration and quality control of x-ray machine

AAPM task group No.4 protocol for quality control (QC) of the x-ray machine was used for the reference to evaluate the status of x-ray machine and components. It is an important task to be performed before starting this experiment because the accuracy of the results from the radiation output, beam quality were used to calculate the fetal dose.

#### 5.1.2 Calculation of fetal doses with the parameters

The doses from exposure parameters were calculated at the surface, 3, 6 and 9 cm depth. In this study, 6 cm depth was selected for the fetal site according to Hufton (1979) [33] who determine fetal depth of 6.3 cm for anterior pacentation (maternal skin surface to nearest fetal surface). The uncertainty of parameter calculation from uncertainty budget was 8.14% for 95% confidence level. The calculated doses depend on the x-ray procedure used, exposure parameters such as kVp, HVL, FSD, mAs and BSF. The parameters used to calculate the absorbed doses obtained from Wagner et al. (1997) [6], Tung et al. (1999) [17] and Damilakis et al. (1997) [20]. The absorbed doses was decreased when kVp was increased because the automatic exposure control was used, it made the mAs decrease when the kVp increased. The decreasing of mAs contributed the low dose for the high kVp technique. The dose at the fetal level for all examinations and kVp studies ranged from 0.13 to 1.05 mGy which the maximum was closed to 1 mGy of the ICRP dose limit to the fetus for both pregnant patient and radiation worker. The technique which the dose was more than 1 mGy occurred at 70

kVp in lumbo-sacral spine AP examination for the dose of 1.05 mGy and 70 kVp in pelvic AP examination for the dose of 1.03 mGy.

### 5.1.3 Thermoluminescent dosimeters calibration

The sensitivity, minimum detectable dose, linearity and energy response of TLDs were observed before using in the RANDO phantom for 70, 80, 90, 100 kVp, Ir-192 (0.38 MeV) and Co-60 (1.25 MeV). The sensitivity was applied for each chip of TLDs. The sensitivity ranged from 0.924 to 1.072. The minimum detectable dose was 0.013 mGy which mean that the doses lower than this value could not be measured. The result showed the good linearity between TLDs response and the absorbed dose. So any level of absorbed doses could be measured by this set of TLDs. The response of TLDs for kilovoltage x-ray beams were higher than the cobalt-60 gamma beams which was used for the calibration of TLDs, so the energy correction factor should be applied. The uncertainty of TLDs in the range of the beam studied from uncertainty budget was 9.42% for 95% confidence level. The TLDs parameters observed in this study agreed with the other studies [30].

### 5.1.4 Measurement of fetal doses in RANDO phantom

The TLDs measurements in each depth of RANDO phantom were obtained from 27 chips; the average dose was calculated for each depth. The dose at the fetal level ranged from 0.15 to 1.39 mGy with the maximum value was higher than the calculation. The pelvic AP technique gave the higher fetal dose of 1.39, 1.26 and 1.14 mGy for 70, 80 and 90 kVp respectively, while it was 1.1 mGy for 70 kVp in lumbo-sacral spine AP examination. The rest of the examinations contributed the dose less than the ICRP dose limit to the fetus. So the careful of the exposure technique of pelvic AP examination should be considered to reduce the fetal dose.

### 5.1.5 Comparison and correlation of fetal doses between TLDs measurement and parameter calculation

For all the examination except some technique of lumbo-sacral spine LAT, absorbed doses at all depth and kVp studied showed the higher dose of measured than calculated. The larger difference occurred at the surface and became smaller when the depths were increased. The highest difference of normalized doses was 23.46%. The difference of both methods may be caused by the method of dose determination. TLDs was calibrated by 0.6 cc ion chamber while the entrance surface dose using in calculation was obtained from Victoreen 4000M+ parallel plate chamber. The factors used for dose determination may also cause the uncertainty.

For the lumbo-sacral spine AP, the normalized absorbed doses difference were lower than the first two methods, the highest normalized dose difference was 6.78%. This is due to the TLDs were placed far from the central axis, while the calculation was made at the central axis. The effect caused some value of absorbed doses from TLDs lower than the calculation. The lower dose of TLDs at the off axis made the compensation for the higher dose of measurement so reduced the dose difference.

For the lumbo-sacral spine LAT, the normalized absorbed doses differences were high at the surface and became low at the deeper depth. The focus to surface

distance was shorter than the other techniques, so the doses at the surface were larger than the other techniques. The large differences also occurred at the surface and reduced for the depth. The highest normalized dose difference value was 23.46%.

The graphs of fetal doses from TLDs measurement and parameter calculation are shown in Figure 4.24 for various depths and Figure 4.25 for fetal depth. They showed a good correlation which mean that the calculation could be performed with the idea of lower dose than measurement within 23%.

#### 5.1.6 Comparison of another published works [19,39,40]

The comparison of fetal dose with the other studies which are the conventional radiography is shown in Table 5.1. Our fetal doses from TLDs are higher than fetal doses of Tung et al. and BrighamRAD but lower than the fetal dose from Baciak et al., However, our measurement showed higher dose than the ICRP dose limit of 1 mGy only for pelvis AP examination. While the study of Baciak et al. and BrighamRAD demonstrated higher fetal dose than 1 mGy for most of the examination. The difference of dose may be from the exposure technique, so the suitable technique to obtain low dose and high quality image should be selected for woman expected to have offspring.

**Table 5.1** The fetal doses from another published works compared with this study.

Examinations	Fetal dose (mGy)			
	Tung et al. (1999)	Baciak et al. (2000)	BrighamRAD (1994-2004)	This study
Pelvis AP	0.33	1.56	0.93	1.39
Abdomen AP	0.08	1.75	2.08	0.87
Lumbo-sacral spine AP	0.07	-	1.36	0.77
Lumbo-sacral spine LAT	0.06	0.78	0.59	0.15



## 5.2 Conclusion

The protection of the unborn children of pregnant women from diagnostic examination is very important because the fetus is damaged due to the effect of ionizing radiation. The pregnant patient or worker has a right to know the magnitude and type of potential radiation effects that might result from in utero exposure. The ICRP recommends that procedures causing exposures of the lower abdomen of women likely to be pregnant should be avoided unless there are strong clinical indications. So it is important to estimate the fetal dose to be the guideline for the pregnant patient underwent the radiographic examination.

Several methods have been developed to estimate conceptus dose from radiographic examination. Our method used the measured free air exposure from difference kVp, mAs, focus skin distance as the starting point, the entrance doses were calculated. Then the backscattered factors and percentage depth doses were employed for calculation the dose at any depth. The Toshiba x-ray machine model KXO-80G/DT-BTH/DST-100A with a tube of 150 kVp maximum was used in this study. The tube current and exposure time for each radiographic examination were adjusted by automatic exposure control. The estimated fetal doses were ranged from 0.13 to 1.05 mGy which mostly were in the ICRP dose limit of 1 mGy.

The thermoluminescence dosimeters, TLD-100 chip were used for direct measurement in Rando phantom, the sensitivity for each detector, linearity for the kVp used in this study together with the iridium-192 and cobalt-60 gamma rays, the minimum detectable and the energy response relative to cobalt-60 gamma rays were studied before using TLDs for the dose measurement. The fetal doses were ranged from 0.15 to 1.39 mGy which were higher than the calculation and mostly occurred in pelvic AP examination.

The calculated and measured dose showed good agreement with the correlation coefficient closed to one. However, our measurement results showed the fetal dose at 6 cm depth that larger than 1.0 mGy as recommended by ICRP publication for the examination in some technique in pelvic AP examination and in lumbo-sacral spine AP examination. While the calculation showed the less dose. Thus using parameter calculation, careful consideration of under dose about 23% should be kept in mind to have the fetal dose in the limit.

## 5.3 Recommendation

The image quality should be considered when reducing the fetal doses lower than ICRP dose limit.

## REFERENCES

- [1] Annals of the ICRP, Pregnancy and medical radiation. Publication 84, Pregnancy and Medical Radiation 30 (1): 2000.
- [2] Polunin N, Lim T A and Tan K P. Reduction in Retake Rates and Radiation Dosage Through Computed Radiography. Ann Acad Med Singapore 27(1998):805-7.
- [3] Don S. Radiosensitivity of children: potential for overexposure in CR and DR and magnitude of doses in ordinary radiographic examinations. Pediatr Radiol. 34 Suppl 3(October 2004): S167-72.
- [4] Compagnone G, Casadio B M, Pagan L, Calzolaio F L, Barozzi L and Bergamini C. Comparison of radiation doses to patients undergoing standart radiographic examinations with conventional screen-film radiography, computed radiography and direct digital radiography. Br J Radiol 79(2006): 899-904.
- [5] Damilakis, J. Pregnancy and diagnostic X-rays. Eur Radiol Syllabus 14(2004): 33-9.
- [6] Wagner L K, Lester R G and Saldana L R. Exposure of the pregnant patient to the diagnostic radiations: a guide to medical management. 2<sup>nd</sup> ed. Madison, Wis: Medical Physics Publishing, 1997.
- [7] Bushberg J T, Siebert J A, Leidholdt E M Jr and Boone J M. The essential physics of medical imaging. Baltimore, Md: Williams & Wilkins, 1994.
- [8] Parry R A, Glaze S A and Archer B R. The AAPM/RSNA physics tutorial for residents: Typical patient radiation doses in diagnostic radiology. RadioGraphics 19(1999): 1289-1302.
- [9] International Atomic Energy Agency. Absorbed dose determination in phantom and electron beams. IAEA TRS 277, 1987.
- [10] Khan F M. The Physic of Radiation Therapy. 3<sup>rd</sup> ed. USA: Lippincott Williams & Wilkins, 2003
- [11] Cameron J R, Suntharalingam N and Kenney G N. Thermoluminescent dosimetry. Milwaukee. The University of Wisconsin Press, 1968.
- [12] Harshaw Bicron radiation measurement produced. Model 5500 automatic TLD reader user's manual. Ohio: Saint – Gobian / Norton industrial ceramics, 1993.

- [13] United Kingdom Accreditation Service (UKAS). The expression of uncertainty and confidence in measurement. UKAS Publication Ref: LAB 12. 2000 ; 1-13.
- [14] International Atomic Energy Agency. Dosimetry in diagnostic radiology: An international code of practice. IAEA TRS 457, Austria. 2007.
- [15] Osei E K and Faulkner K. Fetal doses from radiological examinations. Br J Radiol 72(1999): 773-80.
- [16] Osei E K and Faulkner K. Fetal position and size data for dose estimation. Br J Radiol 72(1999): 363-70.
- [17] Ragozinno M W, Breckle R, Hill L M and Gray J E. Average fetal depth in utero: Data for estimation of fetal absorbed radiation dose. Med Phys 158(1986): 513-15.
- [18] Unlubay D and Bilaloglu P. Fetal risks in radiological examinations and estimated fetal absorption dose. Tani Girisim Radyol 9(1) (2003): 14-8.
- [19] Tung C H and Tsai H. Evaluations of gonad and fetal doses for diagnostic radiology. Proc. Natl. Sci. Counc. ROC (B) 23(1999): 107-13.
- [20] Bradley B, Fleck A and Osei E K. Normalized data for the estimation of fetal radiation dose from radiotherapy of the breast. Br J Radiol 79(2006): 818-27.
- [21] Damilakis J, Perisinakis K, Prassopoulos P, Dimovasili E, Varveris H and Gourtsoyiannis N. Conceptus radiation dose and risk from chest screen-film radiography. Eur Radiol 13(2003): 406-12.
- [22] Damilakis J, Perisinakis K, Koukourakis M and Gourtsoyiannis N. Maximum embryo absorbed dose from intravenous urography: Interhospital variations. Radiation Protection Dosimetry 72(1) (1997): 61-5.
- [23] Aldrich J E, Duran E, Dunlop P and Mayo R. Optimization of dose and image quality for computed radiography and digital radiography. SCAR (Society for Computer Applications in Radiology) 2006: 10.1007/s10278-006-9944-9.
- [24] Compagnane G, Baleni M C, Pagan L, Calzolaio F L, Barozzi L and Bergamini C. Comparison of radiation doses to patients undergoing standard radiographic examinations with conventional screen-film radiography, computed radiography and direct digital radiography. Br J Radiol 79(2006): 899-904.
- [25] Mckinlay A F. The characteristics of thermoluminescence material. Medical physics Hand Books Thermoluminescence Dosimetry. Bristol: Adam Hilger, 1981: 32-8, 83, 132-3.

- [26] Khan FM. Measurement of absorbed dose. The physics of radiation therapy. 2<sup>nd</sup> ed. Baltimore: Williams and Wilkins 1994: 167-71, 179-81, 214-5, 236, 286.
- [27] Harshaw Bicon. Instruction Manual for TLD oven, Saint-Gobain/Norton industrial ceramics Co. Ohio, 1993.
- [28] Harshaw Bicon radiation measurement produced. Model 5500 automatic TLD Reader User's Manual. Saint-Gobain/Norton industrial ceramics Co.: Ohio, 1993.
- [29] International Commission on Radiation Units and Measurements. Tissue substitutes in radiation dosimetry and measurement. Report No.44. Bethesda, MD: International Commission on Radiation Units and Measurements and calculated ranges. Phys. Med BIOL 26(1981): 907.
- [30] Instruction Manual of Victoreen 4000M+ X-ray Test Device. Ohio: Cardinal Health, 2003.
- [31] International Atomic Energy Agency. Absorbed dose determination in phantom and electron beams. IAEA TRS 398, 1987.
- [32] International Atomic Energy Agency and Commission of the European Communities. Radiation doses in diagnostic radiology and methods for dose reduction. Austria. IAEA, 1991-1993; 1-85.
- [33] International Commission on Radiation Units and Measurements. Appendix A: Backscatter factors. ICRU 5(2) (2005): 65-7.
- [34] Kato H. Method of calculating the backscatter factor for diagnostic x-rays using the differential backscatter factor. Jpn. Radiol. Technol 57(12) (1988): 1503-10.
- [35] Hufton A P. Radiation dose to the fetus in obstetric radiography. Br J Radiol 52(1979): 735-40.
- [36] Osei E K and Kotre C J. Equivalent dose to the fetus from occupational exposure of pregnant staff in diagnostic radiology. Br J Radiol 74(2001): 629-37.
- [37] Osei E K and Faulkner K. Radiation risks from exposure to diagnostic x-rays during pregnancy. Radiography 6(2000): 131-44.
- [38] Harrison R M. Backscatter factors for diagnostic radiology (1-4 mm Al HVL). Phy Med Biol 27(12) (1982): 1465-74.
- [39] BrighamRAD. A health care personnel guide for assessing radiation risk and selecting imaging procedures in pregnant women. BWH Radiology 1994-2004. Available from:

<http://brighamrad.harvard.edu/education/fetaldose/diag-exposure.html>  
[2551, January 24]

- [40] Baciak J E and Kearfott K J. Review of fetal radiation dose protection and dosimetry issues for medical procedures. RSO Magazine March/April 2000.



สถาบันวิทยบริการ  
จุฬาลงกรณ์มหาวิทยาลัย



**APPENDICES**

สถาบันวิทยบริการ  
จุฬาลงกรณ์มหาวิทยาลัย

## REPORT OF RADIOGRAPHIC SYSTEM PERFORMANCE

### General Information

<b>Location:</b>	<b>Mongkutpecharat Building King Chulalongkorn Memorial Hospital</b>
<b>Date:</b>	<b>July 26, 2007</b>
<b>Room number:</b>	<b>Emergency room No.1</b>
<b>Manufacturer:</b>	<b>Toshiba Medical System ( Japan, May 2005 )</b>
<b>Model number:</b>	<b>KXO-80G / DT-BTH / DST-100A</b>
<b>Serial number:</b>	<b>99E056 3615</b>

### Checklist

<b>P</b>	<b>General mechanical and electrical condition</b>
<b>P</b>	<b>Tube angle indicator, tube motion and locks</b>
<b>P</b>	<b>Focus to film distance indicator (SID)</b>
<b>P</b>	<b>Field size indicator</b>
<b>P</b>	<b>Congruency of light and radiation fields</b>
<b>P</b>	<b>Crosshair centering</b>
<b>P</b>	<b>Beam Quality (Half Value Layer)</b>
<b>P</b>	<b>Consistency of exposure (mR/mAs)</b>
<b>P</b>	<b>kVp Accuracy</b>
<b>P</b>	<b>Timer accuracy</b>
<b>P</b>	<b>mA Linearity</b>

P = Performed  
 N/P = Not  
 Performed  
 N/A = Not  
 Applicable

### General Condition of Mechanical and Electrical Components

<u>Y</u>	Are there any frayed or exposed electrical wires?
<u>N</u>	Could electrical wires interfere with the use of the unit?
<u>N</u>	Is there play in the couch when it is locked?
<u>Y</u>	Does it have the freedom of movement it was designed for?
<u>Y</u>	Is the couch level in tube and perpendicular directions?
<u>N</u>	Is there play in the tube when it is locked?
<u>Y</u>	Does it have the freedom of movement it was designed to have?
<u>Y</u>	Does the visual, and/or, audible beam-on indicator function?
<u>N/Y</u>	Is the dead man switch installed correctly?

Comments:

### Target to Film Distance Indicator Check (at 40" SID)

SID: 100 cm *Allowable limit = +/- 2% SID*

Measured distance: 100 cm

Indicated distance: 100 cm

Radiographically  
(determined) distance: 100 cm

**% Difference:** 0.00%

**Passed or Failed:** **Passed**

### General Comments



### Tube Angle Indicator Check

CW:		CCW:	
0° -	<u>2</u>	45° -	<u>47</u>
45° -	<u>46</u>	90° -	<u>92</u>
90° -	<u>92</u>		

Allowable  
limit =  $\pm 5^\circ$

### Motion and Lock Check

	<u>Motion</u>	<u>Locks</u>
Tube Longitudinal:	<u>Y</u>	<u>Y</u>
Tube Rotate:	<u>Y</u>	<u>Y</u>
Tube Transverse:	<u>Y</u>	<u>Y</u>
Tube Vertical:	<u>Y</u>	<u>Y</u>
Tube Angulate:	<u>Y</u>	<u>Y</u>
Collimator Jaws:	<u>Y</u>	<u>Y</u>
Collimator Rotation:	<u>Y</u>	<u>Y</u>

### Field Size Indication

Purpose: to insure that the radiographer can set a desired field size using the light field collimator.

Requirement:  $\pm 2\%$  SID.

SID: 100 cm

<u>Indicator Setting</u>	<u>Measured Longitudinal</u>	<u>Measured Transverse</u>	<u>% Variation</u>	<u>Pass/ Fail</u>
8 x 8	<u>7.4</u>	<u>7.9</u>	0.10%	Pass
10 x 10	<u>10.4</u>	<u>9.3</u>	0.70%	Pass
12 x 12	<u>11.8</u>	<u>11.2</u>	0.80%	Pass
14 x 14	<u>13.2</u>	<u>13.4</u>	0.60%	Pass
17 x 17	<u>16.8</u>	<u>16.7</u>	0.30%	Pass
Others:				

### Congruence of Light and Radiation Fields

Purpose: to determine the alignment of the light and radiation fields.

Requirement: alignment to within +/- 2% of indicated SID.

Method: mark corners of light field and compare to radiation field.

SID: 100 cm

Field Size	Light Field Size		Radiation Field Size		% Variation	Pass/ Fail
	Measured Long.	Measured Trans.	Measured Long.	Measured Trans.		
25.5 x 20.5	<u>25.5</u>	<u>20.5</u>	<u>24.3</u>	<u>19.2</u>	1.30%	Pass
30.5 x 25.5	<u>30.5</u>	<u>25.5</u>	<u>29.6</u>	<u>24.5</u>	1.00%	Pass

### Cross Hair Centering

Purpose: to determine if the light field cross hair indicates the central axis of the x-ray beam.

Requirement: must be within +/- 2% of indicated SID.

SID: 100 cm

Deviation between radiation and optical field centers: 0.44

Pass/Fail: **Pass**

General Comments

### Beam Quality (Half Value Layer)

Method: set 70 kVp.

Requirement: NCRP #33 recommends not less than 2.1 mmAl at 70 kVp.

Set kVp: 70

Filter (mmAl)	Instrument Reading
<u>OPEN</u>	<u>213.9</u>
<u>2.5</u>	<u>113.8</u>
<u>3</u>	<u>102.11</u>

**Calculated  
HVL:**

**2.8 mmAl**

### Beam Quality (Half Value Layer)

Method: set 80 kVp.

Requirement: NCRP #33 recommends not less than 2.3 mmAl at 80 kVp.

Set kVp: 80

Filter (mmAl)	Instrument Reading
<u>OPEN</u>	<u>274.7</u>
<u>3</u>	<u>143.9</u>
<u>3.5</u>	<u>133.2</u>

**Calculated  
HVL:**

**3.31 mmAl**

### Beam Quality (Half Value Layer)

Method: set 90 kVp.

Requirement: NCRP #33 recommends not less than 2.5 mmAl at 90 kVp.

Set kVp: 90

Filter (mmAl)	Instrument Reading
<u>OPEN</u>	<u>348.9</u>
<u>3.5</u>	<u>181.4</u>
<u>4</u>	<u>164.8</u>

**Calculated HVL: 3.71 mmAl**

### Beam Quality (Half Value Layer)

Method: set 100 kVp.

Requirement: NCRP #33 recommends not less than 2.7 mmAl at 100

Set kVp: 100

Filter (mmAl)	Instrument Reading
<u>OPEN</u>	<u>415.8</u>
<u>4</u>	<u>218.7</u>
<u>4.5</u>	<u>199.7</u>

**Calculated HVL: 4.28 mmAl**

### Exposure Consistency

Purpose: to determine if the exposure is remaining consistent.

Requirement: coefficient of variation should be  $\leq 0.05$ .

Method: Victoreen 4000M+ procedure.

	Set SCD: <u>66.04</u> cm	Set kVp: <u>80</u>	
Set mA: <u>320</u>	Set time: <u>0.078</u>	Set mAs: <u>25</u>	
	<u>kVp</u>	<u>Time</u>	<u>mR</u>
	<u>79.19</u>	<u>0.0800</u>	<u>281.4</u>
	<u>79.17</u>	<u>0.0801</u>	<u>281.4</u>
	<u>79.19</u>	<u>0.0801</u>	<u>282.4</u>
	<u>79.18</u>	<u>0.0800</u>	<u>282.6</u>
<b>Mean:</b>	<b>79.183</b>	<b>0.0801</b>	<b>281.95</b>
<b>Std. Dev.</b>	<b>0.0083</b>	<b>0.0000</b>	<b>0.5545</b>
<b>C.V.</b>	<b>0.0001</b>	<b>0.0006</b>	<b>0.0020</b>
	<b>Pass/Fail:</b>	<b>Pass</b>	

### General Comments

สถาบันวิทยบริการ  
จุฬาลงกรณ์มหาวิทยาลัย

### Timer Accuracy

Requirement: within 10% of set time.

Method: at about 80 kVp, mid-current mA station, record measured time for each time setting (use Victoreen 4000M+).

SCD: 66.04 cm      Set kVp: 80 mA: 320

<b>Seconds (set)</b>	<b>Measured (milliseconds)</b>	<b>% Variation</b>
<u>0.0500</u>	<u>0.0501</u>	0.20%
<u>0.1000</u>	<u>0.0999</u>	0.10%
<u>0.1969</u>	<u>0.1996</u>	1.38%
<u>0.2500</u>	<u>0.2494</u>	0.24%
<u>0.3125</u>	<u>0.3281</u>	4.99%
<u>0.3906</u>	<u>0.4068</u>	4.14%

### General Comments

สถาบันวิทยบริการ  
จุฬาลงกรณ์มหาวิทยาลัย

### mA or mAs Linearity

Method: select 80 kVp and time close to 0.100 ms (1/10 sec) and cycle through all mA stations and record the exposure in mR (use Victoreen 4000M+).

Requirement: coefficient of variation should not exceed 0.1.

S/L	Ave. kVp	mA	Time	mAs	mR	mR/mAs	C.V.
L	78.81	320	0.1	32.0	335.9	10.5	-0.138
	78.85	400	0.1	40.0	443.5	11.1	-0.126
	79.59	500	0.1	50.0	571.0	11.4	-0.101
	79.92	630	0.1	63.0	700.0	11.1	

**Global Mean: -0.1217**

**Std.**

**Global Dev.: 0.01859**

**Global C.V.: -0.1527**

### General Comments

สถาบันวิทยบริการ

จุฬาลงกรณ์มหาวิทยาลัย

### kVp Linearity

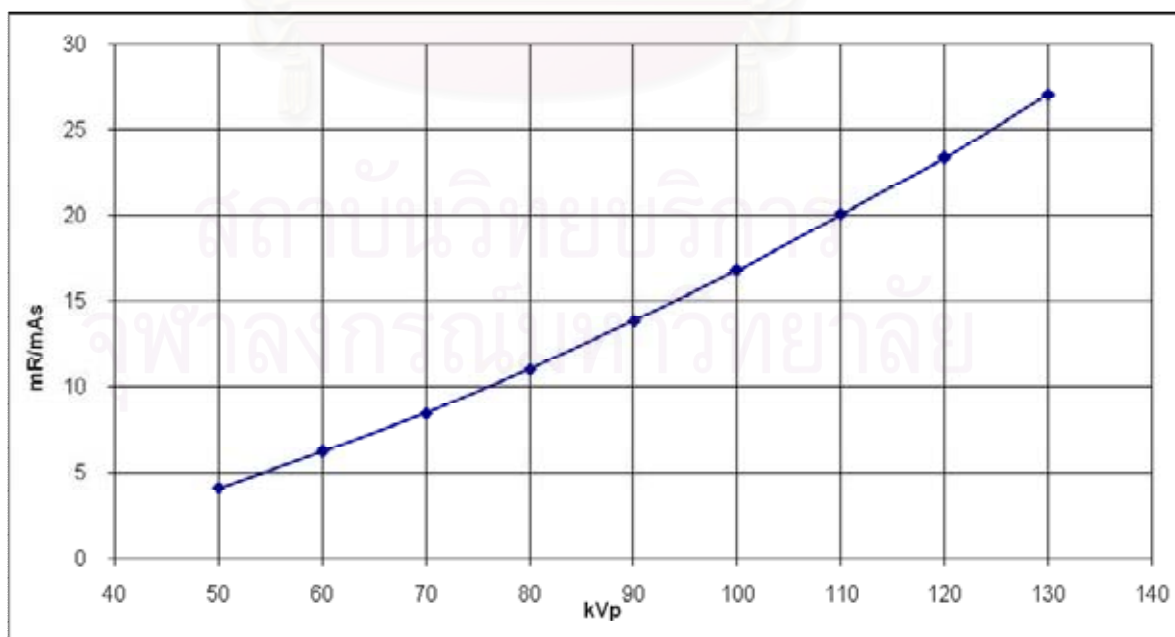
Method: at a mid-current station, vary the kVp from minimum to maximum in steps of 10 kVp. Record the measured kVp. (Use the Victoreen 4000M+).

Requirement: the deviation should not exceed 5 kVp or 10% of set kVp, whichever is larger.

Set SCD: 66.04 cm                      Phase: 3

mA: 320                      Time: 0.1                      mAs: 32

<u>Set kVp</u>	<u>Measured kVp</u>		<u>Max.</u>	<u>% Dev.</u>	<u>mR</u>	<u>mR/mAs</u>
	<u>Avg.</u>	<u>Eff.</u>				
50	50.60	50.55	51.09	1.20%	130.10	4.07
60	59.71	59.63	60.18	0.48%	199.20	6.23
70	70.04	69.95	70.87	0.06%	269.40	8.42
80	78.90	78.79	79.81	1.37%	351.20	10.98
90	89.54	89.43	90.91	0.51%	442.00	13.81
100	99.53	99.24	100.90	0.47%	535.70	16.74
110	108.40	108.10	110.00	1.45%	641.80	20.06
120	116.50	116.30	118.20	2.92%	746.30	23.32
130	128.70	128.40	130.40	1.00%	864.8	27.03





**VITAE**

<b>NAME</b>	Miss Phakamart Thaoyabut
<b>SEX</b>	Female
<b>NATIONALITY</b>	Thai
<b>DATE OF BIRTH</b>	January 6, 1982
<b>PLACE OF BIRTH</b>	Sakon Nakhon, Thailand
<b>INSTITUTIONS ATTENDED</b>	Naresuan University, 2005: Bachelor of Science (Radiological Technology)  Chulalongkorn University, 2008: Master of Science (Medical Imaging)
<b>HOME ADDRESS</b>	117 Moo.6 T. Nongsanom A.Wanorndiwas Sakon Nakhon 47120 Thailand Tel. 042-988094

สถาบันวิทยบริการ  
จุฬาลงกรณ์มหาวิทยาลัย